INSTITUTO SUPERIOR TÉCNICO
Universidade Técnica de Lisboa

Chemical Absorption model in gPROMS for Carbon Capture with Monoethanolamine

Filipe Henriques Mendes Calado

Master's Thesis in

Chemical Engineering

Supervisory committee

President:	Professor João Fareleira, from Instituto Superior Técnico
Supervisors:	Professor Carla Pinheiro, from Instituto Superior Técnico
	Professor Nilay Shah, from Imperial College London
Juror:	Professor Maria Rosinda Ismael, from Instituto Superior Técnico

November 2010

(this page was intentionally left in blank…)

Acknowledgments

I would like to acknowledge the support provided by the thesis co-supervisors Professor Carla Pinheiro from Instituto Superior Técnico in Lisbon, and Professor Nilay Shah and Professor Constantinos Pantelides from Imperial College London in London during the course of this work. The opportunity they presented to me revealed to be an extraordinary life experience and I am eternally grateful to them. I would also like to thank you Professor João Fareleira and Professor Maria Rosinda Ismael for serving in my supervisory committee.

I am also grateful to *Process System Enterprise Ltd* for having me at their office in London for 6 months. In particular I would like to show my appreciation to some of the elements from the Consulting Group, namely Dr. Apostolos Giovanoglou, Dr. Diogo Narciso, Dr. Mark Pinto, Dr. Rodrigo Blanco and Dr. Georgios Koumpouras. Their support made it much easier and enjoyable the time I spent in London. I am grateful to *Det Norske Veritas S.A.* for allowing me to use their experimental data which added great value to work developed in this thesis. Particularly I would like to thanks Dr. Chara Georgopoulou for her support and contribution.

A special thanks to the EngD. student Joana Figueiredo for helping me during the process of reviewing this thesis.

To my beloved parents and family I would like to say I am truly grateful for your support and encouragement during the period I was living in London and also for making it possible for me to grow as a person in such a pleasant environment.

To my closest friends, I could not make it without you and I honestly hope we all succeed in our careers now that we are growing older and we have more responsibilities.

Abstract

A chemical absorption model in gPROMS for CO_2 capture with MEA was developed in this work. The model was organized in two different hierarchical levels. The lower level was composed by five individual sub-models where all the correlations describing this system were implemented. A higher level composite model that established the connections between the individual sub-models was also implemented. The chemical absorption model was developed to allow good flexibility, easy maintenance, and the possibility to use it in a drag-and-drop flowsheeting. The model developed was validated against experimental data available for 4 indicators from Aboudheir (Aboudheir, 2002) and Tontiwachwuthikul *et al.* (Tontiwachwuthikul, *et al.*, 1992). It was found that it could predict these indicators using two different correlations for the effective area for mass transfer within reasonable accuracy (AAD < 21% and $\Delta T_{av} < 3$ K), for CO_2 capture efficiencies up to 90%. It was showed that the correlation proposed by Bravo *et al.* (Equation 2.17) for the effective area was more suitable than the correlation proposed by Onda *et al.* (Equation 2.16) to perform a feasibility study. This study was performed to assess the possibility of removing a significant amount of CO_2 diluted in a flue gas stream within a very restricted space environment. It was showed that for 18 of the 25 operating conditions considered, chemical absorption was a feasible technology according to the space restrictions imposed.

KEYWORDS: CO_2 capture, chemical absorption, MEA, modelling, feasibility study

Abstract (in Portuguese)

Neste trabalho foi desenvolvido um modelo para captura de CO_2 com MEA usando absorção química em linguagem gPROMS. O modelo foi organizado de acordo com dois níveis hierárquicos. No nível da hierarquia mais baixo foram criados 5 sub-modelos onde foram implementadas as equações que traduzem o comportamento do sistema enquanto que no nível hierárquico mais alto foi criado um modelo para estabeler as ligações entre os sub-modelos. Esta organização permitiu uma maior flexibilidade no uso do modelo, assim como uma maior facilidade de manutenção e também facilitou o integração do mesmo em diagramas de processo. O modelo foi validado com resultados experimentais para 4 indicadores da performance do sistema publicados por Aboudheir (Aboudheir, 2002) e Tontiwachwuthikul *et al.* (Tontiwachwuthikul, *et al.*, 1992). Concluiu-se que, para eficiências de captura de CO_2 menores que 90%, o modelo é capaz de prever os resultados experimentais com AAD < 21% e $\Delta T_{av} < 3$ K usando duas correlações diferentes para a área efectiva disponível para a transferência de massa propostas por Bravo *et al.* (Bravo, *et al.*, 1982) e Onda *et al.* (Onda, *et al.*, 1968). Neste trabalho ficou provado que a correlação proposta por Bravo *et al.* é mais adequada para estudos de viabilidade. Um estudo de viabilidade foi efectuado para determinar se a tecnologia de absorção química podia ser instalada num espaço bastante limitado para remoção de CO_2 de uma corrente gasosa diluída. Foi concluído que para 18 das 25 condições operatórias analisadas esta tecnologia poderia ser considerada viável.

PALAVRAS-CHAVE: Captura de CO_2, absorção química, MEA, modelação, viabilidade

Table of Contents

List of Tables

List of Figures

Nomenclature

AAD	absolute average deviation defined by $\left(\frac{\sum\left\|\frac{x_{experimental}-x_{model}}{x_{experimental}}\right\|}{\textbf{number experimental points}}\times\mathbf{100}\right)$
AmH	generic amine
$AmH^+.CO_2^-$	zwitteron
$Am.CO_2^-$	carbamate
B	generic specie which can act as a base
BFDM	backward finite difference method
BH^+	protonated base
CO	carbon monoxide
CO_2	carbon dioxide
DAE	differential algebraic equation
DNV	*Det Norske Veritas S.A.*
FFDM	forward finite difference method
GHG	greenhouse gas
H_2	hydrogen
H_2O	water
$HMEA^+$	protonated MEA
IPCC	Intergovernmental Panel on Climate Change
MDEA	methyldiethanolamine
MEA	monoethanolamine
$MEA.CO_2^-$	MEA Carbamate
MSDS	material safety data sheet
N_2	nitrogen
N_2O	nitrous oxide
O_2	oxygen
OH^-	hydroxide ion
PSE	*Process System Enterprise Ltd*
VLE	vapour-liquid equilibrium

1. Introduction

Climate changes are nowadays a global concern around the world. According to the IPCC's Third Assessment Report there are strong evidences that human activities are responsible for the rapidly increase in the global warming verified over the last 50 years (www.ipcc.ch). If fact the emission of GHG into the atmosphere as the result of fossil fuels combustion is recognized as the main contributor for the global warming. The most significant GHG released into the atmosphere is considered to be CO_2 (www.ipcc.ch).

Several works have been developed in studying alternatives to reduce the CO_2 emissions into the atmosphere. These alternatives can be grouped within three CO_2 capture systems, namely Post-combustion, Pre-combustion and Oxyfuel combustion. These systems differentiate from each other not only in terms of the technology used but also in terms of the location where the CO_2 is removed or, in the case of Oxyfuel fuel combustion, the combustion is performed with O_2 instead of using air. The differences between each CO_2 capture system are schematically illustrated in Figure 1.

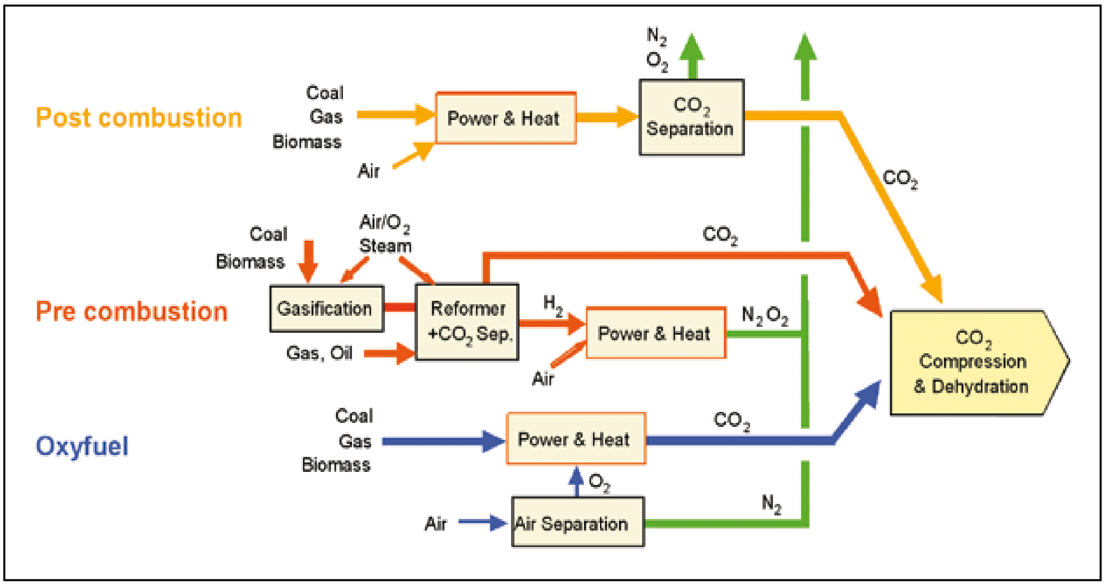

Figure 1 – CO_2 capture systems (www.ipcc.ch).

The Post-combustion system uses air in the fuel combustion resulting in low concentrations of CO_2 in the exhaust gas stream. As the name suggests CO_2 is removed after the combustion occurs. In the Pre-combustion system the original fuel is first gasified leading to the formation of synthesis gas mostly composed by CO and H_2. This gas is reformed with steam to increase the formation of CO_2 and more H_2 after which the highly concentrated CO_2 is removed and the remaining H_2 is then used as fuel to produce power and heat (www.ipcc.ch). In the Oxyfuel system, the fuel is burned with O_2 instead of using air leading to high concentrations of CO_2 in the exhaust gas stream and therefore an easier separation step. On the other hand the required separation of O_2 and N2 is cryogenic and very expensive (www.ipcc.ch). The advantages of each system as well as some key considerations are summarized in Figure 2.

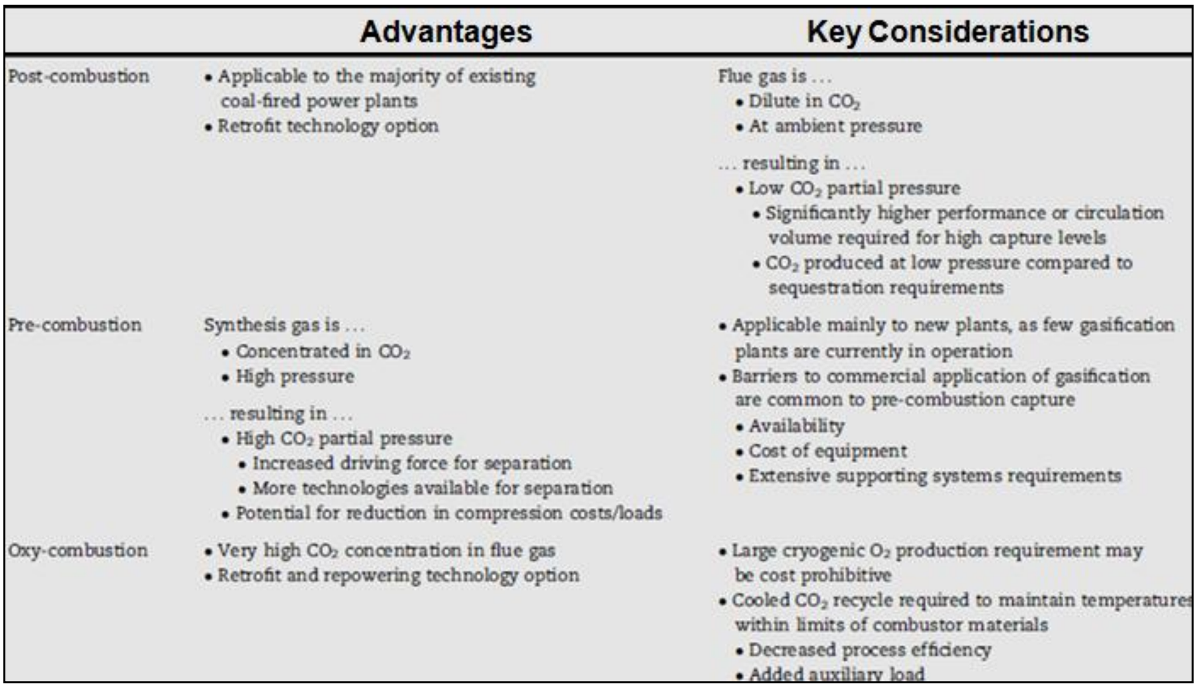

	Advantages	Key Considerations
Post-combustion	• Applicable to the majority of existing coal-fired power plants • Retrofit technology option	Flue gas is ... • Dilute in CO_2 • At ambient pressure ... resulting in ... • Low CO_2 partial pressure • Significantly higher performance or circulation volume required for high capture levels • CO_2 produced at low pressure compared to sequestration requirements
Pre-combustion	Synthesis gas is ... • Concentrated in CO_2 • High pressure ... resulting in ... • High CO_2 partial pressure • Increased driving force for separation • More technologies available for separation • Potential for reduction in compression costs/loads	• Applicable mainly to new plants, as few gasification plants are currently in operation • Barriers to commercial application of gasification are common to pre-combustion capture • Availability • Cost of equipment • Extensive supporting systems requirements
Oxy-combustion	• Very high CO_2 concentration in flue gas • Retrofit and repowering technology option	• Large cryogenic O_2 production requirement may be cost prohibitive • Cooled CO_2 recycle required to maintain temperature within limits of combustor materials • Decreased process efficiency • Added auxiliary load

Figure 2 – Advantages and key considerations of each CO_2 capture system (Figueroa, *et al.*, 2008).

In this work Post-combustion for CO_2 capture was used since this system has the retrofit advantage and can be used without having to modify the combustion system upstream. Several technologies have been proposed that can be applied to Post-combustion CO_2 capture. These technologies are illustrated in the diagram of Figure 3.

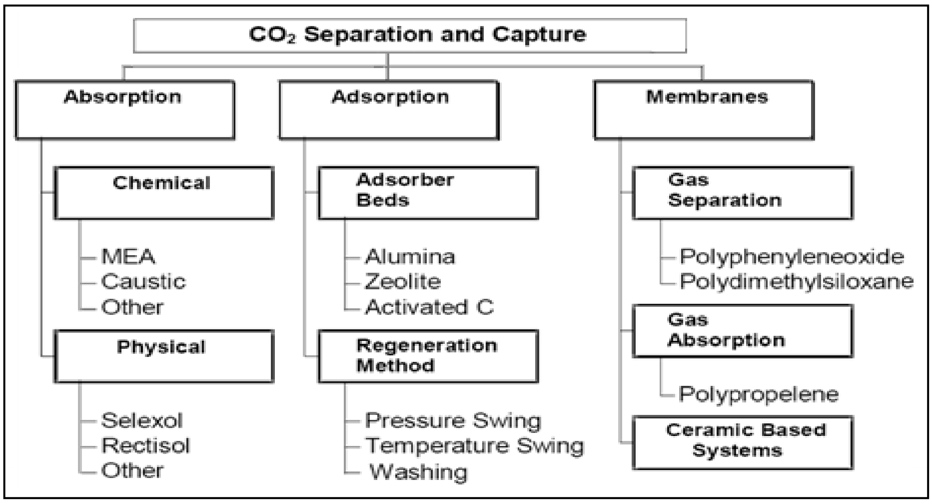

Figure 3 – Technologies available for Post-combustion CO_2 capture (Rubin, *et al.*, 2002).

In their report for the U.S. Department of Energy Rubin *et al.* presented an extensive description about the advantages and disadvantages of each technology used for Post-combustion CO_2 capture (Rubin, *et al.*, 2002). This information was summarized as follows:

Table 1 – Advantages, disadvantages, and system requirements of each technology for Post-combustion CO_2 capture (Rubin, *et al.*, 2002).

Technology	System requirements	Advantages	Disadvantages
Chemical absorption	Absorption and regeneration columns; Chemical solvent; Heat exchangers;	Suitable for dilute CO_2 streams; Operates at ordinary temperature; Commercially available technology;	Heat requirement for solvent regeneration; Solvent losses due impurities in the gas stream;
Physical absorption	Absorption and regeneration columns; Physical solvent;	Less energy requirement for solvent recovery than chemical absorption; Solvents are less susceptible to the impurities in the gas stream;	High operating pressure; Less efficient than chemical absorption;
Adsorption	Adsorber bed(s)	Very high CO_2 removal;	Very high operating pressure; High cost;
Membranes	Membrane filters	Upcoming, promising technology; Space efficient;	Very high operating pressures; May require multiple units and recycling due to lower product purity; Very high cost;

Chemical absorption with amine solvents (in this case MEA) was chosen in this work since it has been successfully used for acid gas purification, including CO_2, in gas industries and ammonia plants since a long time ago (Kohl, *et al.*, 1997). This is considered a well established technology and presents itself as the most reliable Post-combustion technology for CO_2 capture at industrial scale within the timeframe of this work, although in the future other technologies are expected to be more cost efficient as it can be seen in Figure 4:

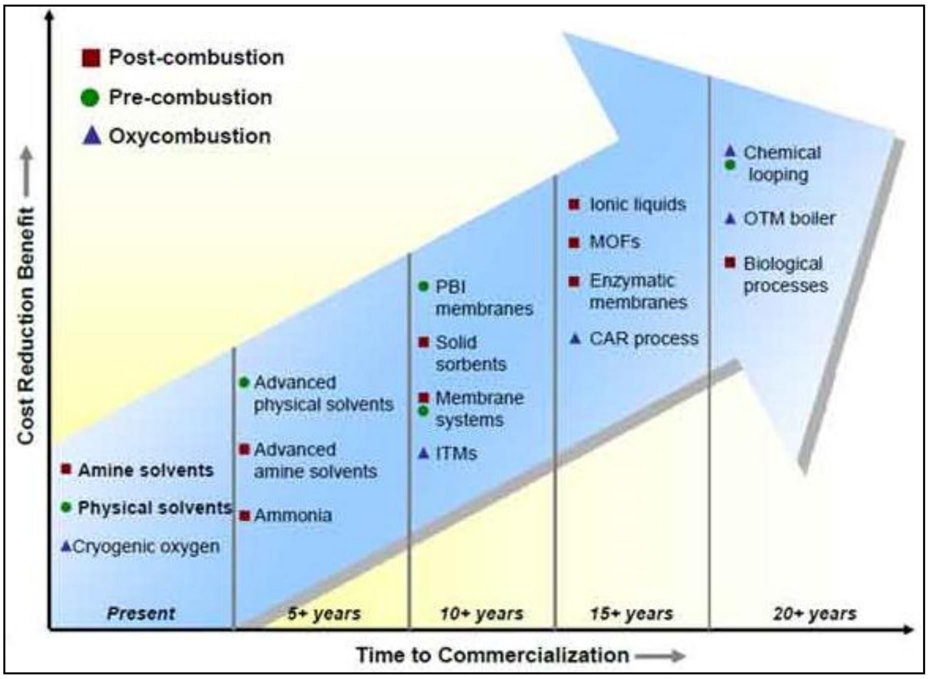

Figure 4 – Predictions of the cost reduction benefit and the time to commercialization of different technologies for CO_2 capture (www.powerplantccs.com).

This technology requires several pieces of equipment. Besides the absorption column where CO_2 is removed from the vapour stream, a regeneration section is also required to regenerate the solvent. Due to the higher temperatures at this step of the process a heat-exchanger is necessary to increase the temperature of the liquid outlet stream from the absorption column. This stream then goes through the regeneration column and, after being regenerated, the lean solvent stream returns to the heat exchanger where it is cooled before entering the absorption column again. The chemical absorption loop is illustrated in Figure 5.

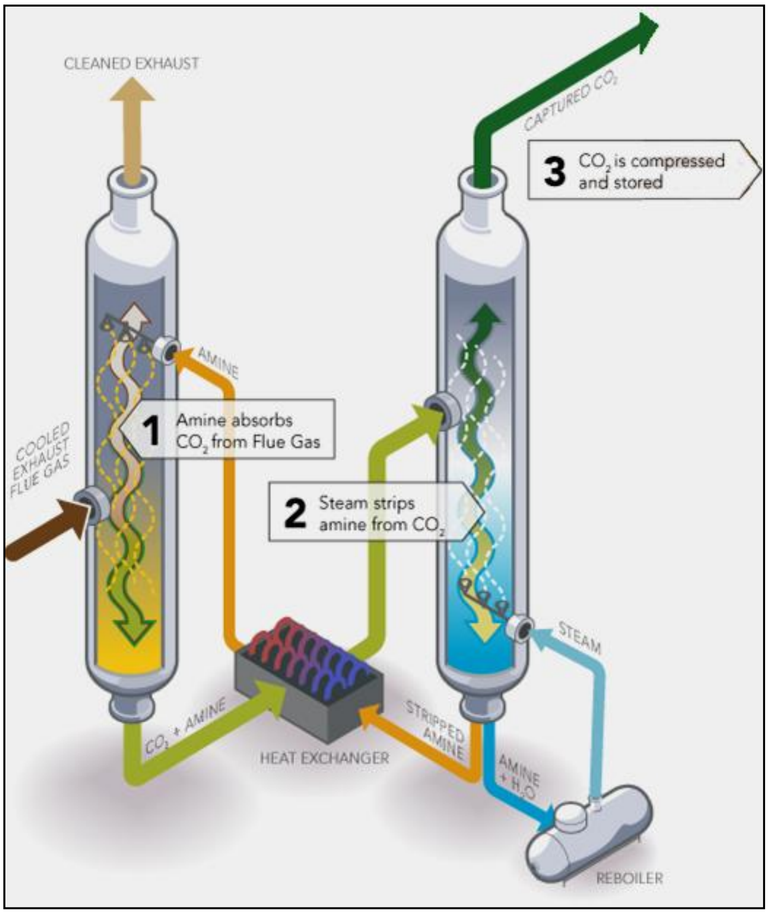

Figure 5 – Chemical absorption loop and flow direction of each stream (www.bantrel.com).

The scope of this work was then to develop a chemical absorption model for CO_2 capture with MEA to assess if this technology could be used to remove a significant amount of CO_2 from a flue gas stream within a restricted space environment. Although other equipment is required, as illustrated in Figure 5, this assessment was made through the determination of the dimensions of the absorption column required to achieve the desired CO_2 removal for steady-state operation.

2. Literature Review

An extensive description regarding the most significant phenomena of a chemical absorption system for CO_2 capture with MEA is presented in this chapter. This description is the result of a collection made from the work published by several authors during the years concerning these phenomena. The correlations used in the model to describe them as well as some of the assumptions made regarding the model development are presented.

2.1. Pressure drop in packed columns

As it is illustrated in Figure 5, the absorption column for CO_2 capture can be described as a packed column where two fluids (vapour phase and liquid phase) in countercurrent flow are contacting each other. To describe the variation of the pressure inside a packed column a momentum balance can be written, however due to the uncertainties of the physical phenomena associated with the pressure drop the most common approach is to use semi-empirical correlations (Pantelides, 2000). In this work, the so-called Ergun's equation at its steady-state form was used to estimate the pressure drop along the axial direction of the column:

$$-\frac{\partial P}{\partial z} = 150\frac{\left(1-\varepsilon_p\right)^2}{\varepsilon_p}\frac{\mu_G.v_G}{{d_p}^2} + 1.75\frac{\left(1-\varepsilon_p\right)}{\varepsilon_p}\frac{\rho_G.{v_G}^2}{d_p}$$

(Equation 2.1)

2.2. Mass transfer

Within a single phase, the different concentrations of the components in a non homogeneous mixture establish driving forces for mass transfer to occur. Hence, fluxes of species occur from the regions where the species are more concentrated to the regions where those concentrations are lower. This phenomenon is known as diffusion and can be described by Fick's law or, in a more detailed approach, Maxwell's law for diffusion (Coulson, *et al.*, 1999). The fluxes of species can also occur due to regions at different temperatures, but in this case the phenomenon is known as thermal diffusion. The approach to determine thermal diffusion in a non homogeneous mixture is also described in Coulson, *et al.*

However, none of these approaches were followed in this work since along the axial direction the diffusion in general was considered to be negligible and both phases were considered to be homogeneous along the radial direction, which mean that the concentrations of all the components and the temperature were considered to be the same at each radial position within the bulk of vapour or the liquid phases.

On the other hand when two different phases are brought into contact, as it happens in an absorption column for CO_2 capture, there is also the possibility of mass transfer to occur across the phase boundary. The mass transfer between two different phases is not only influenced by the concentrations of the components in each phase and its temperature but also by the physical properties and the contact area between the two (Coulson, *et al.*, 1999). In 1923, the *two-film theory* proposed by Whitman (Whitman, 1923) was the first mechanism to be presented as an attempt to describe the conditions near the phase boundary. This mechanism is based on the assumption that two thin films are formed near that interface, one per phase, and it is within those films that are located the resistances for transfer to occur (Coulson, *et al.*, 1999). So within those films the mass transfer equations presented by Fick and Maxwell to describe the diffusion phenomenon are valid. Another mechanism describing the conditions near the two phase boundary called *penetration theory* was proposed by Higbie (Higbie, 1935). It is assumed that for a short contact time, so that the penetration is only confined to layers near the interface of the two fluids, diffusion occurs and elements of one of the fluids are exposed to the other phase. So, the interface is renewed and those elements are remixed into the bulk (Coulson, *et al.*, 1999).

2.2.1. Mass transfer coefficients

Although the fluxes of material can be directly determined applying both of these mechanisms, it implies solving complex systems of equations. Therefore, over the years several correlations based on these two theories were proposed to estimate mass transfer coefficients which can be used to determine the fluxes of material without having to solve those complex systems of equations. A review of these correlations was recently made by Wang and co-workers (Wang, *et al.*, 2005). Hence, the flux of each component per unit of interface area available for mass transfer can be determined based on the estimation of the mass transfer coefficient for that component and the driving force responsible for the transfer, *i.e.* the concentration difference between the interface and the bulk in each phase.

$$\boldsymbol{N_{G,i} = k_{G,i} \times \frac{P}{RT}\left(y_i{}^b - y_i{}^{int}\right)}$$

(Equation 2.2)

$$\boldsymbol{N_{L,i} = k_{L,i} \times \left(C_i{}^{int} - C_i{}^b\right)}$$

(Equation 2.3)

Since there is no accumulation of material near the interface, the rates of mass transfer, *i.e.* the fluxes, of material from one phase to the other must be the same (Coulson, *et al.*, 1999).

According to Wang *et al.*, the correlations developed by Onda and his co-workers (Onda, *et al.*, 1968) are widely used in the prediction of mass transfer coefficients in packed columns. In their work, Onda *et al.* studied the absorption of pure CO_2 with organic solvents in different random packings, and based on those results and experimental data available from other authors proposed correlations to estimate the mass transfer coefficients for both the liquid and the vapour phase in a wide range of flow conditions. It is reported that those correlations predict the coefficients within a ±20% deviation from the experimental data. Recently, the work developed by Sieres *et al.* with ammonia-water absorption in refrigeration systems showed that the Onda's correlations can be used to estimate the experimental mass transfer coefficients with reasonable accuracy and they present better results compared to other commonly used correlations for different kinds of random packings (Sieres, *et al.*, 2007).

Therefore, the Onda's correlations are used in this work to predict the mass transfer coefficients. For the vapour phase, the Onda's correlation is:

$$\boldsymbol{k_{G,i}} = \frac{\boldsymbol{c}}{\boldsymbol{RT_{int}}} \times \left(\frac{\boldsymbol{F_G}}{\boldsymbol{S.a_p.\mu_G}}\right)^{0.7} \left(\frac{\boldsymbol{\mu_G}}{\boldsymbol{\rho_G.D_{G,i}}}\right)^{1/3} \left(\frac{\boldsymbol{a_p}}{\boldsymbol{d_p}}\right)^{-2.0} \left(\boldsymbol{a_p.D_{G,i}}\right)$$

(Equation 2.4)

It is reported in Onda *et al.* that $\boldsymbol{c}$ is a dimensionless constant that takes different values depending on the size of the packing $\boldsymbol{d_p}$. Hence, for values of $\boldsymbol{d_p} < 1.5 \times \mathbf{10^{-2}}$ m, Onda *et al.* suggested that constant should be equal to 2.00 and 5.23 for $\boldsymbol{d_p} \geq \mathbf{1.5} \times \mathbf{10^{-2}}$ m. On the other hand, Sieres *et al.* suggested this constant could be higher than 5.23 for values of $\boldsymbol{d_p} > 1.5 \times \mathbf{10^{-2}}\ \mathbf{m}$ and should be fitted to match the experimental data. Since one of the aims of this work is to develop a model that can be used to predict the behaviour of chemical absorption of CO_2 without fitting any parameter, the values proposed by Onda *et al.* were used. For the liquid phase, the correlation proposed by Onda *et al.* was:

$$\boldsymbol{k_{L,i}} = \mathbf{0.0051} \times \left(\frac{\boldsymbol{F_L}}{\boldsymbol{S.a_e.\mu_L}}\right)^{2/3} \left(\frac{\boldsymbol{\mu_L}}{\boldsymbol{\rho_L.D_{L,i}}}\right)^{-1/2} \left(\boldsymbol{a_p.d_p}\right)^{0.4} \left(\frac{\boldsymbol{\rho_L}}{\boldsymbol{\mu_L.g}}\right)^{-1/3}$$

(Equation 2.5)

Onda *et al.* proposed that the mass transfer coefficient for the liquid phase should be a function of the effective area available for mass transfer $\boldsymbol{a_e}$. This subject is discussed later in the section 2.2.4.

2.2.2. *Diffusivities*

As it can be seen in (Equation 2.4 and (Equation 2.5 the mass transfer coefficients are a function of the components diffusivities in the vapour phase and in the liquid phase respectively. To determine the components diffusivity in the vapour phase, the method proposed by Fuller was used (Poling, *et al.*, 2007). This method is said to predict vapour diffusivities for binary systems at low pressures with an AAD of 4% (Poling, *et al.*, 2007).

$$D_{G,i} = \frac{1.43 \times 10^{-7} \times (T_{int})^{1.75}}{\left(\frac{P}{1 \times 10^5}\right) \times \sqrt{2 \times \left(\frac{1 \times 10^{-3}}{MW_i} + \frac{1 \times 10^{-3}}{MW_j}\right)^{-1}} \times \left[(\sum v)_i{}^{1/3} + (\sum v)_j{}^{1/3}\right]^2}$$

(Equation 2.6)

In (Equation 2.6, $\sum v$ is obtained by summing atomic diffusion volumes of the elements that make part of the molecules of interest. These volumes are presented in Poling *et al.* (Poling, *et al.*, 2007). It is also worth mentioning that in the calculation of the vapour diffusivities of each component i, air or N2 were considered as the jth element of the pair of molecules depending on the inlet composition of the vapour phase.

On the liquid phase an analogy with N_2O has been used over the years to predict the CO_2 diffusivity in aqueous alkanolamine solutions (Ko, *et al.*, 2001). This analogy is based on the N_2O and the CO_2 diffusivities in pure water and also in the diffusivity of N_2O in aqueous alkanolamine solutions (Equation 2.7).

$$D_{L,CO_2} = D_{N_2O,sol} \times \left(\frac{D_{CO_2}}{D_{N_2O}}\right)_{water}$$

(Equation 2.7)

The diffusivities of N_2O and CO_2 in pure water were studied by Versteeg *et al.* (Versteeg, *et al.*, 1988). The following temperature dependencies were reported:

$$D_{CO_2,water} = 2.35 \times 10^{-6} \times exp\left(\frac{-2119}{T_{int}}\right)$$

(Equation 2.8)

$$D_{N_2O,water} = 5.07 \times 10^{-6} \times exp\left(\frac{-2371}{T_{int}}\right)$$

(Equation 2.9)

To determine the diffusivity of CO_2 in aqueous alkanolamine solutions through the "N_2O analogy" Ko *et al.* used the equations proposed by Versteeg *et al.*, (Equation 2.8) and (Equation 2.9), and focused their experiments in determining the diffusivity of N_2O in those solutions. Several amines were studied over a wide range of concentrations and at different temperatures. For the system of interest for this work, respectively MEA+H_2O, the range of concentrations studied were 500 to 5000 mol/m^3 and the measurements were done at 30, 35 and 40 ºC (Ko, *et al.*, 2001). The following correlation to determine the N_2O diffusivity in an MEA+H_2O system was proposed:

$$\boldsymbol{D_{N_2O,sol} = \left(5.07\times10^{-6} + 8.65\times10^{-7}.\frac{C_{MEA}}{1000} + 2.78\times10^{-7}.\left(\frac{C_{MEA}}{1000}\right)^2\right)}$$
$$\boldsymbol{\times\, exp\left[\frac{\left(-2371 - 93.4\times\frac{C_{MEA}}{1000}\right)}{T_{int}}\right]}$$

(Equation 2.10)

The correlations proposed by Versteeg *et al.* and by Ko *et al.* were used in this work to determine the diffusivity of CO_2 in the liquid phase. For the other components of interest, the correlation proposed by Wilke (Poling, *et al.*, 2007) for binary mixtures was used to predict their diffusivities. This correlation is valid for dilute solutions although it does not apply to electrolytes.

$$\boldsymbol{D_{L,i} = \frac{1.173\times10^{-16}\times T_{int}\times\sqrt{(\emptyset_{water}.MW_{water}\times1000)}}{\mu_L.(V_i\times1000)^{0.6}}}$$

(Equation 2.11)

In (Equation 2.11), $\boldsymbol{\emptyset_{water}}$ is an association factor for the solvent, which for the remaining components of interest besides CO_2 was considered to be pure H_2O and $\boldsymbol{V_i}$ is the molar volume of the component $\boldsymbol{i}$ at its normal boiling temperature (Poling, *et al.*, 2007). As a result of this assumption, the diffusivity of H_2O in the solvent was considered to be equal to unity.

2.2.3. Enhancement factor

The chemical absorption of CO_2 with MEA is a reactive system. In fact, the reaction of CO_2 with MEA taking place near the phase boundary between the vapour and the liquid phases enhance the flux of material of CO_2 into the liquid phase, since the concentration of this component is being kept low due to the reaction and therefore, the driving force for mass transfer to occur between the two phases remains high. To account for the above mentioned, an enhancement factor was considered in the equation of flux of material for CO_2. Hence (Equation 2.3) assumed the following format for CO_2:

$$N_{L,CO_2} = k_{L,CO_2} \times E_{CO_2} \times \left({C_{CO_2}}^{int} - {C_{CO_2}}^{b}\right)$$

(Equation 2.12)

In their work with chemical absorption of CO_2 with MDEA, Carey *et al.* (Carey, *et al.*, 1991) reported the following correlation to predict the enhancement factor:

$$E_{CO_2} = 1 + (E_{int} - 1).\left(1 - \theta - \frac{\theta}{E_{int} + 1.5}\right)$$

(Equation 2.13)

Carey *et al.* also reported that E_{int} represented the enhancement factor at the interface and such was function of the forward reaction rate constant r_{for} of the reaction of CO_2 with the solvent as well as the concentration of the solvent $\mathrm{C_{sol}}$ (Carey, *et al.*, 1991). This said, they reported the following correlation to predict the enhancement factor at the interface:

$$E_{int} = \sqrt{1 + \frac{D_{CO_2}}{\left(k_{L,CO_2}\right)^2} \times r_{for}.C_{sol}}$$

(Equation 2.14)

They also reported that θ was a dimensionless factor which represented the distance the reaction was to reach chemical equilibrium (Carey, *et al.*, 1991).

$$\theta = \frac{{C_{CO_2,eq}}^{int} - {C_{CO_2}}^{b}}{{C_{CO_2}}^{int} - {C_{CO_2}}^{b}}$$

(Equation 2.15)

It is worth mentioning that for the limiting case of high values of E_{int} and $\theta \ll 1$, (Equation 2.13) resumes to (Equation 2.14). In their recent review on the reaction kinetics of CO_2 absorption with alkanolamines Vaidya *et al.* reported that the reaction mechanisms used to describe the behaviour of CO_2 absorption with MEA were rate-based and also that the reaction of CO_2 with primary amines as MEA was very fast (Vaidya, *et al.*, 2007), which match exactly the conditions of the limiting case referred. Therefore E_{CO_2} was determined using only (Equation 2.14) applied to MEA.

2.2.4. *Effective area for mass transfer*

In their work, Onda *et al.* assumed that the effective area available for mass transfer between the two phases should be equal to the surface area of the packing that was actually wetted by the liquid phase (Onda, *et al.*, 1968). They assumed that the wetted area of the packing was only function of the flow conditions of the liquid phase and therefore proposed the following correlation:

$$\frac{a_e}{a_p} = 1 - exp\left(1.45 \times \left(\frac{\sigma_p}{\sigma_L}\right)^{0.75} \times {Re_L}^{0.1} \times {Fr_L}^{-0.05} \times {We_L}^{0.2}\right)$$

(Equation 2.16)

According to Onda *et al.*, σ_p is the critical surface tension of the packing. The values of σ_p for different packing materials are presented in (Perry, *et al.*, 1984). The correlation given by (Equation 2.16) was validated for the following operating conditions:

$$0.3 < \left(\frac{\sigma_p}{\sigma_L}\right) < 2$$

$$0.04 < Re_L < 500$$

$$5.0 \times 10^{-9} < Fr_L < 1.8 \times 10^{-2}$$

$$1.2 \times 10^{-8} < We_L < 0.272$$

Within these range of operating conditions, Onda and his co-workers showed that (Equation 2.16) could be used to determine the wetted area with a deviation of ±20% from the experimental data for several kinds of random packing (Onda, *et al.*, 1968), which within the scope of this work was considered to be a reasonable agreement.

A few years later Bravo *et al.* proposed a new correlation to determine the effective area available for mass transfer in commercial-scale packed columns based on their experiments with random packings (Bravo, *et al.*, 1982). Bravo *et al.* considered that the effective area available for mass transfer should also be a function of the flow conditions of the vapour phase (Wang, *et al.*, 2005). Hence, they proposed the following correlation:

$$\frac{a_e}{a_p} = \frac{0.498}{1.6}\left(\frac{(\sigma_L \times 1000)^{0.5}}{L^{0.4}}\right)\left(\frac{\mu_L.F_L}{S.\rho_L.\sigma_L} \times \frac{6 \times F_G}{S.a_p.\mu_G}\right)^{0.392}$$

(Equation 2.17)

In their work, Bravo *et al.* reported that the correlation given by (Equation 2.17) is an improvement of the one proposed by Onda *et al.* and it can be used to determine the effective area available for mass transfer with an AAD of 22% (Bravo, *et al.*, 1982). No restrictions were mentioned in terms of range of applicability of this correlation.

Both the correlations given by (Equation 2.16) and (Equation 2.17) were used in this work during the model validation step. A discussion concerning this subject is later included in the section 3.3.

2.3. Liquid holdup up to the flooding point

The mass transfer behaviour of a two phase countercurrent flow in a packed column is strongly influenced by the flow conditions of each phase (Billet, *et al.*, 1995). Hence for a wide range of flow conditions the two fluids flow separately, but as the vapour flowrate increases it starts supporting a higher amount of descending liquid and as a consequence the liquid holdup in the column becomes higher too (Billet, *et al.*, 1995). The point when the liquid holdup starts to increase due to the velocity of the vapour phase is called loading point. For even higher vapour flowrates, the flow of the two fluids becomes instable and mass transfer calculations become inaccurate. This is known as the point when the column starts to flood and therefore is called the flooding point (Billet, *et al.*, 1995).

In their work Billet *et al.* studied the fluid dynamics of a two phase countercurrent flow inside packed columns and they proposed correlations to determine the liquid holdup in these different ranges of flow conditions. Hence they proposed a correlation to determine the liquid holdup below the loading point $\boldsymbol{\omega_L}$ as follows:

$$\boldsymbol{\omega_L = \left(\frac{12 \times \mu_L . v_L . {a_p}^2}{g . \rho_L}\right)^{1/3}}$$

(Equation 2.18)

According to Billet *et al.* the exact location of the loading point is difficult to determine (Billet, *et al.*, 1999). Even though they presented a set of correlations to estimate the location of the loading point, that level of detail was considered to be out of the scope of this work. Instead, it was assumed that (Equation 2.18) could be used to determine the holdup of the liquid within the range of conditions up to the flooding point.

To determine the vapour and the liquid velocities at the flooding point Billet *et al.* (Billet, *et al.*, 1999) proposed the following set of equations:

$$v_{G,flood} = \sqrt{2 \times \left(\frac{g}{\Psi_{flood}}\right) \times \frac{\left(\varepsilon_p - \omega_{L,flood}\right)^{3/2}}{\varepsilon_p^{1/2}} \times \sqrt{\frac{\omega_{L,flood}}{a_p}} \times \sqrt{\frac{\rho_L}{\rho_G}}}$$

(Equation 2.19)

$$v_{L,flood} = \frac{\rho_G}{\rho_L} \times \frac{F_L}{F_G} \times v_{G,flood}$$

(Equation 2.20)

According to Billet *et al.* Ψ_{flood} is a resistance factor at flooding conditions and should be determined by (Billet, *et al.*, 1999):

$$\Psi_{flood} = \frac{g}{C_{flood}^{2}} \times \left[\frac{F_L}{F_G} \times \sqrt{\frac{\rho_G}{\rho_L}} \times \left(\frac{\mu_L}{\mu_G}\right)^{0.2}\right]^{(-2.n_{flood})}$$

(Equation 2.21)

They also mentioned that the flooding constant C_{flood} and the exponent n_{flood} in (Equation 2.21) can take different values depending of the operating conditions (Billet, *et al.*, 1999). Hence for:

$$\frac{F_L}{F_G} \times \sqrt{\frac{\rho_G}{\rho_L}} \leq 0.4 :\ n_{flood} = -0.194 ;\ C_{flood} = C_{flood,Billet}$$

$$\frac{F_L}{F_G} \times \sqrt{\frac{\rho_G}{\rho_L}} > 0.4 :\ n_{flood} = -0.708 ;\ C_{flood} = 0.6244 \times C_{flood,Billet} \times \left(\frac{\mu_L}{\mu_G}\right)^{0.1028}$$

(Equation 2.22)

In (Equation 2.22) $C_{flood,Billet}$ represents a flooding constant which can take different values for different kinds of packing. Such values can be found in (Billet, *et al.*, 1999). For the liquid holdup at the flooding point $\omega_{L,flood}$ Billet *et al.* proposed the following correlation:

$$\omega_{L,flood}^{3} \times \left(3.\omega_{L,flood} - \varepsilon_p\right) = \frac{6}{g} \times a_p^{2}.\varepsilon_p \times \frac{\mu_L.F_L.\rho_G}{\rho_L^{2}.F_G} \times v_{G,flood}$$

(Equation 2.23)

The set of (Equation 2.19) to (Equation 2.23) was only used in this work for the feasibility study.

2.4. Heat transfer

As it was mentioned above for the mass transfer in packed columns, fluxes of heat can also be established between two different phases when their temperatures are different. In this case, the difference in the temperatures of each phase provides a driving force for heat transfer to occur across the phase boundary. Hence, the heat flux can be determined using a set of equations very similar to those proposed for mass transfer, respectively (Equation 2.2) and (Equation 2.3). When applied to heat transfer, these equations are as follows:

$$\boldsymbol{Q_G = h_G \times \left(T_G - T^{int}\right)}$$

(Equation 2.24)

$$\boldsymbol{Q_L = h_L \times \left(T^{int} - T_L\right)}$$

(Equation 2.25)

Due to the same reasons mentioned for the mass transfer, *i.e.* no accumulation of heat near the phase boundary, $\boldsymbol{Q_G = Q_L}$ was assumed.

In opposition to the approach followed for the mass transfer no correlations to predict the heat transfer coefficients were used. Also no analogy between the mass transfer and heat transfer was considered to determine the heat transfer coefficients. It was assumed that the heat transfer coefficients in each phase were constant inside the column and that the heat transfer coefficient in the liquid phase, $\boldsymbol{h_L}$ was much higher than the one in the vapour phase, $\boldsymbol{h_G}$. This assumption was made since in general the thermal conductivity of the liquids is higher than the thermal conductivity of gases (Coulson, *et al.*, 1999).

It is worth mentioning that no studies about the direct influence of the heat transfer coefficients in the CO_2 absorption with MEA were found in the literature, which seems to indicate that its accurate estimation is not very significant for this particular system. However the use of an analogy between the mass transfer and the heat transfer is recommended to determine the heat transfer coefficients of the vapour phase and the liquid phase in more detailed studies. This procedure can be found in the work develop by Coulson *et al.* (Coulson, *et al.*, 1999).

2.5. Vapour-Liquid equilibrium

As it was described in section 2.2, fluxes of material can occur across the phase boundary when there is a difference between the concentrations of the components in each phase. To take this into account, phase equilibrium between those components must be considered. In this work however VLE was only considered for CO_2 and H_2O.

Since CO_2 is often very dilute in the flue gas streams, herein considered as the vapour phase, the Henry's law was considered to describe the VLE of CO_2 in this absorption system (Aboudheir, 2002). Hence, the amount of CO_2 at the interface in the vapour side was related to the concentration of CO_2 at the interface in the liquid side as follows:

$$\boldsymbol{y_{CO_2}}^{\boldsymbol{int}} = \frac{\boldsymbol{He_{CO_2}}}{\boldsymbol{P}} \times \boldsymbol{C_{CO_2}}^{\boldsymbol{int}}$$

(Equation 2.26)

An analogy similar to the one used for the determination of the diffusivity of CO_2 in aqueous alkanolamine solutions (Equation 2.7) has been used by several authors, according to Tsai *et al.* (Tsai, *et al.*, 2000), to determine the solubility of CO_2 in aqueous alkanolamine solutions, herein given by the Henry constant $\boldsymbol{He_{CO_2}}$.

$$\boldsymbol{He_{CO_2}} = \boldsymbol{He_{N_2O,sol}} \times \left(\frac{\boldsymbol{He_{CO_2}}}{\boldsymbol{He_{N_2O}}}\right)_{\boldsymbol{water}}$$

(Equation 2.27)

The Henry constants of N_2O and CO_2 in pure water were also studied by Versteeg *et al.* (Versteeg, *et al.*, 1988). The following temperature dependencies were reported:

$$\boldsymbol{He_{CO_2,water}} = \boldsymbol{2.8249 \times 10^6 \times exp\left(\frac{-2284}{T_{int}}\right)}$$

(Equation 2.28)

$$\boldsymbol{He_{N_2O,water}} = \boldsymbol{8.5470 \times 10^6 \times exp\left(\frac{-2284}{T_{int}}\right)}$$

(Equation 2.29)

In their work Tsai *et al.* focused in determining the solubility of N_2O in aqueous alkanolamine solutions and used the equations proposed by Versteeg *et al.* for the solubility of CO_2 and N_2O in pure water. They measured the solubilities of N_2O at 30, 35 and 40 ºC over a wide range of amine concentrations. For the solvent of interest in this work, *i.e.* MEA, the range of concentrations considered was 1000 to 6000 mol/m^3 (Tsai, *et al.*, 2000). Based on their measurements, these authors were able to use a model that correlates the Henry's constant of N_2O in aqueous alkanolamine solutions $\boldsymbol{He_{N_2O,sol}}$ with the Henry's constant of this component in pure solutions of amine and water. Hence, Tsai *et al.* reported the following correlation to determine $\boldsymbol{He_{N_2O,sol}}$:

$$\boldsymbol{He_{N_2O,sol}} = \left(\boldsymbol{He_{N_2O,water}}\right)^{\varphi_{water}} \times \left(\boldsymbol{He_{N_2O,MEA}}\right)^{\varphi_{MEA}} \times \boldsymbol{exp}\left(\boldsymbol{He_{N_2O}}^{excess}\right)$$

(Equation 2.30)

It is worth mentioning that (Equation 2.30) is presented in a different format from the one reported on the work of Tsai *et al.* This was done to prevent numerical problems that could arise using the original equation during the simulations.

According to Tsai *et al.* $\boldsymbol{\varphi_{water}}$ and $\boldsymbol{\varphi_{MEA}}$ represent the volume fraction of each component in the binary system MEA+H_2O. It was also reported that $\boldsymbol{He_{N_2O}}^{excess}$ is a Henry's excess quantity which accounts with the interactions between the two components considered in the binary systems (Tsai, *et al.*, 2000).

$$\boldsymbol{He_{N_2O}}^{excess} = \boldsymbol{\varphi_{water}}.\boldsymbol{\varphi_{MEA}} \times \left(\boldsymbol{a_1} + \boldsymbol{a_2}.\boldsymbol{T_{int}} + \boldsymbol{a_3}.\boldsymbol{T_{int}}^2 + \boldsymbol{a_4}.\boldsymbol{\varphi_{water}}\right)$$

(Equation 2.31)

The interaction parameters $\boldsymbol{a_i, i = 1,..,4}$ for the binary system MEA+H_2O were reported by Tsai *et al.* as follows (Tsai, *et al.*, 2000):

Table 2 – Interaction parameters in the Henry's excess quantity correlation (Equation 2.31).

system	MEA+H_2O
$\boldsymbol{a_1}$	4.793
$\boldsymbol{a_2}$	-7.446×10^{-3}
$\boldsymbol{a_3}$	0
$\boldsymbol{a_4}$	-2.201

The solubility of N_2O in pure MEA was reported by (Aboudheir, 2002) as being given by:

$$He_{N_2O,MEA} = 1.207 \times 10^5 \times exp\left(\frac{-1136.5}{T_{int}}\right)$$

(Equation 2.32)

On the other hand for H_2O it was considered that the system was saturated in this component and Raoult's law could be applied (Aboudheir, 2002). Therefore the amount of H_2O at the interface on the vapour phase side was related with the amount of H_2O on the liquid phase side by the following correlation:

$$y_{H_2O}{}^{int} = \frac{P_{vap,H_2O}}{P} \times C_{H_2O}{}^{int}$$

(Equation 2.33)

2.6. Reaction kinetics

The reaction kinetics of CO_2 with alkanolamines has been one of the most studied subjects concerning the chemical absorption of CO_2. Recently a review on the published studies was presented by Vaidya *et al.* (Vaidya, *et al.*, 2007). According to them, there are two well established mechanisms used to describe the kinetic behaviour of a chemical absorption system of CO_2 with primary and secondary alkanolamines, the Zwitteron mechanism and the Termolecular mechanism, and a third mechanism to describe the kinetic behaviour of systems with tertiary amines (Vaidya, *et al.*, 2007). Since MEA is a primary amine, only the Zwitteron and Termolecular mechanisms were described in this work. To further understanding of the principles behind these two mechanisms the reading of the kinetics review presented by Vaidya *et al.* is strongly recommended.

The Zwitteron mechanism suggests that the reaction of CO_2 with primary and secondary amines (AmH) occurs in a two-step mechanism via formation of an intermediate specie called Zwitteron (Vaidya, *et al.*, 2007). The first step is a reversible reaction of CO_2 with the amine to produce the intermediate.

$$CO_2 + AmH \leftrightharpoons AmH^+.CO_2{}^-$$

(Equation 2.34)

The second step is the deprotonation of the Zwitteron by a base (B) with the formation of carbamate. In an aqueous solution of amines several species can be found which can act as a base (the amine itself, H_2O and OH^-) and according to this mechanism all of them should be accountable in the reaction kinetics of CO_2 with MEA (Vaidya, *et al.*, 2007).

$$\boldsymbol{AmH^+.CO_2{}^- + B \leftrightharpoons Am.CO_2{}^- + BH^+}$$

(Equation 2.35)

It is also reported that according to the Zwitteron mechanism the overall reaction order of the reaction of CO_2 with these amines can be first order in respect to the amine in situations when the Zwitteron deprotonation is a very fast reaction. On the other hand, if the deprotonation of the Zwitteron is made mainly by the amine itself and the rate of this step is comparable to the rate of the reversible reaction of the first step, the overall reaction order in respect to the amine is 2 (Vaidya, *et al.*, 2007).

The Termolecular mechanism suggests that the reaction of CO_2 with the amine to produce carbamate occurs only in one step, without the formation of the Zwitteron:

$$\boldsymbol{CO_2 + AmH + B \leftrightharpoons Am.CO_2{}^- + BH^+}$$

(Equation 2.36)

According to the reported by Vaidya *et al.* in their review the reaction kinetics is second order in respect to the amine and can be higher in the case base $\boldsymbol{B}$ is the amine itself.

In this work the Termolecular mechanism was used. As it was already mentioned the amine considered was MEA and H_2O was considered as a base in (Equation 2.36). Therefore the reaction of CO_2 with MEA used in this work was:

$$\boldsymbol{CO_2 + MEA + H_2O \leftrightharpoons MEA.CO_2{}^- + H_3O^+}$$

(Equation 2.37)

This approach was also followed by Aboudheir in his work of modelling chemical absorption of CO_2 with MEA (Aboudheir, 2002). For the reaction rate of (Equation 2.37) Aboudheir proposed the following equation (Aboudheir, 2002):

$$\boldsymbol{\Gamma_4 = r_{for}.\left(C_{CO_2}.C_{MEA} - \frac{1}{K_4} \times C_{MEA.CO_2^-}.C_{H_3O^+}\right)}$$

(Equation 2.38)

with $\boldsymbol{r_{for}}$ given by:

$$r_{for} = \left(r_{MEA}.C_{MEA} + r_{H_2O}.C_{H_2O}\right)$$

(Equation 2.39)

In his work Aboudheir also studied the temperature dependencies of r_{MEA} and r_{H_2O} based on experimental measurements using a laminar jet absorber. The experiments were carried out within the range of MEA concentrations from 3000 mol/m^3 to 9000 mol/m^3 and temperatures between 20 ºC and 60 ºC. Further description about the experimental apparatus can be found in the work published by Aboudheir (Aboudheir, 2002). After fitting the relevant parameters the following correlations were proposed with a reported 16% AAD from the experimental data:

$$r_{MEA} = 4.61 \times 10^3 \times exp\left(\frac{-4412}{T_{int}}\right)$$

(Equation 2.40)

$$r_{H_2O} = 4.55 \times exp\left(\frac{-3287}{T_{int}}\right)$$

(Equation 2.41)

The temperature dependency of (Equation 2.37) equilibrium constant K_4 was proposed by Barth *et al.* (Barth, *et al.*, 1986) as follows:

$$K_4 = 6.00 \times 10^{-9} \times exp\left(\frac{2856}{T_{int}}\right)$$

(Equation 2.42)

The set of (Equation 2.38) to (Equation 2.42) was used in this work to describe the kinetic behaviour of the chemical absorption system of CO_2 with MEA. Several other reactions were proposed as possibly occurring in this system (Aboudheir, *et al.*, 2003), however only one of them was considered. This approach was followed since such level of detail was out of the scope of this work. Hence the dissociation of protonated MEA was also considered (Equation 2.43).

$$HMEA^+ + H_2O \leftrightharpoons MEA + H_3O^+$$

(Equation 2.43)

This reaction was considered to be at chemical equilibrium. According to Aboudheir the equilibrium constant $\boldsymbol{K_5}$ of (Equation 2.43) can be considered independent of the concentration of H_2O (Aboudheir, 2002). He reported the following correlation to determine $\boldsymbol{K_5}$:

$$\boldsymbol{K_5 = \frac{C_{MEA} \cdot C_{H_3O^+}}{C_{HMEA^+}}}$$

(Equation 2.44)

In his work Aboudheir also reported the following temperature dependency for $\boldsymbol{K_5}$ (Aboudheir, 2002):

$$\boldsymbol{K_5 = 1.00 \times 10^3 \times exp\left(\frac{-5811}{T_{int}} - 3.3636\right)}$$

(Equation 2.45)

3. Model development

The chemical absorption model for CO_2 capture with MEA presented in this work was developed in gPROMS. This software offers an Advanced Process Modelling environment where it is possible to create their by either writing down the equations or using the gPROMS model libraries within a flowsheet framework. In conjunction with the model development the gPROMS software also allows the users to perform steady-state and dynamic simulations, parameter estimation, and process optimization among other activities (www.psenterprise.com). In gPROMS the numerical resolution is not sequential since this is an equation-orientated tool, which means the set of equations that constitute the model are all solved at the same time. This increases the model robustness and its ability to converge for the desired solution. Its architecture also provides access to all the equations that are part of the model allowing a deep comprehension and an easy maintenance (www.psenterprise.com). These are the main reasons why gPROMS was used in this work.

3.1. Model architecture

The chemical absorption model developed for CO_2 capture with MEA was organized according to a hierarchical architecture. Hence in the bottom of the hierarchy five individual sub-models were created namely: *Gas bulk*, *Interface*, *Liquid bulk*, *Mass Transfer* and *Reaction kinetics*. These sub-models include all the equations used to describe the different chemical and physical phenomena considered in this work. As their names suggest two of these sub-models are concerned with the flow conditions of the vapour and liquid phases and the remaining three are focused on the description of all the transfer phenomena, the reaction kinetics and the vapour-liquid equilibrium at the phase boundary. A full description of the contents of each sub-model is on section 3.2.

The interactions between the sub-models were written down in a high hierarchical composite model called *Absorption column*. This composite model did not contain any equations regarding the behaviour of the chemical absorption system but rather made use of all the low hierarchical sub-models and established the links between them.

It is also worth mentioning that a thermo-physical properties package provided along with the gPROMS software license was used to determine the physical properties required by each sub-model. Hence these were determined using *Multiflash* thermo-physical properties package based on the operating conditions of pressure, temperature and composition.

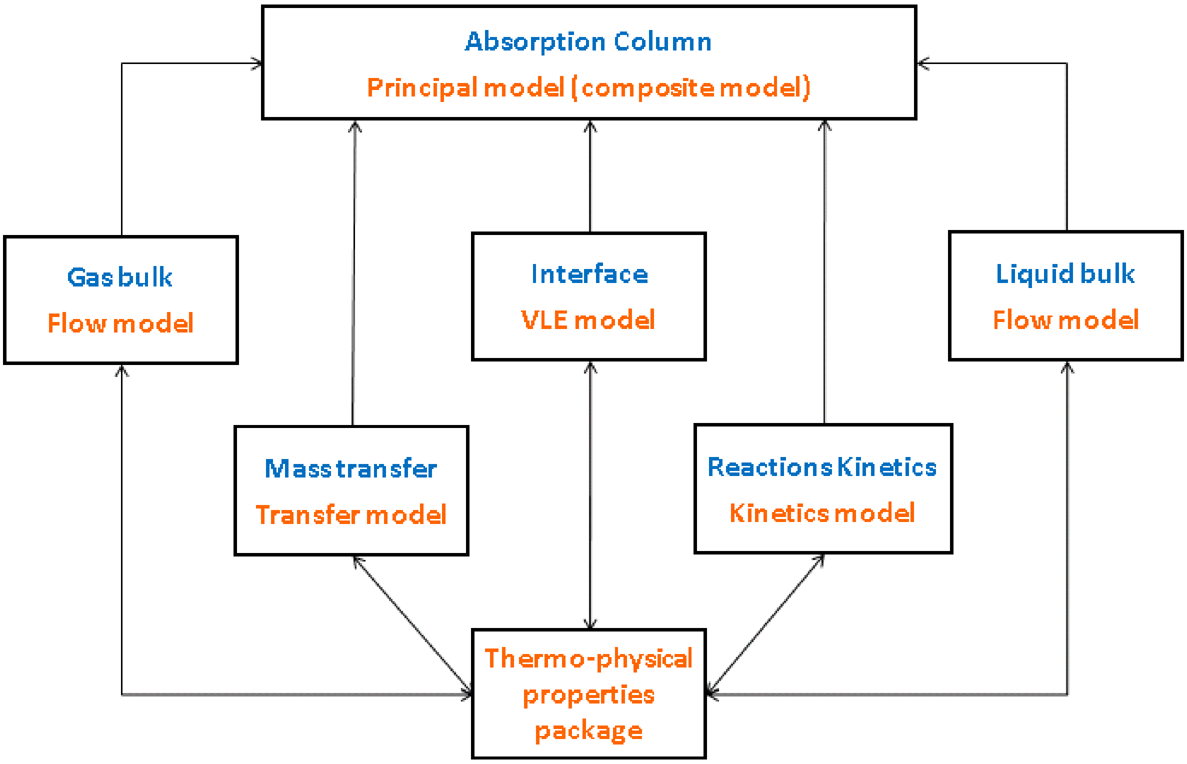

Figure 6 – Architecture of the chemical absorption model for CO_2 capture with MEA developed in this work.

The architecture illustrated in Figure 6 was chosen because it presents some advantages. One of the main advantages is that it allows the comprehension of the chemical absorption system in terms of what are the most significant phenomena taking place and how they interact with each other, since those links can easily be found in the composite model. It also allows great flexibility since it is easy to locate a particular equation based on its physical meaning and replace it if a lower/higher level of detail is desired. The user is able to experiment different kinds of situations either by disabling a complete sub-model or just the equations regarding a particular phenomenon, for instance the behaviour of the system might be studied if no reactions were actually taking place just by disabling the links of this sub-model with the others. This flexibility also allows easy maintenance since several different tests can be performed and critical equations responsible for numerical instability can be easily located with the help of gPROMS simulation reports.

Other advantage of this architecture is that the composite model comprises all the information related with the chemical absorption system and it can be used in a drag-and-drop flowsheeting. For the *Absorption Column* composite model an icon was created as well as dialog boxes where the user can fill all the input information required for the sub-models to perform simulations. This procedure is described in more detail further in this work on the section 3.2 of this chapter.

3.2. Model formulation

The scope of this work was to develop a chemical absorption model for CO_2 capture with MEA that could be used in feasibility studies for a specific set of operating conditions and limiting space available for the installation of the equipment. Since these were preliminary studies the model did not required a high level of detail. As a consequence several assumptions were made, some of which were already presented in chapter 2 since they concerned some specific correlations or phenomena.

3.2.1. Main assumptions

The main assumptions made during the development of the chemical absorption model are indicated in Table 3. These assumptions were made regarding the scope of this work and the fact that a high level of detail was not required.

Table 3 – Assumptions made during the development of the chemical absorption model.

Assumptions	Consequences
Axially distributed material and energy balances for both vapour and liquid phases	The model variables were allowed to vary with time and along the axial direction
Dynamics of the liquid phase was considered	
Pressure drop determined by (Equation 2.1) along the axial direction	
Ideal behaviour for the vapour phase	Phase properties were determined based on pure component physical properties
Perfect mixing for the liquid phase	
Mass and heat transfers based on transfer coefficients	Low level of detail on the *Mass transfer* sub-model
Mass transfer enhancement factor	
Phase equilibrium for CO_2 and H_2O	No solvent loss was considered
Reversible rate-based reaction between CO_2 and MEA	Low level of detail on the *Reaction kinetics* sub-model
Chemical equilibrium between $HMEA^+$/MEA	
Adiabatic operation	No heat loss was considered

Some of the assumptions were already discussed as a consequence of the level of detail required within the scope of this work, for instance those related with transfer, reaction kinetics, and thermodynamic behaviour. It was assumed that the system dynamics was given by the dynamics of the liquid phase since usually the vapour phase has higher velocities inside the absorption columns due to the flowrates considered and therefore has lower residence times than the liquid phase. Hence the dynamics of the vapour phase was disregarded. The assumption of ideal behaviour for the vapour phase is explained because the absorption column usually operates at low pressure (Kvamsdal, *et al.*, 2008). In his work Aboudheir reported that heat loss could be disregarded while describing his experimental absorption column and that its operation was essentially adiabatic (Aboudheir, 2002). The assumption of modelling phase equilibrium only for CO_2 and H_2O was also considered since the models available in the literature to predict the amine partial pressure are often inaccurate, as reported by Hessen *et al.* in their work regarding the thermodynamics of aqueous alkanolamines solutions (Hessen, *et al.*, 2009). The vapour pressure at 293.15 K of pure MEA is reported in its MSDS as being equal to 100 Pa while for pure water the reported value is 2300 Pa (www.sciencelab.com). The vapour pressure of the pure solvent is therefore very small compared with the vapour pressure of pure water. The assumption of not considering VLE for MEA was also followed by Aboudheir (Aboudheir, 2002) and Austgen *et al.* (Austgen, *et al.*, 1989) in their VLE models.

Following the assumptions made during the model development, a description of the modelling procedures and the algebraic equations used in each sub-model is presented.

3.2.2. Gas bulk sub-model

The *Gas bulk* sub-model was developed to describe the flow conditions of the vapour phase inside the absorption column. Material balances were implemented for each component (Equation 3.1). In the material balances the diffusion along the radial direction was disregarded and no vapour holdup was considered. This said, the material balances in the vapour phase consisted in two terms, one concerning the flow of material along the axial direction and another to account with the material flux of the components across the phase boundary. No accumulation term was considered since the vapour velocity inside the column is much higher than the liquid and therefore the dynamics of the vapour phase was disregarded.

$$\mathbf{0} = -\frac{\mathbf{1}}{\boldsymbol{S}} \times \frac{\partial\left(\boldsymbol{F_{G,i}}\right)}{\partial \boldsymbol{z}} \times \frac{\mathbf{1}}{\boldsymbol{L}} + \boldsymbol{N_{G,i}}.\boldsymbol{MW_i}.\boldsymbol{a_e} \quad \mathbf{,z} \in [\mathbf{0},\mathbf{1}[$$

(Equation 3.1)

It is worth mentioning that in (Equation 3.1) the term $\frac{1}{L}$ was included because the numerical discretisation of the partial derivatives was normalized to the domain 0 (top of the column) to 1 (bottom of the column) instead of 0 to L. The numerical method used to discretise this equation was FFDM with an order of approximation of 1. This method was chosen so that the discretisation was made in the opposite direction of material flow. During this work this option proved to produce better numerical results when discretisation methods were applied. The number of grid points used in all the discretisations was included as a model parameter to allow some flexibility. Further information on the numerical discretisation methods used in this work can be found on the tab Help → Documentation on gPROMS working environment.

An energy balance was also included in the *Gas bulk* sub-model as follows:

$$\mathbf{0} = -\frac{\mathbf{1}}{\boldsymbol{S}} \times \frac{\partial(\boldsymbol{H_G})}{\partial \boldsymbol{z}} \times \frac{\mathbf{1}}{\boldsymbol{L}} + \boldsymbol{Q_G}.\boldsymbol{a_e} \quad \mathbf{,z} \in [\mathbf{0},\mathbf{1}[$$

(Equation 3.2)

The above mentioned assumptions for the material balances are also considered for the energy balance given by (Equation 3.2). As it was referred in the section 3.2.1 of this chapter no heat loss was considered.

The pressure drop correlation given by (Equation 2.1) presented in section 2.1 was also included in the *Gas bulk* sub-model. The discretisation method used in the latter was BFDM with an order of approximation 1 and because BFDM was used the domain of the pressure drop equation was $\mathbf{z} \in]\mathbf{0}, \mathbf{1}]$. This option proved to produce better numerical results than using FFDM. A procedure followed in this thesis was to indicate only the definition domains for the equations that were not defined within the entire length of the absorption column. When no reference was made it means the equation was defined for $\mathbf{z} \in [\mathbf{0}, \mathbf{1}]$.

To complete the *Gas bulk* sub-model the following algebraic equations were considered:

$$\boldsymbol{S = \frac{\pi}{4}.d^2}$$

(Equation 3.3)

$$\boldsymbol{F_G = v_G.S.\rho_G}$$

(Equation 3.4)

$$\boldsymbol{F_G = \sum\left(F_{G,i}\right) \qquad , z \in [0,1[}$$

(Equation 3.5)

$$\boldsymbol{F_{G,i} = m_{G,i}.F_G}$$

(Equation 3.6)

$$\boldsymbol{F_{G,i} = F_{mol_{G,i}}.MW_i}$$

(Equation 3.7)

$$\boldsymbol{F_{mol_{G,i}} = y_i.F_{mol_G}}$$

(Equation 3.8)

$$\boldsymbol{F_{mol_G} = \sum\left(F_{mol_{G,i}}\right)}$$

(Equation 3.9)

$$\boldsymbol{H_G = F_G.\overline{h}_G}$$

(Equation 3.10)

The physical properties $\bar{h}_G$, ρ_G and μ_G were determined using the physical properties package *Multiflash*. The molecular weights of the components in the vapour phase were also determined by the physical properties package.

In this model the CO_2 capture efficiency was also determined based on the inlet and the outlet mass flowrates of CO_2 in the vapour phase respectively $F_{G,CO_2|1}$ and $F_{G,CO_2|0}$.

$$\eta_{CO_2} = \frac{F_{G,CO_2|1} - F_{G,CO_2|0}}{F_{G,CO_2|1}} \times 100$$

(Equation 3.11)

A selector was also included in this sub-model to allow some flexibility in terms of considering the column height as an input or as a result. Therefore if the column height is a known parameter, for instance when simulations are performed with experimental data, this selector is defined for the column height to be provided as an input. On the other hand if a determined CO_2 capture efficiency is desired at the top of the column the selector is defined for the column height to be determined as a result considering the desired efficiency.

3.2.3. Liquid bulk sub-model

The *Liquid bulk* sub-model was created to describe the behaviour of the liquid phase inside the absorption column. Material balances in a molar base were implemented but in this case an accumulation term and a term related with the reaction kinetics were included. As presented in chapter 2, two reactions were considered, (Equation 2.37) and (Equation 2.43), one of them as a chemical equilibrium. Since the reaction given by (Equation 2.43) was considered to be at chemical equilibrium the resolution of the DAE system became a high index DAE problem. Further information regarding the high index DAE systems can be found in the work developed by Pantelides (Pantelides, 2000).

An index reduction had to be performed. Hence instead of implementing a material balance equation for each component, the number of material balances in the liquid phase was determined by the number of linearly independent equations related to material conservation or, in other words, the result of the difference between the number of components in this phase and the number of numerical constrains in the liquid phase. In addition to the chemical equilibrium considered for (Equation 2.43), it was considered that the liquid phase was electrically neutral. Therefore the following charge balance was implemented:

$$C_{MEA.CO_2^-} = C_{HMEA^+} + C_{H_3O^+}$$

(Equation 3.12)

This means there were two numerical constrains in the liquid phase, the constrain given by the chemical equilibrium (Equation 2.44), and the constrain given by the charge balance (Equation 3.12). The number of material balances implemented in the *Liquid Bulk* sub-model was then equal to $(\boldsymbol{n}-\mathbf{2})$, where $\boldsymbol{n}$ represents the number of components considered. The material balances were then implemented as follows:

$$\frac{\partial\left(A_{j,i}.\omega_{mol,i}\right)}{\partial t}=-\frac{1}{S}\times\frac{\partial\left(F_{mol_L}\times\left(A_{j,i}.x_i\right)\right)}{\partial z}\times\frac{1}{L}+\left(A_{j,i}.N_{L,i}\right).a_e+\left(A_{j,i}.\Gamma_i\right) \quad , \ z\in\left]0,1\right]$$

(Equation 3.13)

In (Equation 3.13), $\boldsymbol{A_{j,i}}$ represents the matrix used to reduce the number of material balances originally from the number of components $\boldsymbol{n}$ to $\boldsymbol{j}=(\boldsymbol{n}-\mathbf{2})$. The dimensions of this matrix are $(\boldsymbol{n}-\mathbf{2})\times\boldsymbol{n}$. A description of the procedure followed to determine the matrix $\boldsymbol{A_{j,i}}$ is presented in Appendix E. Also in this equation $\boldsymbol{\Gamma_i}$ represents the overall reaction rate for each component. They were determined by summing the product of the reaction rates for the respective stoichiometric coefficient of the component for all the non-equilibrium reactions considered. In this case only (Equation 2.37) was considered as a rate-based reaction. In addition to the material balances the two constrain given by the equilibrium constant $\boldsymbol{K_5}$ equation and the charge balance (Equation 3.12) were used to complete the set of equations that describe the material conservation in the liquid phase.

This procedure was followed to increase the generality of the model developed in this work. Hence this procedure allowed the model to automatically determine the dimensions of the matrix $\boldsymbol{A_{j,i}}$, and therefore the number of material balances equations without having to manually change the implementation of (Equation 3.13), even when the number of components, the number of non-equilibrium reactions or the number of equilibrium reactions considered were changed.

An energy balance was also included in the *Liquid bulk* sub-model. Compared to the vapour phase energy balance equation, the energy balance in the *Liquid bulk* sub-model includes a term regarding the heat released in the liquid phase by the absorption of CO_2 and also an accumulation term. The following energy balance was implemented:

$$\frac{\partial(U_L)}{\partial t}=-\frac{1}{S}\times\frac{\partial(H_L)}{\partial z}\times\frac{1}{L}+Q_L.a_e+H_{abs}.N_{G,CO_2}.a_e \quad , z\in\left]0,1\right]$$

(Equation 3.14)

It was assumed that the heat of absorption of CO_2 with an aqueous MEA solution was 85000 J/mol (Kohl, *et al.*, 1997). According to Kohl *et al.* this assumption is valid within the range of CO_2 loadings from 0 to 0.5 (Kohl, *et al.*, 1997). The discretisation method used for (Equation 3.13) and (Equation 3.14) was BFDM with an order of approximation of 1 since the liquid flows in the opposite direction of the vapour. As it can be seen in the two above mentioned equations, the material and energy balances implemented in the *Liquid bulk* sub-model presented dynamic behaviour. Therefore to perform simulations some initial conditions must be provided. In this work steady-state initial conditions were considered.

Algebraic equations were used to complete this sub-model. Some of them were similar to those presented in the section 3.2.2 of this chapter but in this case applied to the liquid phase so they will not be presented again, namely (Equation 3.3), (Equation 3.4), (Equation 3.6) and (Equation 3.10). Hence along with the above mentioned, the auxiliary equations used in the *Liquid bulk* sub-model were:

$$\boldsymbol{F_L = \sum (F_{L,i}) \qquad , z \in]0,1]}$$

(Equation 3.15)

$$\boldsymbol{x_i = \frac{\frac{m_{L,i}}{MW_i}}{\sum\left(\frac{m_{L,i}}{MW_i}\right)}}$$

(Equation 3.16)

$$\boldsymbol{1 = \sum (x_i)}$$

(Equation 3.17)

$$\boldsymbol{F_{mol_L} = \sum \left(\frac{F_{L,i}}{MW_i}\right)}$$

(Equation 3.18)

$$\boldsymbol{\rho_{mol_L} = \left[\sum \left(\frac{m_{L,i}}{MW_i}\right)\right] \times \rho_L}$$

(Equation 3.19)

$$\boldsymbol{C_i = x_i \times \rho_{mol_L}}$$

(Equation 3.20)

$$\boldsymbol{U_L = \overline{u}_L \times \rho_L}$$

(Equation 3.21)

$$\boldsymbol{\overline{u}_L = \overline{h}_L - \frac{P}{\rho_L}}$$

(Equation 3.22)

Since liquid holdup $\boldsymbol{\omega_L}$ was considered, (Equation 2.18) presented in the section 2.3 of the chapter 2 was implemented in the *Liquid bulk* sub-model. Hence the two following algebraic equations were used:

$$\boldsymbol{\omega_{mol} = \omega_L \times \rho_{mol_L}}$$

(Equation 3.23)

$$\boldsymbol{\omega_{mol,i} = x_i . \omega_{mol}}$$

(Equation 3.24)

The physical properties $\boldsymbol{\bar{h}_L}$, $\boldsymbol{\rho_L}$ and $\boldsymbol{\mu_L}$ were determined using *Multiflash*. The pressure in the liquid phase was considered to be the same as the pressure in the vapour phase. Due to the fact that the ionic species considered in the liquid phase were not included in the database of compounds used by *Multiflash* these species had to be contracted into the amounts of the pure components CO_2, H_2O and MEA. This contraction was made as follows:

$$\boldsymbol{C_{CO_2,tot} = C_{CO_2} + C_{MEA.CO_2^-}}$$

(Equation 3.25)

$$\boldsymbol{C_{MEA,tot} = C_{MEA} + C_{MEA.CO_2^-} + C_{HMEA^+}}$$

(Equation 3.26)

$$\boldsymbol{C_{H_2O,tot} = C_{H_2O} + C_{H_3O^+}}$$

(Equation 3.27)

$$\boldsymbol{\frac{C_{CO_2,tot}}{C_{MEA,tot}} = \frac{\bar{x}_{CO_2}}{\bar{x}_{MEA}}}$$

(Equation 3.28)

$$\boldsymbol{1 = \bar{x}_{CO_2} + \bar{x}_{MEA} + \bar{x}_{H_2O}}$$

(Equation 3.29)

$$\boldsymbol{\bar{m}_i = \frac{\bar{x}_i \times MW_i}{\sum(\bar{x}_i \times MW_i)} \qquad , i = CO_2, MEA, H_2O;}$$

(Equation 3.30)

$$C_{MEA,tot} = \bar{\rho}_L \times \frac{\bar{m}_{MEA}}{MW_{MEA}}$$

(Equation 3.31)

For this contraction to be initialized, an initial guess had to be made for the mass density $\bar{\rho}_L$ of the liquid phase. Hence $\bar{\rho}_L$ was considered to be equal to 1000 Kg/m^3. This procedure allowed the determination by *Multiflash* of the liquid phase physical properties based on the total quantities of CO_2, MEA and H_2O. However the molecular weights were still determined by the physical properties package for all the components considered in the liquid phase since these were added manually.

In the *Liquid bulk* sub-model the CO_2 loading was also included. This quantity was implemented as the ratio between the total amount of CO_2 and the total amount of MEA in the liquid phase:

$$CO2_{loading} = \frac{C_{CO_2,tot}}{C_{MEA,tot}}$$

(Equation 3.32)

Other quantity sometimes indicated in the studies referred in this work is the MEA weight concentration $C_{MEA}(w/w)$. As the CO_2 loading this quantity was also included in the *Liquid bulk* sub-model.

$$C_{MEA}(w/w) = \frac{C_{MEA,tot} \times MW_{MEA}}{C_{H_2O,tot} \times MW_{H_2O}} \times 100$$

(Equation 3.33)

Both the CO_2 loading and the MEA weight concentration are often used by some authors referred in this work to characterize the conditions within the liquid phase. These quantities were particularly important at the model validation stage to make sure that the simulated conditions were as similar as possible to the ones for which the experimental data were obtained.

3.2.4. Interface sub-model

The *Interface sub-model* includes the VLE described in the section 2.5 of chapter 2. In the Henry's excess quantity calculation by (Equation 2.31) the volume fractions of MEA and H_2O in the binary system MEA+H_2O were used, respectively φ_{MEA} and φ_{H_2O}. Since perfect mixing was assumed these quantities were determined based on the properties of the pure components as follows:

$$\varphi_{MEA} = \frac{x_{MEA,bin} \cdot V_{m_{MEA}}}{\left(x_{MEA,bin} \cdot V_{m_{MEA}} + x_{H_2O,bin} \cdot V_{m_{H_2O}}\right)}$$

(Equation 3.34)

$$1 = \varphi_{MEA} + \varphi_{H_2O}$$

(Equation 3.35)

$$x_{MEA,bin} = \frac{C_{MEA}}{C_{MEA} + C_{H_2O}}$$

(Equation 3.36)

$$1 = x_{MEA,bin} + x_{H_2O,bin}$$

(Equation 3.37)

Multiflash was used to determine $V_{m_{MEA}}$, $V_{m_{H_2O}}$ and P_{vap,H_2O} the latter was used in the VLE equations.

This sub-model also included (Equation 2.2) and (Equation 2.3) and the equations related with the enhancement factor for the CO_2 flux across the phase boundary, (Equation 2.12) to (Equation 2.15) respectively presented in the section 2.2.3. The equations described in section 2.4 were also implemented in the *Interface* sub-model. To increase the flexibility of the model two selectors were created to allow the user the possibility to input the mass transfer and heat transfer coefficients desired or let these quantities being determined by the correlations presented in this work. Although no correlation was presented to predict the heat transfer coefficients its selector accounts for the possibility of including one in future work.

3.2.5. Mass transfer and Reaction kinetics sub-models

The mass transfer and the reaction kinetics phenomena are often referred as occurring in the regions near the phase boundary. One approach commonly used is to consider these phenomena to occur within thin films near the boundary. Some authors as Aboudheir (Aboudheir, 2002) or Tontiwachwuthikul *et al.* (Tontiwachwuthikul, *et al.*, 1992) actually modeled those regions but as mentioned before that approach was not followed in this work. Therefore the phenomena were considered as occurring at the phase boundary conditions of temperature and pressure.

The *Mass transfer* sub-model included all the equations presented in the section 2.2 excluding those previously mentioned as being part of the *Interface* sub-model, and (Equation 2.18) for the liquid holdup calculation, already referred as being part of the *Liquid bulk* sub-model. The reason for the inclusion of the correlations presented in the section 2.3 in here is that most of the variables used in those equations were already defined in the *Mass transfer* sub-model. The only physical property determined by *Multiflash* was the surface tension $\boldsymbol{\sigma_L}$.

In this sub-model was also included a selector. This selector allowed the user to decide whether if the column diameter was one of the required inputs of the model or if the diameter was determined as a result of the flooding calculations. When the latter option was chosen an array of diameters was obtained. For each of these diameters the velocity of the vapour phase corresponded to 80% of the flooding velocity (Billet, *et al.*, 1999). The maximum value of that array was then chosen as the column diameter which meant the velocity of the vapour phase never exceeded the condition mentioned.

For the *Reaction kinetics* sub-model the set of equation from (Equation 2.38) to (Equation 2.42) and also (Equation 2.45) were implemented. (Equation 2.44) was implemented in the *Liquid bulk* sub-model as mentioned.

3.2.6. Absorption column model (composite model)

In section 3.1 it was referred that the *Absorption column* model established the links between the 5 sub-models considered. In fact and contrarily to the other models no variables or parameters were implemented in this model besides the number of grid points used by the discretisation methods. The reason underlying the option to implement this parameter here was because the same number of grid points was desired for all the discretisations. Since this was a high hierarchical model it was possible to make use of the parameter propagation property of gPROMS and so this parameter only had to be set a value once. In all the simulations performed 50 points were used. The number of grid points used is by far higher than the number of experimental measurements found in the literature along the axial direction of the absorption column. The parameter propagation property could be extended for other parameters included in the sub-models but that procedure was not followed for any other.

Since this model made use of the low hierarchical sub-models the desired connection equations could be implemented without having to define any variable. These connection equations were important to pass information from the sub-model where these quantities were being determined to other sub-model where they were being used in a correlation.

To make it easy to use the *Absorption column* model in flowsheeting an icon was created. This allowed the model to be easily integrated in a flowsheet using drag-and-drop. As it was mentioned some equations in the *Gas bulk* and the *Liquid bulk* sub-models were not defined within the entire domain of the absorption column. The reason behind this was to prevent the *Absorption column* model to be overspecified at the top and at the bottom of the column since connection equations were implemented at these boundaries through the specification of ports. Each port allowed the model to be connected with other models from the gPROMS libraries like sinks and sources and information to be passed between the two.

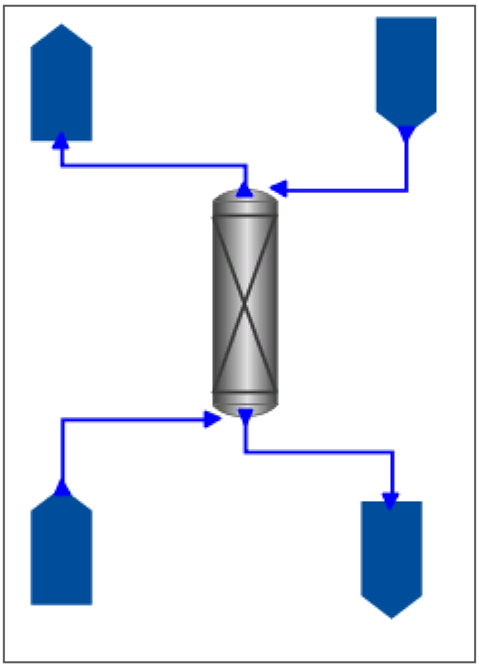

Figure 7 – Absorption column model developed in this work integrated in a simple flowsheet connected with sinks and sources.

The *Absorption column* model required some inputs to be provided. In a simple flowsheet like the one presented in Figure 7 the following inputs required by the model should be provided within the source:

- Inlet mass flowrate of the vapour and liquid phases, $\boldsymbol{F_{G|1}}$ and $\boldsymbol{F_{L|0}}$;
- Inlet mass composition of the vapour and liquid phases, $\boldsymbol{m_{G,i|1}}$ and $\boldsymbol{m_{L,i|0}}$;
- Inlet temperature of the vapour and liquid phases, $\boldsymbol{T_{G|1}}$ and $\boldsymbol{T_{L|1}}$;
- Inlet pressure of the vapour and liquid phases, $\boldsymbol{P_{G|1}}$ and $\boldsymbol{P_{L|0}}$;

The model developed also required the specification of the path to the file generated by *Multiflash* where the thermodynamic models and the components were defined. The thermodynamic models used in this work were ideal behaviour for the vapour phase and ideal mixing for the liquid phase. The components considered were: CO_2, N_2, O_2, H_2O, MEA, $MEA.CO_2^-$, H_3O^+ and $HMEA^+$.

To provide the remaining inputs required by the *Absorption column* model dialog boxes were created so the user could easily fill that information. These dialog boxes are presented in Figure 8 to Figure 10.

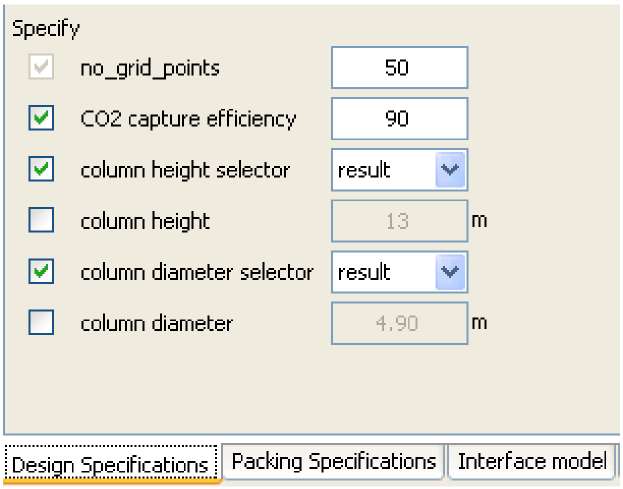

Specify

☑ no_grid_points: 50

☑ CO2 capture efficiency: 90

☑ column height selector: result

☐ column height: 13 m

☑ column diameter selector: result

☐ column diameter: 4.90 m

Figure 8 – Example of the design specifications required by the Absorption column model developed in this work (for column height and diameter selectors defined as results).

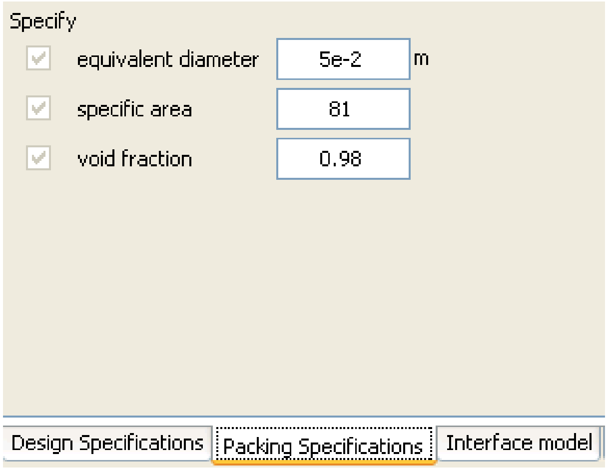

Specify

☑ equivalent diameter: 5e-2 m

☑ specific area: 81

☑ void fraction: 0.98

Figure 9 – Example of the packing specifications required by the Absorption column model developed in this work.

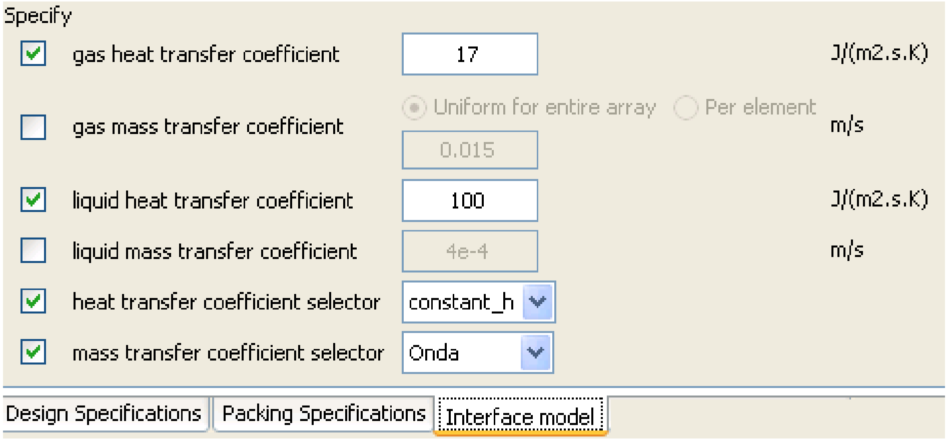

Specify

☑ gas heat transfer coefficient: 17 J/(m2.s.K)

☐ gas mass transfer coefficient: ● Uniform for entire array ○ Per element; 0.015 m/s

☑ liquid heat transfer coefficient: 100 J/(m2.s.K)

☐ liquid mass transfer coefficient: 4e-4 m/s

☑ heat transfer coefficient selector: constant_h

☑ mass transfer coefficient selector: Onda

Figure 10 – Example of the mass and heat transfer options available in the Absorption column model developed in this work (for mass transfer coefficients determined by Onda's correlation and constant heat transfer coefficients).

During the course of every simulation a structural analysis report is initially provided by gPROMS. This report is very useful to understand if the problem is structurally well posed, particularly for very large models. It is also in this report that information regarding the index of the DAE problem is provided. An example of this analysis for the *Absorption column* developed in this work can be seen in Figure 11.

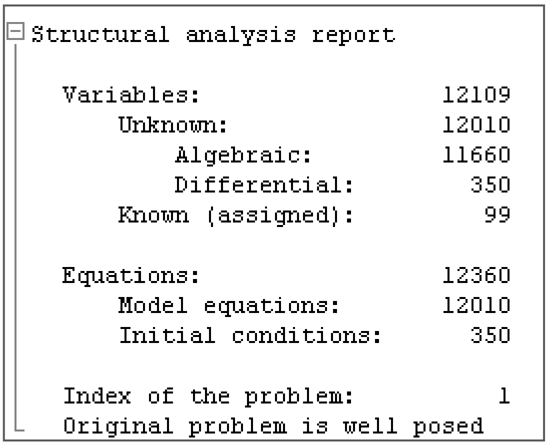

```
Structural analysis report

   Variables:                    12109
       Unknown:                  12010
           Algebraic:            11660
           Differential:           350
       Known (assigned):            99

   Equations:                    12360
       Model equations:          12010
       Initial conditions:         350

   Index of the problem:             1
   Original problem is well posed
```

Figure 11 – Example of the structural analysis report for the Absorption column model developed in this work provided by gPROMS.

In the example presented in Figure 11 it can be seen that this model included a total of 12010 equations and the same number of unknown variables, 11660 of each were algebraic and 350 were differential variables. Hence a total of 350 initial conditions were provided, one for each differential variable. The number of degrees of freedom was 99, as the result of the difference between the total number of variables and the number of unknown variables. Therefore for the problem to be structurally well posed 99 inputs were also provided. Is it worth mentioning that gPROMS considers the identity elimination which means the actual number of variables implemented in the model can be significantly higher than those presented in this report.

After each simulation, gPROMS generates a file where the values of all the variables defined in the model are saved. Using its feature gRMS, plots can be created with the profiles of these variables along the axial direction of the column or its variation with time, in the case of dynamic simulations.

3.3. Model validation

Once developed, the *Absorption column* model was validated against experimental data published by Tontiwachwuthikul *et al.* (Tontiwachwuthikul, *et al.*, 1992) and Aboudheir (Aboudheir, 2002) for the chemical absorption of CO_2 with MEA. According to both authors these experimental data were obtained at steady-state conditions. From all the published data available, two runs for each author were chosen and used for the validation of the *Absorption column* model developed in this work. For each set of data, the model predictive behaviour of the CO_2 molar fraction in the vapour phase and the liquid phase temperature is presented and analyzed considering the two correlations for the effective area reported in this work, respectively (Equation 2.16) and (Equation 2.17).

3.3.1. Inputs used in each simulation

From the experimental data published by Tontiwachwuthikul *et al.*, runs T14 and T18 were chosen (Tontiwachwuthikul, *et al.*, 1992). Run T18 was chosen because it was the only one for which the reported CO_2 capture efficiency was not 100%. As for run T14 it was chosen because CO_2 was more diluted in the vapour phase than in run T18 and the capture efficiency was 100%. For the model validation the experimental flowrates and vapour composition reported by Tontiwachwuthikul *et al.* the conditions presented in Table 4 were used. The original experimental data reported by Tontiwachwuthikul *et al.* are included in Appendix A.

Table 4 – Inlet conditions from the experimental data published by (Tontiwachwuthikul, *et al.*, 1992) for the runs T14 and T18 used as input for the *Absorption column* model validation.

	T14	**T18**
Inlet vapour flowrate (kg/s)	4.298×10^{-3}	4.560×10^{-3}
Inlet liquid flowrate (kg/s)	2.940×10^{-2}	2.069×10^{-2}
Inlet vapour temperature (K)	293.15	293.15
Inlet liquid temperature (K)	292.15	293.15
Pressure (Pa)	103150	103150
Inlet MEA concentration (mol/m^3)	2000	2000
Inlet CO_2 loading	0.118	0
Inlet vapour composition (mass):		
CO_2	0.220	0.265
Air (N_2 + O_2)	0.780	0.735

It must be mentioned that the MEA molar concentrations reported by Tontiwachwuthikul *et al.* for runs T14 and T18 is out of the range for which the kinetic mechanism used in this work was validated (see section 2.6). Hence this was in fact another reason why these runs were chosen since then the predictive behaviour of the model developed in this work could be evaluated for a wider range of operating conditions.

The inlet temperature of the vapour was not reported by Tontiwachwuthikul *et al.* Instead they referred the experiments were carried out at near atmospheric conditions (Tontiwachwuthikul, *et al.*, 1992).

Therefore 293.15 K was assumed as the inlet temperature of the vapour phase. It was also reported the column had 6.55m height and an inside diameter of 0.10m, and it was packed with ½" Berl saddles (Tontiwachwuthikul, *et al.*, 1992). In their evaluation of the performance of random and structured packings for air dehumidification Chung *et al.* reported the following packing specification for ½" Berl saddles (Chung, *et al.*, 1996):

Table 5 – Packing specifications for Berl saddles used in the model validation with the experimental data from Tontiwachwuthikul *et al.* (Chung, *et al.*, 1996).

	Berl saddles
Material	ceramic
Packing specific area (m^2/m^3)	465
Packing equivalent diameter (m)	1.27×10^{-2}
Packing void fraction	0.620

From the experimental data published by Aboudheir, runs B011 and B012 were chosen (Aboudheir, 2002). The reasons underlying the choice of these runs were similar to the ones reported for the model validation with experimental data presented by Tontiwachwuthikul *et al.* Hence run B011 had a lower CO_2 capture efficiency than run B012, which had near 100% capture efficiency and a lower inlet molar fraction of CO_2 in the vapour phase (Aboudheir, 2002). The experimental data reported by Aboudheir for runs B011 and B012 can be found in Appendix B. The use of experimental data from two different authors for similar CO_2 capture efficiency conditions was intended to reinforce the conclusions made during the validation process of the *Absorption column* model.

As well as for the above mentioned for the experimental data from Tontiwachwuthikul *et al.* the total flowrates of the vapour and liquid phases were determined from the original experimental data available, which is presented in Appendix B. The conditions used in the simulations are presented as follows:

Table 6 – Inlet conditions from the experimental data published (Aboudheir, 2002) for the runs B011 and B012 used as input for the *Absorption column* model validation.

	B011	**B012**
Inlet vapour flowrate (kg/s)	2.810×10^{-3}	2.160×10^{-3}
Inlet liquid flowrate (kg/s)	1.630×10^{-2}	1.630×10^{-2}
Inlet vapour temperature (K)	296.65	296.65
Inlet liquid temperature (K)	297.35	298.05
Pressure (Pa)	103150	103150
Inlet MEA concentration (mol/m^3)	3000	3000
Inlet CO_2 loading	0.188	0.195
Inlet vapour composition (mass):		
CO_2	0.275	0.074
Air ($N_2 + O_2$)	0.725	0.926

In the description of the experimental apparatus Aboudheir reported the experimental runs B011 and B012 were carried out in a column 2.40m height and an internal diameter of 0.10m, and also that the column was packed with the high performance random packing IMTP#15 (Aboudheir, 2002). Since no information was reported by Aboudheir about the packing specifications, and no useful information was found on the manufacturer brochure (www.koch-glitsch.com), the packing specifications for the 15mm high performance random packing AlphaPACK I$^+$, which is commercialized by a different manufacturer were used (www.hatltd.com). It was assumed that the performance of these two high performance packings was similar. The packing specifications used for the simulations are presented in Table 7.

Table 7 – Packing specifications for the high performance random packing AlphaPACK I$^+$ used in the model validation with the experimental data from Aboudheir (www.hatltd.com).

	AlphaPACK I$^+$
Material	Steel
Packing specific area (m^2/m^3)	325
Packing equivalent diameter (m)	1.50×10^{-2}
Packing void fraction	0.966

For the simulations it was still required to provide information regarding the mass and heat transfer coefficients. As mentioned in section 2.2.1 the mass transfer coefficients for the vapour and liquid phases were determined using the correlations proposed by Onda *et al.*, respectively (Equation 2.4) and (Equation 2.5). As explained in section 2.4 some values were assumed for the heat transfer coefficients since no information was found regarding this subject in the literature. The heat transfer coefficient for the vapour phase was considered to be 10 J/(m^2.s.K) and for the liquid phase coefficient 100 J/(m^2.s.K) was considered. A discussion regarding this assumption is presented in the section 3.3.2.

3.3.2. Simulations Results

Once defined the input requirements, steady-state simulations were performed and profiles for the CO_2 molar fraction in the vapour phase and the temperature of the liquid phase along the column were analyzed against each experimental run. The CO_2 capture efficiency and the CO_2 outlet loading of the liquid phase were also compared with the experimental data reported.

The predictive behaviour of the model was evaluated using the two different effective area correlations proposed by Onda *et al.* and Bravo *et al.*, respectively (Equation 2.16) and (Equation 2.17). The suitability of each correlation was analyzed through the determination of the AAD from the experimental data reported for all the indicators mentioned above with exception of the temperature in the liquid phase, namely CO_2 molar fraction in the vapour phase, CO_2 capture efficiency and CO_2 outlet loading of the liquid phase. For the liquid temperature, the average temperature deviation in Kelvin degrees was determined (ΔT_{av}). The obtained results are presented in Table 8 and from Figure 12 to Figure 19 (see also Appendix C).

Table 8 – Comparison between the experimental data and the simulations results for the CO_2 outlet loading of the liquid phase and the CO_2 capture efficiency using the correlations proposed by Onda *et al.* and Bravo *et al.* for the effective area for mass transfer presented in section 2.2.4.

	$CO_{2_{loading}}$	AAD (%)	η_{CO_2}	AAD (%)
T14	0.480	----	100	----
this work - Bravo *et al.*	0.478	0.3	97	3
this work - Onda *et al.*	0.489	2	99	1
T18	0.558	----	85	----
this work - Bravo *et al.*	0.497	11	77	9
this work - Onda *et al.*	0.478	14	78	8
B011	0.470	----	79	----
this work - Bravo *et al.*	0.485	3	84	6
this work - Onda *et al.*	0.494	5	87	10
B012	0.268	----	99	----
this work - Bravo *et al.*	0.267	0.4	94	6
this work - Onda *et al.*	0.276	3	98	1

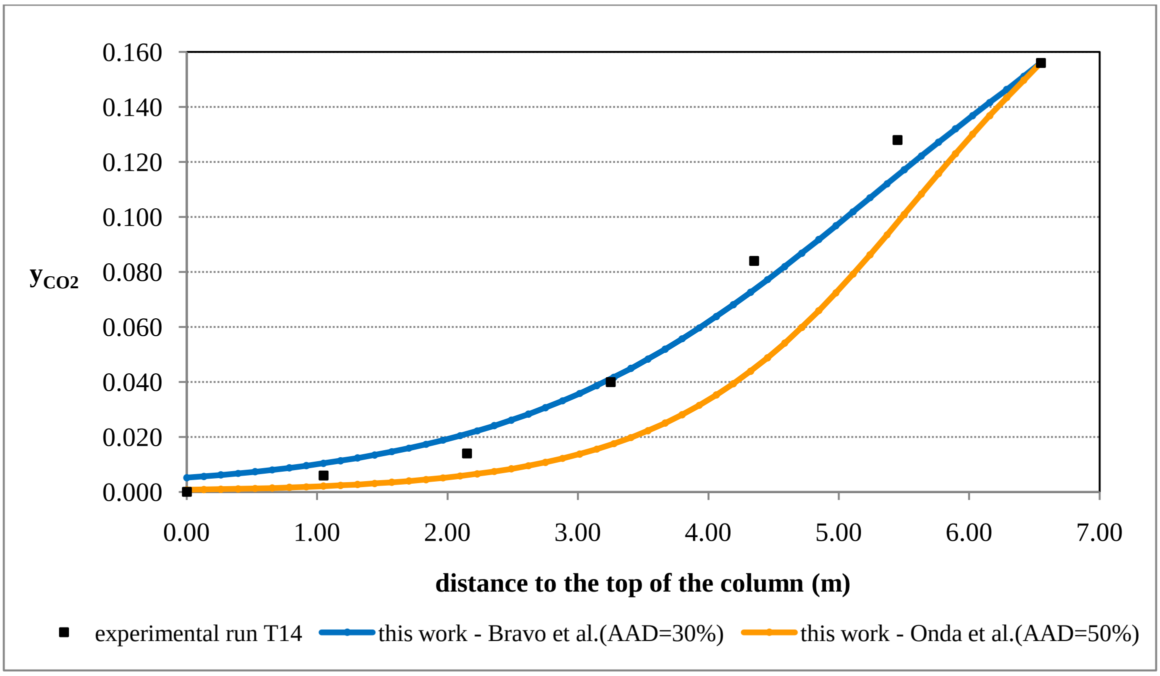

Figure 12 – CO_2 molar fraction profile in the vapour phase for the experimental run T14 (Tontiwachwuthikul, *et al.*, 1992) and predicted by the Absorption column model using the correlations proposed by Onda *et al.* and Bravo *et al.* for the effective area for mass transfer presented in section 2.2.4.

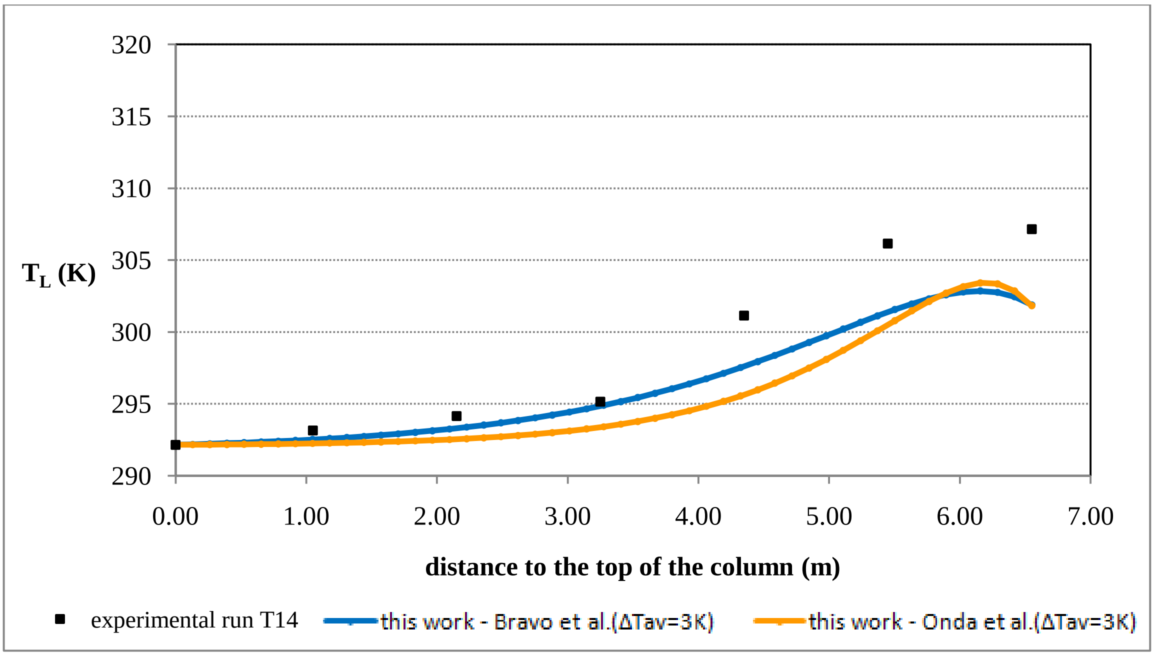

Figure 13 – Liquid phase temperature profile for the experimental run T14 (Tontiwachwuthikul, *et al.*, 1992) and predicted by the Absorption column model using the correlations proposed by Onda *et al.* and Bravo *et al.* for the effective area for mass transfer presented in section 2.2.4.

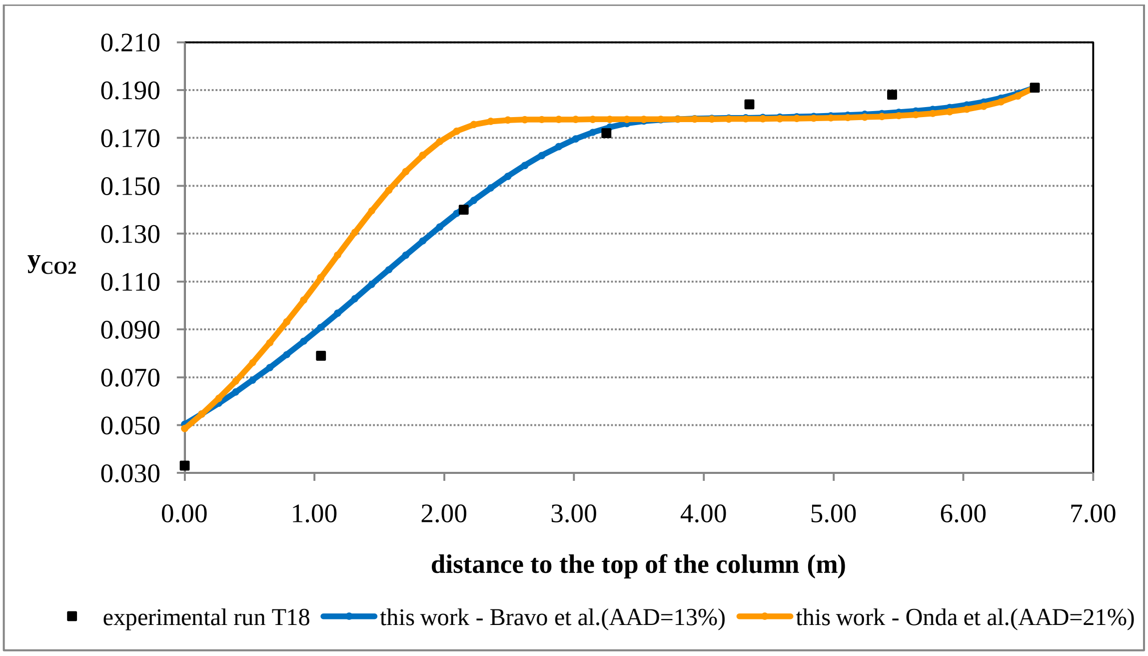

Figure 14 – CO_2 molar fraction profile in the vapour phase for the experimental run T18 (Tontiwachwuthikul, *et al.*, 1992) and predicted by the Absorption column model using the correlations proposed by Onda *et al.* and Bravo *et al.* for the effective area for mass transfer presented in section 2.2.4.

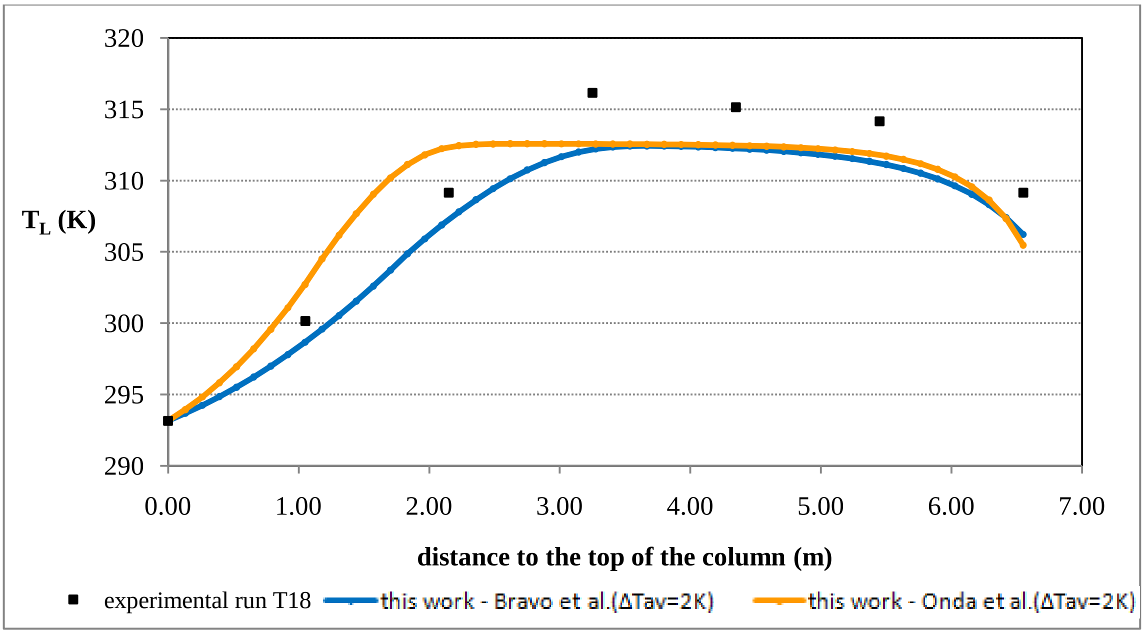

Figure 15 – Liquid phase temperature profile for the experimental run T18 (Tontiwachwuthikul, *et al.*, 1992) and predicted by the Absorption column model using the correlations proposed by Onda *et al.* and Bravo *et al.* for the effective area for mass transfer presented in section 2.2.4.

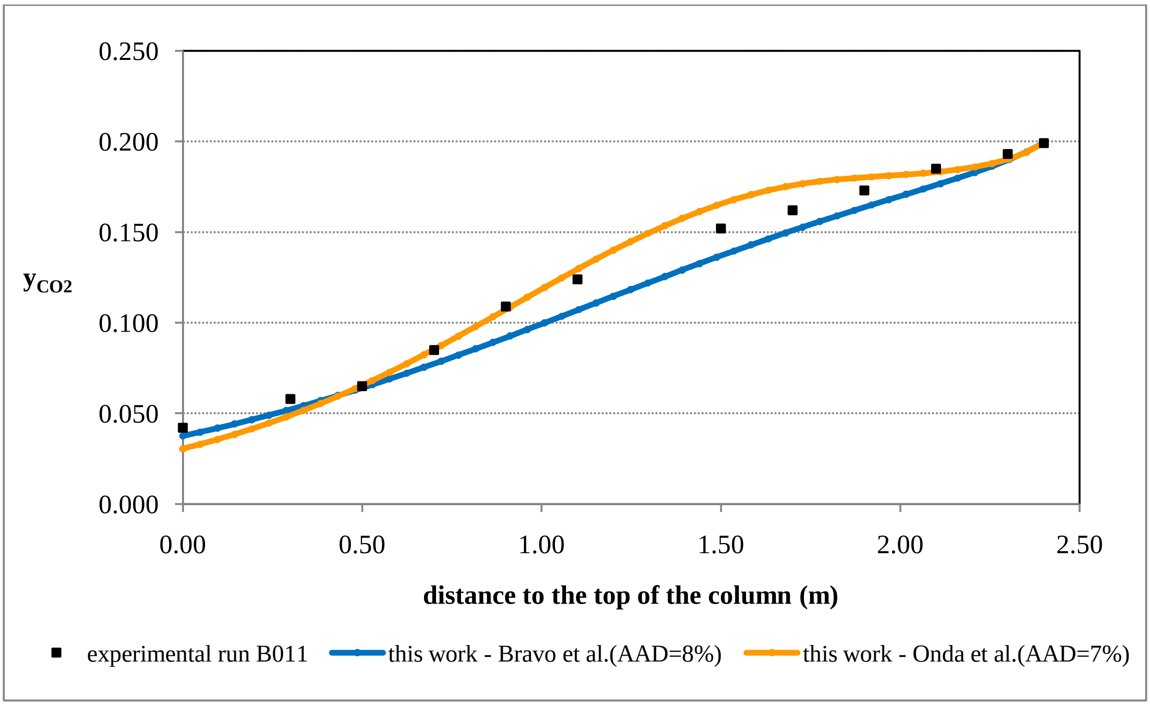

Figure 16 – CO_2 molar fraction profile in the vapour phase for the experimental run B011 (Aboudheir, 2002) and predicted by the Absorption column model using the correlations proposed by Onda *et al.* and Bravo *et al.* for the effective area for mass transfer presented in section 2.2.4.

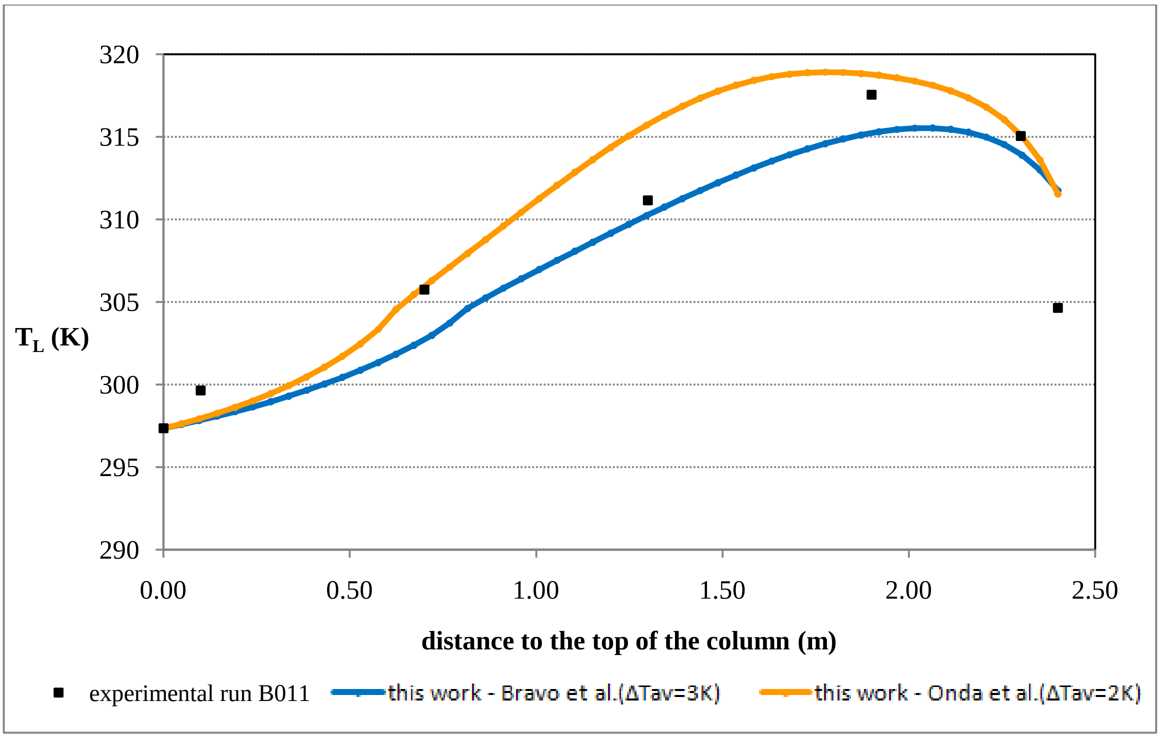

Figure 17 – Liquid phase temperature profile for the experimental run B011 (Aboudheir, 2002) and predicted by the Absorption column model using the correlations proposed by Onda *et al.* and Bravo *et al.* for the effective area for mass transfer presented in section 2.2.4.

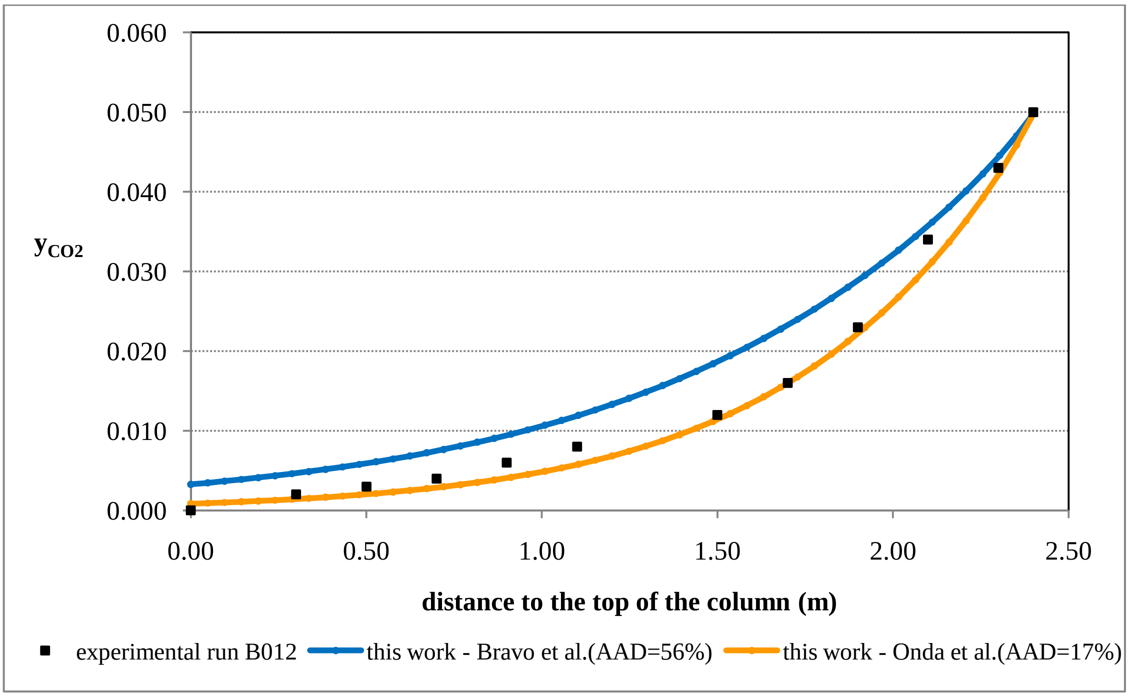

Figure 18 – CO_2 molar fraction profile in the vapour phase for the experimental run B012 (Aboudheir, 2002) and predicted by the Absorption column model using the correlations proposed by Onda *et al.* and Bravo *et al.* for the effective area for mass transfer presented in section 2.2.4.

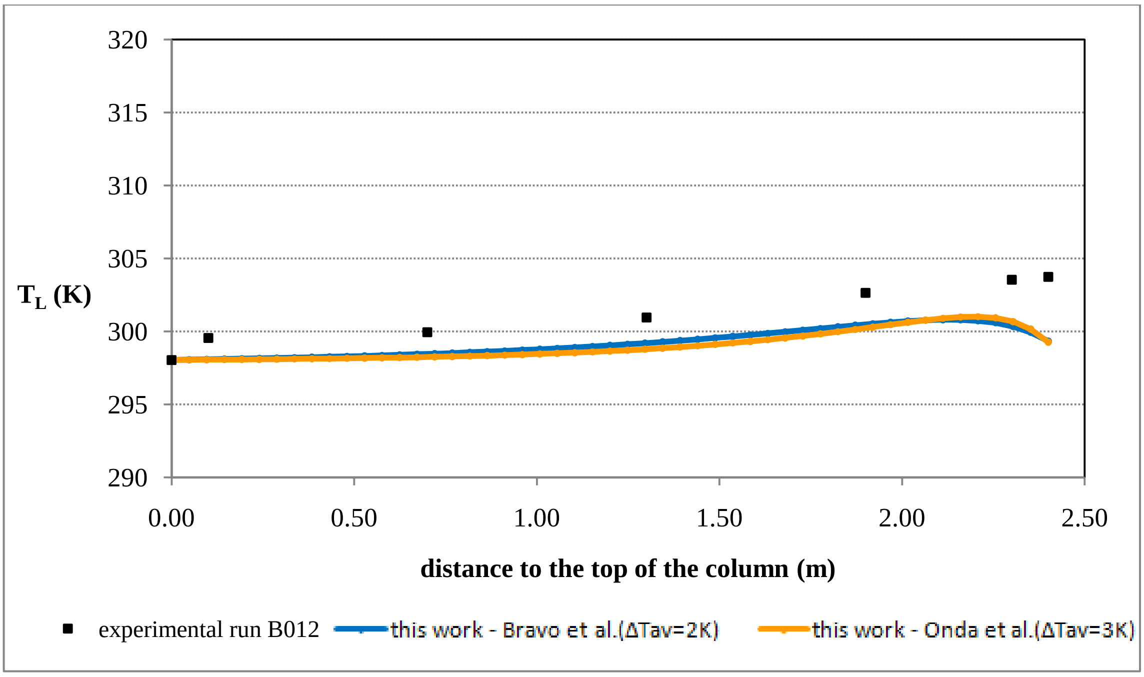

Figure 19 – Liquid phase temperature profile for the experimental run B012 (Aboudheir, 2002) and predicted by the Absorption column model using the correlations proposed by Onda *et al.* and Bravo *et al.* for the effective area for mass transfer presented in section 2.2.4.

From the model validation results it can be seen the ΔT_{av} determined for the temperature in the liquid phase were very small using both correlations for the effective area for mass transfer for all the experimental data considered . These values are presented in Figure 13, Figure 15, Figure 17, and Figure 19. This said, these small ΔT_{av} showed the values assumed for the heat transfer coefficients did not result in significant deviations of the temperature of the liquid phase predicted by the model and the experimental data reported by Tontiwachwuthikul *et al.* and Aboudheir and this assumption was therefore supported by the obtained results.

It can also be seen that for CO_2 capture efficiencies near 100% (100% for run T14 and 99% for run B012) the model predictions for the CO_2 molar fractions in the vapour phase presented a much higher AAD than for the remaining runs that presented smaller efficiencies (85% capture efficiency for run T18 and 79% for run B011). The AAD of the CO_2 molar fractions profile for each simulation can be seen in Figure 12, Figure 14, Figure 16, and Figure 18.

Since for runs T14 and B012 the CO_2 capture efficiency was near 100%, the CO_2 molar fractions at the region near the top of the absorption column, corresponding to the exit of the vapour stream were very small for both cases. Therefore deviations from the experimental data resulted in high AAD's due to the way this indicator was defined (see AAD definition in the chapter *Nomenclature*) since the experimental molar fractions were also very small in this region. These deviations were the result of the simplifications made during the development of this model specially the fact that no phase equilibrium was considered for MEA. Hence even if, for instance, the amount of MEA going into the vapour phase in a chemical absorption system for CO_2 capture is small, in the regions near the top of the column this amount of MEA could be significant to accurate determine the molar fractions of the components more diluted in the vapour phase, in this case CO_2. It is worth mentioning that for the remaining parameters analyzed AAD's that high were not verified which seems to support the reasons presented to explain the results for the CO_2 molar fractions in the vapour phase in runs T14 and B012.

On the other hand the simulations results showed that for smaller CO_2 capture efficiencies (runs T18 and B011), the model was able to predict every indicator analyzed within reasonable accuracy. The highest AAD was verified for the prediction of the CO_2 molar fractions in the vapour phase for run T18 using the correlation proposed by Onda *et al.* (AAD=21%).

After the model validation it was not entirely clear which of the correlations used to determine the effective area for mass transfer was more accurate. Hence with exception of the simulations results presented in Figure 12 and Figure 18, the determined AAD's for the other indicators were not significantly different. According to the AAD's determined in this work, using the correlation proposed by Bravo *et al.* for the effective area for mass transfer produced better results in the estimation of the CO_2 outlet loading in the liquid phase for all the cases considered (see Table 8). For the experimental data reported by Tontiwachwuthikul *et al.* the CO_2 molar fractions in the vapour phase were better predicted using this correlation (see Figure 12 and Figure 14). Using this correlation also resulted in a lower CO_2 capture efficiency AAD from the experimental data reported by Aboudheir for run B011 (see Table 8). On the other hand the results obtained using the correlation for the effective area for mass transfer proposed by Onda *et al.* were more accurate for the CO_2 capture efficiencies of the remaining 3 runs considered (see Table 8) and also for the CO_2 molar fractions in the vapour phase for the experimental data reported by Aboudheir (see Figure 16 and Figure 18).

Previous to the model validation it was expected that the results obtained using the correlation proposed by Bravo *et al.* were more accurate since, unlike the correlation proposed by Onda *et al.*, it accounts with the flow conditions of the vapour phase. According to Bravo *et al.* the flow conditions of the vapour phase can create discontinuities or ruptures in the surface shape of the liquid phase and also affect its dispersion droplets, and therefore influence the effective area available for mass transfer (Bravo, *et al.*, 1982). In a compilation of papers presented in the *8th Distillation and Absorption* conference held in London in 2006, Sorensen reported that for high liquid flowrates the effect of dispersion droplets in randomly packed columns can result in an effective area for mass transfer higher than the total surface area of the packing, or in other words, higher than the specific area of the packing (Sorensen, 2006). This behaviour cannot be predicted using the correlation proposed by Onda *et al.* (Equation 2.16) since according to it the higher value the effective area for mass transfer could take is equal to the total surface area of the packing. Furthermore the correlation proposed by Bravo *et al.* also included a direct influence of the column height in the effective area for mass transfer which is useful for scale-up of the absorption column. Therefore this correlation was considered to be more suitable for the feasibility study performed in this work.

3.4. Feasibility study

After being validated, the Absorption column model was used for a feasibility study. This study was done in collaboration with the companies *Process System Enterprise Ltd* (PSE) and *Det Norske Veritas S.A.* (DNV). The scope of this study was to assess if chemical absorption of CO_2 with MEA could be used to remove a significant amount of CO_2 from a flue gas stream within a very restricted space environment. Although a chemical absorption system requires other equipment besides the absorption column, this assessment was made considering only the size of this column since that was the main focus of this work. Hence the assessment presented in this work is preliminary and for a definitive conclusion the remaining equipment required for a chemical absorption system must be considered.

Therefore the model developed was used to determine the size of the absorption column required to remove 90% of the CO_2 from a flue gas stream for steady-state operating conditions. As explained in the section 3.2.5 the column diameter was determined considering that the vapour velocity inside the column was never higher than 80% of the vapour velocity determined for the flooding point. The inlet vapour composition was reported by DNV in a case study and due to a confidentiality agreement it was not presented in this work, apart from the CO_2 mass fraction that was 0.080 kg/kg, which means CO_2 was diluted in the flue gas stream. The inlet mass flowrate of the vapour phase $\boldsymbol{F_{G|1}}$ was also provided by DNV. The actual value of vapour flowrate is not presented. Instead it is only referred as $\boldsymbol{F_{G|1}}$. This mass flowrate corresponded to the combustion system upstream of the absorption column operating at 100% of its capacity. While performing this feasibility study the following inlet conditions were assumed:

Table 9 – Operating conditions used for the feasibility study.

	Feasibility study
Inlet vapour temperature (K)	313.15
Inlet liquid temperature (K)	308.15
Pressure (Pa)	105000
Inlet MEA weight concentration (%)	31
Inlet MEA concentration (mol/m^3)	3600
Inlet CO_2 loading	0.175
Inlet vapour composition (mass):	
CO_2	0.080
Other components	0.920

As mentioned above, there were restricted space requirements ($\boldsymbol{L_1}$, $\boldsymbol{L_2}$) that should be met in order for the absorption column to be considered as a feasible technology for the particular case study reported by DNV. Hence the absorption column should be able to fit in a house with the following dimensions ($\boldsymbol{L_1} > \boldsymbol{L_2}$):

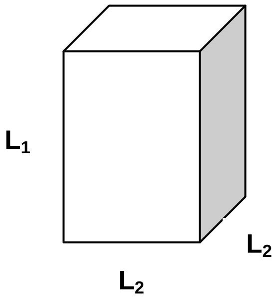

Figure 20 – Space restrictions for the absorption column to be considered as a feasible technology for CO2 capture in the case study reported by DNV.

The actual values of these dimensions are not presented due to the confidentiality agreement, as well as the column dimensions obtained as results of the feasibility study. Instead the results for the column height $\boldsymbol{L}$ are presented as function of $\boldsymbol{L_1}$ and the results for the column diameter $\boldsymbol{d}$ are presented as function of $\boldsymbol{L_2}$. As this was a preliminary feasibility study based on the dimensions of the absorption column, this technology was assumed to be feasible at operating conditions for which $\boldsymbol{L/L_1} < 1$ and $\boldsymbol{d/L_2} < 1$ were both verified.

As mentioned the correlation proposed by Bravo *et al.* (Equation 2.17) was used to determine the effective area for mass transfer. The simulations were performed considering the high performance random packing AlphaPACK I$^+$. Different packing sizes were used to assess the influence of this parameter in the size of the column. Each packing size was represented in Figure 21 and Figure 22 by the symbol #, followed by the characteristic dimension of the packing in millimeter units. All the specifications used for each packing size are available in the manufacturer website (www.hatltd.com).

Also analyzed in this feasibility study was the size of the column for different inlet mass flowrates for the liquid phase $\boldsymbol{F_{L|0}}$. In fact it was expected that the amount of solvent used in the absorption column influenced the height of the column required to remove the desired amount of CO_2, *i.e.* for the same MEA concentration a higher liquid flowrate should means more solvent available to react with CO_2 and therefore a smaller column. On the other hand, a higher liquid flowrate should also means a larger column and higher costs in terms of solvent consumption, although no cost estimation was considered in this feasibility study. The liquid mass flowrates $\boldsymbol{F_{L|0}}$ considered in this study are presented as function of the inlet mass flowrate of the vapour phase $\boldsymbol{F_{G|1}}$ due to the confidentiality agreement.

The results of the feasibility study for the column height are presented in Figure 21 and for the column diameter are presented in Figure 22 (see also Appendix D).

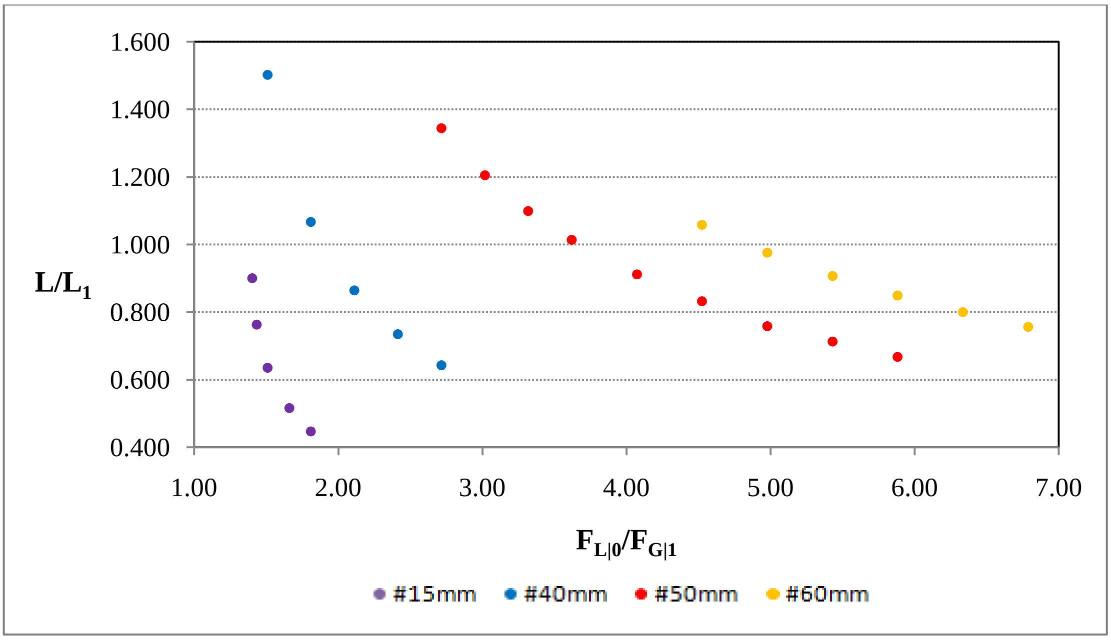

Figure 21 – Results obtained in the feasibility study for the column height L for different inlet mass flowrates in the liquid phase $F_{L|0}$ and packing sizes using the operating conditions mentioned.

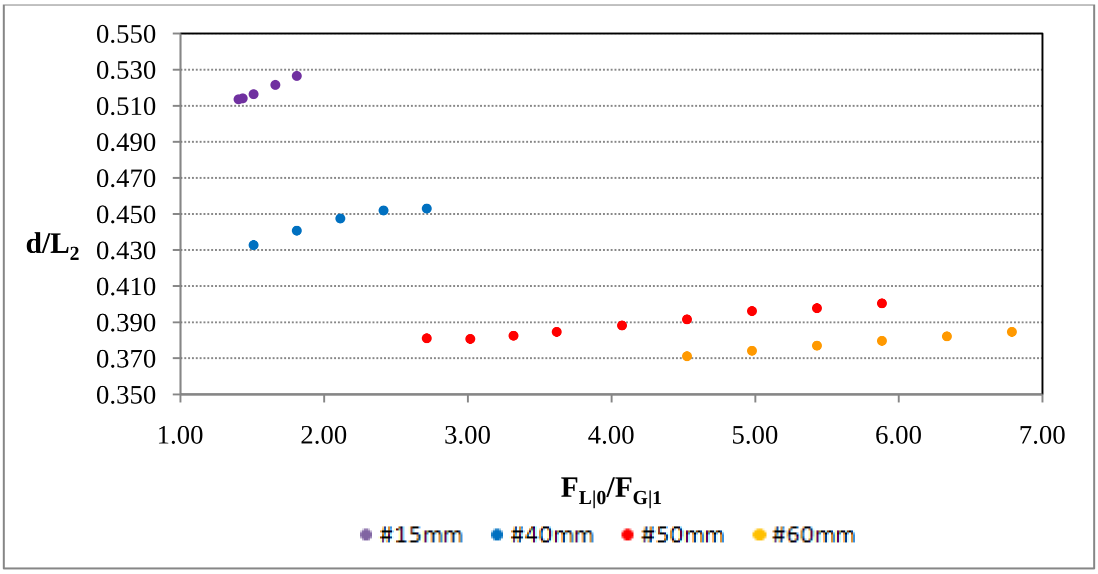

Figure 22 – Results obtained in the feasibility study for the column diameter d for different inlet mass flowrates in the liquid phase $F_{L|0}$ and packing sizes using the operating conditions mentioned.

As expected, for the conditions considered in this study the height of the absorption column required to remove 90% of CO_2 from the vapour phase decreases with the increase of the liquid mass flowrate (see Figure 21). This behaviour is attributed to the fact that, as reported by Sorensen, with the increase of the mass flowrate of the liquid phase the effective area available for mass transfer between the vapour and the liquid phases becomes higher (Sorensen, 2006). Another expected behaviour that can be seen in Figure 21 was that for the same liquid flowrates the column height increases when higher packing sizes are considered. According to the manufacturer the packings with bigger dimensions had lower specific areas (www.hatltd.com) which in this case reduced the effective area available for mass transfer and therefore reduced the mass transfer between the two phases. On the other hand considering bigger packing sizes reduces the column diameter as can be seen in Figure 22, and since the space available for the installation of the chemical absorption unit as reported by DNV is very restricted, this option should be considered during the design studies.

4. Conclusions

A chemical absorption model in gPROMS for CO_2 capture with MEA was developed in this work. The model was organized in two different hierarchical levels; the lowest level was composed by five individual sub-models where the all the equations which described the behaviour of the chemical absorption system were implemented. The high hierarchical level was composed by one model which established the connections between the individual sub-models. This architecture was chosen to allow great flexibility, easiness to use this model in a drag-and-drop flowsheeting and easy maintenance.

The model was validated against experimental data reported by Aboudheir and Tontiwachwuthikul *et al.* for chemical absorption of CO_2 with MEA. Two runs were chosen from the experimental data reported by each author, T14 and T18 for Tontiwachwuthikul *et al.* (Tontiwachwuthikul, *et al.*, 1992) and B011 and B012 for Aboudheir (Aboudheir, 2002). These runs were chosen to assess the suitability of the model developed in this work to predict the behaviour of the chemical absorption system in a wide range of operating conditions. This assessment was made through the determination of the AAD from the experimental data for the CO_2 molar fraction in the vapour phase, the outlet CO_2 loading in the liquid phase, and the CO_2 capture efficiency and ΔT_{av} for the liquid temperature in the liquid phase, using two different correlations for the effective area available for mass transfer, (Equation 2.16) and (Equation 2.17), proposed respectively by Onda *et al.* (Onda, *et al.*, 1968) and Bravo *et al.* (Bravo, *et al.*, 1982). From the simulation results it was concluded that the model developed in this work was suitable to predict all the 4 indicators considered in this work as describing the behaviour of a chemical absorption system for CO_2 capture with MEA for CO_2 capture efficiencies up to 90%.

The model validation results with experimental data using the two correlations for the effective area for mass transfer were found to be very similar in terms of accuracy. Yet it was concluded that the correlation proposed by Bravo *et al.* (Equation 2.17) was more suitable for the scope of the feasibility study performed in this work. Therefore this correlation was used in this study. It was also concluded that the reaction kinetics used in the absorption column model could be successfully used to predict the behaviour of the chemical absorption system for MEA concentrations as low as 2000 mol/m^3, as it can be seen in the results obtained for the run T18.

As mentioned the absorption column model developed in this work was used in a feasibility study. The scope of this study was to assess if chemical absorption with MEA could be used to remove a significant amount of CO_2 that was diluted in a flue gas stream within a very restricted space environment. The composition and the inlet mass flowrate of the vapour stream were provided by DNV as well as the space restrictions $\boldsymbol{L_1}$ and $\boldsymbol{L_2}$ (Figure 20). The dimensions of the absorption column were determined as the result of two assumptions made. Hence the column height was determined as the height required to achieve a CO_2 capture efficiency in the vapour phase of 90%. As for the column diameter, this was determined so that the maximum velocity of the vapour phase inside the column was 80% of the vapour velocity determined for the flooding point. The chemical absorption was considered to be a feasible technology for the operating conditions for which the dimensions of the absorption column are smaller than the maximum dimensions of the house ($\boldsymbol{L_1}$, $\boldsymbol{L_2}$) where the equipment is supposed to be installed. Although a chemical absorption system requires more equipment than the absorption column, this equipment was not taking into account in the feasibility study. Therefore the conclusions presented in this work regarding the feasibility of this technology are preliminary and further work should be employed to take definitive conclusions concerning this matter.

For this study different packing sizes and inlet mass flowrates for the liquid phase were evaluated. It was found that for 18 of the 25 operating conditions analyzed the size of the absorption column met the space requirements imposed by DNV. Therefore chemical absorption with MEA was considered to be a feasible technology to remove CO_2 from the flue gas stream given by DNV.

5. Future work

As it was presented in the chapter 3.3 a chemical absorption model in gPROMS capable of predicting the CO_2 chemical absorption with MEA was developed. Although this model was suitable within the scope of this work there is still further work to be done due to the simplifications assumed during the development of the model.

One of the limitations of the model developed is the fact that no phase equilibrium was considered for MEA. This assumption was particularly relevant when CO_2 capture efficiencies were considered near 100%. In fact is was noted that for capture efficiencies of 99% and 100% the CO_2 molar fractions in the region near the top of the absorption column predicted by the model presented significant deviations from the experimental data used to validate the model. Hence since the molar fractions of CO_2 were very small in this region these inaccuracies in its prediction were attributed to the fact that no phase equilibrium was considered for the MEA. Also since no phase equilibrium was considered for MEA the model was unable to determine the solvent loss during the chemical absorption of CO_2. Therefore it is recommended as future work that phase equilibrium must be considered for MEA to allow the absorption column model to be used for CO_2 capture efficiencies as high as 100%.

One other subject that was disregarded during the development of this work was the fact that MEA is a corrosive substance (www.sciencelab.com). In his work experimental apparatus Aboudheir reported that a small amount of an inhibitor was added to the liquid phase to prevent the corrosion of the equipment (Aboudheir, 2002). As expected the corrosion effects become more significant the higher the concentration of MEA used in the liquid phase. In addiction the increase of acid gases loading in the liquid phase due to the absorption, in this work represented by CO_2 only, also increases the possibility for corrosion to occur, particularly located corrosion in welds (www.dow.com). The corrosion in amine absorption columns was already responsible for major accidents such as the one that occurred at the Union Oil refinery, Illinois in 1984 which took the life of 17 workers (www.twi.co.uk). Therefore as future work the amount of corrosion inhibitor should also be considered.

The feasibility study performed in this work showed that the size of the absorption column fitted the space restrictions imposed by DNV for several operating conditions considered. For the remaining equipment of the chemical absorption system to be considered further experimental work is required to validate the regeneration column since no relevant experimental data was found for this step. The final assessment of the feasibility of this technology for the case study presented by DNV can only be made considering the dimensions of all the equipment required for the chemical absorption system. During this step alternative configurations should be evaluated, as for instance the possibility of using two absorption columns in parallel or eventually one absorption column with a non uniform diameter. If this technology considering the entire equipment proved to be feasible within the space restrictions imposed by DNV, a rigorous design study should be performed and the size of the packing and the inlet mass flowrate of the liquid phase should be optimized. For this design study higher levels of detail should be used for the *Reaction kinetics* and the *Mass transfer* sub-models, particularly more components and reactions should be considered, as reported by Vaidya et al in their review (Vaidya, *et al.*, 2007) and the behaviour of mass and heat transfer for each phase within the thin films near the phase boundary should be modeled using distributed variables along the radial direction.

List of symbols

$\boldsymbol{a_p}$	total surface area of the packing [m^{2}.m^{-3}]
$\boldsymbol{a_e}$	effective area for mass transfer [m^{2}.m^{-3}]
$\boldsymbol{A_{j,i}}$	matrix of null vectors
$\boldsymbol{c}$	constant in the correlation for the mass transfer coefficient in the vapour phase [dimensionless]
$\boldsymbol{C}$	molar concentration [mol.m^{-3}]
$\boldsymbol{C_{flood}}$	flooding constant [dimensionless]
$\boldsymbol{d}$	column diameter [m]
$\boldsymbol{d_p}$	packing equivalent diameter [m]
$\boldsymbol{D}$	diffusivity [m^{2}.s^{-1}]
$\boldsymbol{E}$	enhancement factor [dimensionless]
$\boldsymbol{F}$	mass flowrate [kg.s^{-1}]
$\boldsymbol{F_{mol}}$	molar flowrate [mol.s^{-1}]
$\boldsymbol{Fr}$	Froude number defined by $\left(\frac{a_p}{g.\rho^2}\left(\frac{F}{S}\right)^2\right)$ [dimensionless]
$\boldsymbol{g}$	gravitational constant [m.s^{-2}]
$\boldsymbol{h}$	heat transfer coefficient [J.m^{-2}.s^{-1}.K^{-1}]
$\boldsymbol{\bar{h}}$	mass specific enthalpy [J.Kg^{-1}]
$\boldsymbol{H}$	enthalpy [J.s^{-1}]
$\boldsymbol{H_{abs}}$	heat of absorption of CO_2 [J.mol^{-1}]
$\boldsymbol{He}$	Henry constant [Pa.m^{3}.mol^{-1}]
$\boldsymbol{k}$	mass transfer coefficient [m.s^{-1}]

$\boldsymbol{K_4}$	equilibrium constant of (Equation 2.37) [dimensionless]
$\boldsymbol{K_5}$	equilibrium constant of (Equation 2.43) [mol.m^{-3}]
$\boldsymbol{L}$	column height [m]
$\boldsymbol{L_1}$	maximum value for the column height in the feasibility study [m]
$\boldsymbol{L_2}$	maximum value for the column diameter in the feasibility study [m]
$\boldsymbol{m}$	mass fraction [kg.kg^{-1}]
$\boldsymbol{\bar{m}}$	mass fraction contracted in the liquid phase [kg.kg^{-1}]
$\boldsymbol{MW}$	molecular weight [kg.mol^{-1}]
$\boldsymbol{n}$	number of components [dimensionless]
$\boldsymbol{N}$	rate of mass transfer [mol.m^{-2}.s^{-1}]
$\boldsymbol{n_{flood}}$	exponent in (Equation 2.21) [dimensionless]
$\boldsymbol{P}$	pressure [Pa]
$\boldsymbol{P_{vap}}$	vapour pressure [Pa]
$\boldsymbol{Q}$	rate of heat transfer [J.m^{-2}.s^{-1}]
$\boldsymbol{r}$	reaction rate constant [m^{6}.mol^{-2}.s^{-1}]
$\boldsymbol{r_{for}}$	reaction rate constant of the forward reaction [m^{3}.mol^{-1}.s^{-1}]
$\boldsymbol{R}$	ideal gas constant [J.mol^{-1}.K^{-1}]
$\boldsymbol{Re}$	Reynolds number defined by $\left(\boldsymbol{\frac{F}{S.a_p.\mu}}\right)$ [dimensionless]
$\boldsymbol{S}$	cross sectional area of the column [m^{2}]
$\boldsymbol{T}$	temperature [K]
$\boldsymbol{\bar{u}}$	mass specific internal energy [J.kg^{-1}]
$\boldsymbol{U}$	volume specific internal energy [J.m^{-3}]
$\boldsymbol{v}$	superficial velocity [m.s^{-1}]

V	molar volume [$m^3.mol^{-1}$]
We	Weber number defined by $\left(\frac{1}{a_p.\sigma.\rho}\left(\frac{F}{S}\right)^2\right)$ [dimensionless]
x	molar fraction in the liquid phase [$mol.mol^{-1}$]
$\overline{x}$	molar fraction contracted in the liquid phase [$mol.mol^{-1}$]
y	molar fraction in the vapour phase [$mol.mol^{-1}$]
$\frac{\partial}{\partial z}$	operator for partial differentiation along the axial direction
$(\sum v)$	sum of the atomic diffusion volumes

Greek Letters

ε	void fraction [$m^3.m^{-3}$]
μ	viscosity [Pa.s]
$\emptyset$	association factor for the solvent [dimensionless]
ρ	density [$kg.m^{-3}$]
ρ_{mol}	molar density [$mol.m^{-3}$]
$\overline{\rho}$	initial guess for the density of the liquid phase [$kg.m^{-3}$]
σ	surface tension [$N.m^{-1}$]
σ_p	critical surface tension of the packing [$N.m^{-1}$]
φ	volume fraction [$m^3.m^{-3}$]
Γ	rate of reaction [$mol.m^{-3}.s^{-1}$]
ω	liquid holdup [$m^3.m^{-3}$]
ω_{mol}	molar liquid holdup [$mol.m^{-3}$]
Ψ	resistance factor [dimensionless]
π	number Pi [dimensionless]

$\boldsymbol{\eta_{CO_2}}$	CO_2 capture efficiency [%]
$\boldsymbol{\Delta T_{av}}$	average temperature deviation, defined as $\left(\left\|T_{experimental} - T_{model}\right\|\right)$ [K]

Subscripts

bin	binary system MEA+H_2O
eq	equilibrium
flood	flooding point
G	vapour phase
i	i^{th} component of the mixture
int	interface
j	j^{th} component of the mixture
L	liquid phase
p	packing
sol	solution
tot	total
0	top of the column
1	bottom of the column

Supercripts

b	bulk
int	interface

Bibliography

Aboudheir, A. 2002. *Kinetics, Modelling, and Simulation of carbon dioxide absorption into highly concentrated and loaded monoethanolamine solutions.* Canada : University of Regina, 2002. PhD Thesis.

Aboudheir, A., *et al.* 2003. Kinetics of the reactive absorption of carbon dioxide in high CO_2-loaded, concentrated aqueous monoethanolamine solutions. *Chem. Eng. Sci.* 58, 2003, pp. 5195 – 5210.

Austgen, D and Rochelle, G. 1989. Model of Vapour-Liquid Equilibria for aqueous acid gas alkanolamine systems using the electrolyte-NRTL equation. *Ind. Eng. Chem. Res.* 28, 1989, pp. 1060-1073.

Barth, D., Tondre, C. and Delpuech, J. 1986. Stopped-flow investigations of the reaction kinetics of carbon dioxide with some primary and secondary alkanolamines in aqueous solutions. *Int. J. Chem. Kinetics.* 18, 1986, pp. 445-457.

Billet, R. and Schultes, M. 1995. Fluid dynamics and mass transfer in the total capacity range of packed columns up to the flood point. *Chem. Eng. Technol.* 18, 1995, pp. 371-379.

Billet, R. and Schultes, M. 1999. Prediction of mass transfer columns with dumped and arranged packings - Updated summary of the calculation method of Billet and Schultes. *IChemE.* 1999, Vol. 77, pp. 498-504.

Bravo, J. and Fair, J. 1982. Generalized correlation for mass transfer in packed distillation columns. *Ind. Eng. Chem. Process Des. Dev.* 21, 1982, pp. 162-170.

Carey, T., Hermes, J. and Rochelle, G. 1991. A model of acid gas absorption/stripping using methyldiethanolamine with added acid. *Gas Separation and Purification.* United Kingdom : Butterworth-Heinemann, 1991, Vol. 5.

Chung, T., Ghosh, T. and Hines, A. 1996. Comparison between random and structured packings for dehumidification of air by lithium chloride solutions in a packed column and their Heat and Mass transfer correlations. *Ind. Eng. Chem. Res.* 35, 1996, pp. 192-198.

Coulson, J. and Richardson, J. 1999. *Chemical Engineering - Fluid Flow, Heat Transfer and Mass Transfer.* 6th Edition. Oxford : Butterworth-Heinemann, 1999. pp. 573-599. Vol. 1.

Figueroa, J., *et al.* 2008. Advances in CO_2 capture technology—The U.S. Department of Energy's Carbon Sequestration Program. *International Journal of Greenhouse gas control.* 2, 2008, pp. 9-20.

Hessen, E, Warberg, T. and Svendsen, H. 2009. Thermodynamic models for CO_2-H_2O-alkanolamine systems, a discussion. *Energy Procedia.* 1, 2009, pp. 971–978.

Higbie, R. 1935. The rate of absorption of pure gas into a still liquid during short periods of exposure. *Trans. Am. Inst. Chem. Eng.* 31, 1935, p. 365.

Ko, J., *et al.* 2001. Diffusivity of Nitrous Oxide in aqueous alkanolamine solutions. *J. Chem. Eng. Data.* 46, 2001, pp. 160-165.

Kohl, A. and Nielsen, R. 1997. *Gas Purification.* 5th Edition. Houston : Gulf Publishing Company, 1997. pp. 49-50 and 91-98.

Kvamsdal, H., Jakobsen, J. and Hoff, K. 2008. Dynamic modeling and simulation of a CO_2 absorber column for post-combustion CO_2 capture. *Chem. Eng. Process.* doi:10.1016/j.cep.2008.03.002, 2008.

Onda, K., Kakeuchi, H. and Okumoto, Y. 1968. Mass transfer coefficients between gas and liquid phases in packed columns. *J. Chem. Eng. Japan.* 1, 1968, pp. 57-61.

Pantelides, C. 2000. *The mathematical modelling of the dynamic behaviour of Process Systems.* London : Imperial College of Science, Technology and Medicine, 2000. pp. 54-61 and 101-102.

Perry, R. and Green, D. 1984. *Perry's Chemical Engineers' Handbook.* 6th Edition. Singapore : McGraw-Hill, 1984. pp. 18-34.

Poling, B., Prausnitz, J. and O'Connell, J. 2007. *The Properties of Gases and Liquids.* 5th Edition. Singapore : McGraw-Hill, 2007. p. 11.10.

Rubin, E. and Rao, A. 2002. *A technical, economic and environmental assessment of amine-based* CO_2 *Capture technology for power plant greenhouse gas control.* Annual Technical Progress Report , Carnegie Mellon University. Pittsburgh : U.S. Department of Energy, 2002.

Sieres, J. and Seara, J. 2007. Experimental investigation of mass transfer performance with some random packings for ammonia rectification in ammonia-water absorption refrigeration systems. *Int. J. Therm. Sci.* 46, 2007, pp. 699-706.

Sorensen, E. 2006. *Distillation and Absorption.* London : Institution of Chemical Engineers, 2006. pp. 754-763.

Tontiwachwuthikul, P, Meisen, A and Lim, J. 1992. CO_2 Absorption by NaOH, Monoethanolamine and 2-amino-2-methyl-1-propanol solutions in a packed column. *Chem. Eng. Sci.* 1992, Vol. 47, pp. 381-390.

Tsai, T., *et al.* 2000. Solubility of Nitrous Oxide in Alkanolamine Aqueous Solutions. *J. Chem. Eng. Data.* 45, 2000, pp. 341-347.

Vaidya, P. and Kenig, E. 2007. CO_2-Alkanolamine reaction kinetics, A review of recent studies. *Chem. Eng. Technol.* 30, 2007, pp. 1467-1474.

Versteeg, G. and Swaalj, W. 1988. Solubility and diffusivity of acid gases (carbon dioxide, nitrous oxide) in aqueous alkanolamine solutions. *J. Chem. Eng. Data.* 33, 1988, Vol. 1, pp. 29-34.

Wang, G., Yuan, X. and Yu, K. 2005. Review of Mass-Transfer Correlations for Packed Columns. *Ind. Eng. Chem. Res.* 44, 2005, pp. 8715-8729.

Whitman, W. 1923. The two-film theory of absortion. *Chem. and Met. Eng.* 29, 1923, p. 147.

Wilke, C. and Chang, P. 1955. Correlation of diffusion coefficients in dilute solutions. *A.I.Ch.E. Journal.* 2, 1955, Vol. 1, pp. 264-270.

www.bantrel.com. [Online] [Cited: November 8th, 2010.] http://bantrel.com/markets/carboncapture.aspx.

www.dow.com. [Online] [Cited: 1st November 2010.] http://www.dow.com/PublishedLiterature/dh_0039/0901b803800391f8.pdf?filepath=gastreating/pdfs/noreg/170-01395.pdf&fromPage=GetDoc.

www.hatltd.com. [Online] [Cited: 28th October 2010.] http://www.hatltd.com/hosted/55000702/home.nsf/lp/cpoexvmmwmwn?OpenDocument.

www.ipcc.ch. [Online] [Cited: 8th November 2010.] http://www.ipcc.ch/publications_and_data/publications_and_data_reports_carbon_dioxide.htm.

www.koch-glitsch.com. [Online] [Cited: 28th October 2010.] http://www.koch-glitsch.com/masstransfer/pages/metal_random_packing.aspx.

www.powerplantccs.com. [Online] [Cited: 14th September 2010.] http://www.powerplantccs.com/ccs/cap/fut/sns/sns.html.

www.psenterprise.com. [Online] [Cited: 15th October 2010.] http://www.psenterprise.com/gproms/index.html.

www.sciencelab.com. [Online] [Cited: 1st November 2010.] http://www.sciencelab.com/xMSDS-Monoethanolamine-9922885.

www.sciencelab.com. [Online] [Cited: 1st November 2010.] http://www.sciencelab.com/msds.php?msdsId=9927321.

www.twi.co.uk. [Online] [Cited: 1st November 2010.] http://www.twi.co.uk/content/spjsjan2005.html.

Appendixes

Appendix A – Experimental data for runs T14 and T18 from Tontiwachwuthikul *et al.* (Tontiwachwuthikul, *et al.*, 1992).

Table 10 – Experimental data for runs T14 and T18 for the CO_2 molar fraction in the vapour phase and for the temperature in the liquid phase (Tontiwachwuthikul, *et al.*, 1992).

	T14		**T18**	
distance to the top of the column (m)	y_{CO2}	T_L(K)	y_{CO2}	T_L(K)
0	0	292.15	0.033	293.15
1.05	0.006	293.15	0.079	300.15
2.15	0.014	294.15	0.140	309.15
3.25	0.040	295.15	0.172	316.15
4.35	0.084	301.15	0.184	315.15
5.45	0.128	306.15	0.188	314.15
6.55	0.156	307.15	0.191	309.15

Appendix B – Experimental data for runs B011 and B012 from Aboudheir (Aboudheir, 2002).

Table 11 – Experimental data for runs B011 and B012 for the CO_2 molar fraction in the vapour phase (Aboudheir, 2002).

	y_{CO2}	
distance to the top of the column (m)	**B011**	**B012**
0	0.042	0
0.30	0.058	0.002
0.50	0.065	0.003
0.70	0.085	0.004
0.90	0.109	0.006
1.10	0.124	0.008
1.50	0.152	0.012
1.70	0.162	0.016
1.90	0.173	0.023
2.10	0.185	0.034
2.30	0.193	0.043
2.40	0.199	0.050

Table 12 – Experimental data for the runs B011 and B012 for the temperature in the liquid phase (Aboudheir, 2002).

	T_L(K)	
distance to the top of the column (m)	**B011**	**B012**
0	297.35	298.05
0.10	299.65	299.55
0.70	305.75	299.95
1.30	311.15	300.95
1.90	317.55	302.65
2.30	315.05	303.55
2.40	304.65	303.75

Appendix C – Simulation results for the tested cases.

Table 13 – Simulation results for operating conditions from run T14 for the CO_2 molar fractions in the vapour phase and temperatures in the liquid phase using the correlations proposed by Bravo *et al.* and Onda *et al.* for the effective area for mass transfer.

	y_{CO2}		T_L(K)	
distance to the top of the column (m)	**Bravo *et al.***	**Onda *et al.***	**Bravo *et al.***	**Onda *et al.***
0	0.005	0.001	292.15	292.15
0.13	0.006	0.001	292.18	292.15
0.26	0.006	0.001	292.22	292.16
0.39	0.007	0.001	292.26	292.17
0.52	0.007	0.001	292.30	292.18
0.66	0.008	0.001	292.35	292.20
0.79	0.009	0.002	292.40	292.21
0.92	0.010	0.002	292.45	292.23
1.05	0.010	0.002	292.52	292.24
1.18	0.011	0.002	292.58	292.27
1.31	0.012	0.003	292.66	292.29
1.44	0.013	0.003	292.74	292.32
1.57	0.015	0.003	292.82	292.35
1.70	0.016	0.004	292.92	292.38
1.83	0.017	0.005	293.02	292.42
1.97	0.019	0.005	293.13	292.46
2.10	0.020	0.006	293.25	292.51
2.23	0.022	0.007	293.38	292.57
2.36	0.024	0.007	293.52	292.64
2.49	0.026	0.008	293.68	292.71
2.62	0.028	0.010	293.84	292.79
2.75	0.031	0.011	294.02	292.89
2.88	0.033	0.012	294.22	293.00
3.01	0.036	0.014	294.43	293.12
3.14	0.039	0.016	294.65	293.25
3.28	0.042	0.018	294.90	293.41
3.41	0.045	0.020	295.16	293.58
3.54	0.048	0.022	295.43	293.77
3.67	0.052	0.025	295.73	293.99
3.80	0.056	0.028	296.05	294.24
3.93	0.060	0.032	296.39	294.52
4.06	0.064	0.035	296.75	294.83
4.19	0.068	0.039	297.12	295.17

(continue to the next page…)

(continuation from the previous page…)				
	y_{CO2}		T_L(K)	
distance to the top of the column (m)	**Bravo *et al.***	**Onda *et al.***	**Bravo *et al.***	**Onda *et al.***
4.32	0.073	0.044	297.52	295.55
4.45	0.077	0.049	297.93	295.97
4.58	0.082	0.054	298.37	296.44
4.72	0.087	0.060	298.81	296.94
4.85	0.092	0.066	299.27	297.49
4.98	0.097	0.072	299.74	298.09
5.11	0.102	0.079	300.20	298.72
5.24	0.107	0.086	300.67	299.39
5.37	0.112	0.094	301.12	300.08
5.50	0.117	0.101	301.56	300.78
5.63	0.122	0.108	301.96	301.47
5.76	0.127	0.116	302.31	302.12
5.89	0.132	0.123	302.59	302.70
6.03	0.137	0.130	302.79	303.16
6.16	0.142	0.137	302.85	303.41
6.29	0.146	0.143	302.75	303.35
6.42	0.151	0.150	302.45	302.85
6.55	0.156	0.156	301.89	301.83

Table 14 – Simulation results for operating conditions from run T18 for the CO_2 molar fractions in the vapour phase and temperatures in the liquid phase using the correlations proposed by Bravo *et al.* and Onda *et al.* for the effective area for mass transfer.

	y_{CO2}		T_L(K)	
distance to the top of the column (m)	**Bravo *et al.***	**Onda *et al.***	**Bravo *et al.***	**Onda *et al.***
0	0.050	0.049	293.15	293.15
0.13	0.055	0.055	293.67	293.93
0.26	0.059	0.061	294.24	294.82
0.39	0.064	0.068	294.85	295.82
0.52	0.069	0.076	295.51	296.94
0.66	0.074	0.084	296.22	298.19
0.79	0.079	0.093	296.98	299.57
0.92	0.085	0.102	297.80	301.08
1.05	0.091	0.112	298.66	302.71
1.18	0.097	0.121	299.57	304.51
1.31	0.103	0.130	300.54	306.17
(continue to the next page…)				

(continuation from the previous page…)				
	y_{CO2}		**T_L(K)**	
distance to the top of the column (m)	**Bravo *et al.***	**Onda *et al.***	**Bravo *et al.***	**Onda *et al.***
1.44	0.109	0.140	301.54	307.68
1.57	0.115	0.148	302.60	309.03
1.70	0.121	0.156	303.71	310.19
1.83	0.127	0.163	304.86	311.12
1.97	0.133	0.168	305.90	311.80
2.10	0.138	0.173	306.88	312.23
2.23	0.144	0.176	307.80	312.45
2.36	0.149	0.177	308.65	312.53
2.49	0.154	0.177	309.43	312.56
2.62	0.158	0.178	310.13	312.57
2.75	0.163	0.178	310.74	312.58
2.88	0.166	0.178	311.25	312.57
3.01	0.170	0.178	311.68	312.57
3.14	0.172	0.178	312.00	312.57
3.28	0.174	0.178	312.22	312.56
3.41	0.176	0.178	312.35	312.56
3.54	0.177	0.178	312.41	312.55
3.67	0.178	0.178	312.43	312.54
3.80	0.178	0.178	312.42	312.53
3.93	0.178	0.178	312.40	312.52
4.06	0.178	0.178	312.36	312.51
4.19	0.178	0.178	312.32	312.49
4.32	0.178	0.178	312.27	312.47
4.45	0.179	0.178	312.21	312.44
4.58	0.179	0.178	312.13	312.40
4.72	0.179	0.178	312.05	312.36
4.85	0.179	0.178	311.95	312.30
4.98	0.179	0.178	311.84	312.23
5.11	0.180	0.178	311.70	312.15
5.24	0.180	0.179	311.54	312.04
5.37	0.180	0.179	311.34	311.89
5.50	0.181	0.179	311.12	311.71
5.63	0.181	0.180	310.84	311.48
5.76	0.182	0.180	310.51	311.18
5.89	0.183	0.181	310.12	310.78
6.03	0.184	0.182	309.63	310.26
6.16	0.185	0.183	309.04	309.57
6.29	0.187	0.185	308.31	308.63
6.42	0.189	0.188	307.39	307.33
6.55	0.191	0.191	306.22	305.47

Table 15 – Simulation results for operating conditions from run B011 for the CO_2 molar fractions in the vapour phase and temperatures in the liquid phase using the correlations proposed by Bravo *et al.* and Onda *et al.* for the effective area for mass transfer.

	y_{CO2}		T_L(K)	
distance to the top of the column (m)	**Bravo *et al.***	**Onda *et al.***	**Bravo *et al.***	**Onda *et al.***
0	0.038	0.030	297.35	297.35
0.05	0.040	0.033	297.58	297.62
0.10	0.042	0.036	297.82	297.92
0.14	0.044	0.038	298.08	298.25
0.19	0.047	0.041	298.36	298.62
0.24	0.049	0.045	298.65	299.01
0.29	0.052	0.048	298.96	299.45
0.34	0.054	0.052	299.30	299.93
0.38	0.057	0.055	299.65	300.46
0.43	0.060	0.059	300.03	301.05
0.48	0.063	0.064	300.44	301.71
0.53	0.066	0.068	300.87	302.45
0.58	0.069	0.073	301.33	303.33
0.62	0.072	0.077	301.83	304.55
0.67	0.075	0.082	302.38	305.45
0.72	0.079	0.087	302.98	306.29
0.77	0.082	0.093	303.72	307.11
0.82	0.086	0.098	304.61	307.94
0.86	0.089	0.103	305.24	308.77
0.91	0.093	0.109	305.83	309.60
0.96	0.096	0.114	306.40	310.43
1.01	0.100	0.119	306.96	311.25
1.06	0.104	0.125	307.52	312.06
1.10	0.107	0.130	308.07	312.85
1.15	0.111	0.135	308.62	313.62
1.20	0.115	0.140	309.16	314.35
1.25	0.118	0.145	309.70	315.05
1.30	0.122	0.149	310.23	315.70
1.34	0.125	0.154	310.74	316.30
1.39	0.129	0.158	311.25	316.85
1.44	0.133	0.161	311.74	317.34
1.49	0.136	0.165	312.22	317.76
1.54	0.140	0.168	312.68	318.12
1.58	0.143	0.171	313.12	318.42
1.63	0.146	0.173	313.53	318.64
1.68	0.150	0.175	313.91	318.79
1.73	0.153	0.177	314.27	318.88

(continue to the next page…)

(continuation from the previous page…)

	y_{CO2}		T_L(K)	
distance to the top of the column (m)	**Bravo *et al.***	**Onda *et al.***	**Bravo *et al.***	**Onda *et al.***
1.78	0.156	0.178	314.59	318.92
1.82	0.159	0.179	314.87	318.90
1.87	0.162	0.180	315.11	318.83
1.92	0.165	0.180	315.30	318.72
1.97	0.168	0.181	315.44	318.57
2.02	0.171	0.182	315.52	318.37
2.06	0.174	0.182	315.53	318.12
2.11	0.177	0.183	315.45	317.79
2.16	0.180	0.184	315.28	317.36
2.21	0.183	0.186	314.98	316.79
2.26	0.186	0.188	314.53	316.04
2.30	0.190	0.190	313.89	315.02
2.35	0.194	0.194	312.99	313.59
2.40	0.199	0.199	311.75	311.53

Table 16 – Simulation results for operating conditions from run B012 for the CO_2 molar fractions in the vapour phase and temperatures in the liquid phase using the correlations proposed by Bravo *et al.* and Onda *et al.* for the effective area for mass transfer.

	y_{CO2}		T_L(K)	
distance to the top of the column (m)	**Bravo *et al.***	**Onda *et al.***	**Bravo *et al.***	**Onda *et al.***
0	0.003	0.001	298.05	298.05
0.05	0.003	0.001	298.07	298.06
0.10	0.004	0.001	298.09	298.06
0.14	0.004	0.001	298.11	298.07
0.19	0.004	0.001	298.13	298.08
0.24	0.004	0.001	298.15	298.09
0.29	0.005	0.001	298.18	298.10
0.34	0.005	0.002	298.20	298.12
0.38	0.005	0.002	298.23	298.13
0.43	0.005	0.002	298.26	298.14
0.48	0.006	0.002	298.29	298.16
0.53	0.006	0.002	298.33	298.18
0.58	0.006	0.002	298.36	298.20
0.62	0.007	0.003	298.40	298.22
0.67	0.007	0.003	298.44	298.24

(continue to the next page…)

(continuation from the previous page…)				
	y_{CO2}		T_L(K)	
distance to the top of the column (m)	**Bravo *et al.***	**Onda *et al.***	**Bravo *et al.***	**Onda *et al.***
0.72	0.008	0.003	298.48	298.26
0.77	0.008	0.003	298.52	298.29
0.82	0.009	0.004	298.57	298.32
0.86	0.009	0.004	298.62	298.35
0.91	0.010	0.004	298.67	298.38
0.96	0.010	0.005	298.72	298.42
1.01	0.011	0.005	298.78	298.46
1.06	0.011	0.005	298.84	298.50
1.10	0.012	0.006	298.91	298.55
1.15	0.013	0.006	298.98	298.60
1.20	0.013	0.007	299.05	298.66
1.25	0.014	0.007	299.12	298.72
1.30	0.015	0.008	299.20	298.78
1.34	0.016	0.009	299.29	298.86
1.39	0.017	0.010	299.37	298.94
1.44	0.017	0.010	299.46	299.02
1.49	0.018	0.011	299.56	299.11
1.54	0.019	0.012	299.66	299.21
1.58	0.020	0.013	299.76	299.32
1.63	0.022	0.014	299.87	299.43
1.68	0.023	0.015	299.98	299.56
1.73	0.024	0.017	300.09	299.69
1.78	0.025	0.018	300.20	299.83
1.82	0.027	0.020	300.31	299.98
1.87	0.028	0.021	300.43	300.14
1.92	0.029	0.023	300.53	300.30
1.97	0.031	0.025	300.63	300.46
2.02	0.033	0.027	300.71	300.63
2.06	0.034	0.029	300.77	300.78
2.11	0.036	0.031	300.81	300.91
2.16	0.038	0.034	300.80	300.99
2.21	0.040	0.036	300.74	301.01
2.26	0.042	0.039	300.59	300.93
2.30	0.045	0.042	300.34	300.68
2.35	0.047	0.046	299.94	300.17
2.40	0.050	0.050	299.34	299.27

Appendix D – Simulation results for the feasibility study

Table 17 – Simulation results for the feasibility study considering a packing size of 15 mm and different $F_{L|0}/F_{G|1}$.

Packing size #15		
$F_{L|0}/F_{G|1}$	L/L_1	d/L_2
1.40	0.900	0.514
1.43	0.763	0.514
1.51	0.635	0.516
1.66	0.516	0.522
1.81	0.446	0.527

Table 18 – Simulation results for the feasibility study considering a packing size of 40 mm and different $F_{L|0}/F_{G|1}$.

Packing size #40		
$F_{L|0}/F_{G|1}$	L/L_1	d/L_2
1.51	1.502	0.433
1.81	1.066	0.441
2.11	0.864	0.448
2.41	0.734	0.452
2.71	0.642	0.453

Table 19 – Simulation results for the feasibility study considering a packing size of 50 mm and different $F_{L|0}/F_{G|1}$.

Packing size #50		
$F_{L|0}/F_{G|1}$	L/L_1	d/L_2
2.71	1.344	0.381
3.02	1.205	0.381
3.32	1.099	0.383
3.62	1.014	0.385
4.07	0.912	0.388
4.52	0.832	0.392
4.98	0.758	0.396
5.43	0.713	0.398
5.88	0.668	0.401

Table 20 – Simulation results for the feasibility study considering a packing size of 50 mm and different $F_{L|0}/F_{G|1}$.

Packing size #60		
$F_{L\|0}/F_{G\|1}$	L/L_1	d/L_2
4.52	1.058	0.371
4.98	0.976	0.374
5.43	0.907	0.377
5.88	0.849	0.380
6.33	0.800	0.382
6.79	0.756	0.385

Appendix E – Example of the procedure followed in the determination of matrix $A_{j,i}$ in (Equation 3.13) (Pantelides, 2000)

Consider the following reaction scheme, where A, B, C and D represent some components:

$$A \leftrightharpoons B$$

Equation E-1

$$B + C \leftrightharpoons D$$

Equation E-2

Initially consider that both reactions are rate-based. Then the material balances for each component in this system are given by:

$$\frac{\partial M_A}{\partial t} = F_{A,in} - F_{A,out} + V.(-1 \times r_1)$$

$$\frac{\partial M_B}{\partial t} = F_{B,in} - F_{B,out} + V.(1 \times r_1 - 1 \times r_2)$$

$$\frac{\partial M_C}{\partial t} = F_{C,in} - F_{C,out} + V.(-1 \times r_2)$$

$$\frac{\partial M_D}{\partial t} = F_{D,in} - F_{D,out} + V.(1 \times r_2)$$

Each material balance can be re-write as follows:

$$w_A \frac{\partial M_A}{\partial t} = w_A . F_{A,in} - w_A . F_{A,out} + V . w_A . (-1 \times r_1)$$

$$w_B \frac{\partial M_B}{\partial t} = w_B . F_{B,in} - w_B . F_{B,out} + V . w_B . (1 \times r_1 - 1 \times r_2)$$

$$w_C \frac{\partial M_C}{\partial t} = w_C . F_{C,in} - w_C . F_{C,out} + V . w_C . (-1 \times r_2)$$

$$w_D \frac{\partial M_D}{\partial t} = w_D . F_{D,in} - w_D . F_{D,out} + V . w_D . (1 \times r_2)$$

Hence the overall material balance is given by the summation of all the individual material balances:

$$\sum_{i=A}^{D} w_i \frac{\partial M_i}{\partial t} = \sum_{i=A}^{D} w_i . F_{i,in} - \sum_{i=A}^{D} w_i . F_{i,out} + V . \sum_{i=A}^{D} w_i \left(\sum_{j=1}^{2} \nu_{i,j} . r_j \right)$$

Equation E-3

The last term of the above equation can be rearranged as follows:

$$V . \sum_{i=A}^{D} w_i \left(\sum_{j=1}^{2} \nu_{i,j} . r_j \right) = V . \sum_{j=1}^{2} r_j \left(\sum_{i=A}^{D} w_i . \nu_{i,j} \right)$$

Now consider that Equation E-1 is at chemical equilibrium and therefore to eliminate r_1 from Equation E-3 we have to choose the coefficients $w_i,\ i = A, . . , D$ so that:

$$\sum_{i=A}^{D} w_i . \nu_{i,1} = 0$$

Equation E-4

Equation E-4 can be written in terms of a product of matrixes as:

$$[w_A \quad w_B \quad w_C \quad w_D] . \begin{bmatrix} -1 \\ 1 \\ 0 \\ 0 \end{bmatrix} = 0$$

Equation E-5

In other words, the matrix $\begin{bmatrix} -1 \\ 1 \\ 0 \\ 0 \end{bmatrix}$ is the matrix of the stoichiometric coefficients of the reaction at chemical equilibrium which in this case was Equation E-1. Consider now that $\nu^{eq} = \begin{bmatrix} -1 \\ 1 \\ 0 \\ 0 \end{bmatrix}$.

Then Equation E-5 can be written as:

$$w^T . \nu^{eq} = 0$$

Equation E-6

Equation E-6 indicates that the required $w^{(k)}$ are the null vectors of the matrix ν^{eq}. Since ν^{eq} has 4 rows and 1 column there are 3 linearly independent null vectors (k = 3). Therefore the matrix w^T is given by:

$$w^T = \begin{bmatrix} w_A^{(1)} & w_B^{(1)} & w_C^{(1)} & w_D^{(1)} \\ w_A^{(2)} & w_B^{(2)} & w_C^{(2)} & w_D^{(2)} \\ w_A^{(3)} & w_B^{(3)} & w_C^{(3)} & w_D^{(3)} \end{bmatrix}$$

Finally the new equation for the overall material balance for this example is given by:

$$w_i{}^T \times \frac{\partial M_i}{\partial t} = w_i{}^T . F_{i,in} - w_i{}^T . F_{i,out} + V . \left[w_i{}^T . \left(\sum_{j=1}^{2} \nu_{i,j} . r_j \right) \right]$$

This was the procedure followed to determine the matrix $\boldsymbol{A_{j,i}}$ used in the material balances of the liquid phase. In this example the matrix $\boldsymbol{A_{j,i}}$ was equal to the matrix $w_i{}^T$.

Appendix F – gPROMS implementation code

Absorption Column (composite model)

```
PARAMETER
   no_grid_points      AS INTEGER

UNIT
   gas_bulk            AS Gas_bulk
   liquid_bulk         AS Liquid_bulk
   interface           AS Interface
   reaction_kinetics   AS Reaction_kinetics
   MTC                 AS Mass_transfer

PORT
   gas_inlet           AS PMLMaterial
   gas_outlet          AS PMLMaterial
   liquid_inlet        AS PMLMaterial
   liquid_outlet       AS PMLMaterial

PORTSET
   # Start Port Sets
      "flow" AS [gas_inlet, gas_outlet, liquid_inlet, liquid_outlet]
   # End Port Sets

TOPOLOGY
   gas_inlet = gas_bulk.inlet ;
   gas_outlet = gas_bulk.Outlet ;
   liquid_inlet = liquid_bulk.inlet ;
   liquid_outlet = liquid_bulk.Outlet ;

EQUATION
# Connectivity equations
   gas_bulk.molar_fraction(,)          = interface.gas_molar_fraction(,) ;
   gas_bulk.temperature()              = interface.gas_temperature() ;
   gas_bulk.pressure()                 = interface.pressure() ;
   gas_bulk.component_molar_flux(,)    = interface.gas_molar_flux(,) ;
   gas_bulk.heat_flux()                = interface.gas_heat_flux() ;
   interface.molar_concentration(,)    = liquid_bulk.molar_concentration(,) ;
   interface.liquid_molar_density()    = liquid_bulk.molar_density() ;
   interface.liquid_temperature()      = liquid_bulk.temperature() ;
   interface.pressure()                = liquid_bulk.pressure() ;
   interface.liquid_molar_flux(,)      = liquid_bulk.component_molar_flux(,) ;
   interface.liquid_heat_flux()        = liquid_bulk.heat_flux() ;
   liquid_bulk.molar_concentration(,)  = reaction_kinetics.component_molar_concentration(,) ;
   liquid_bulk.component_global_reaction_rate(,)       = reaction_kinetics.component_reaction_rate(,) ;
   liquid_bulk.equilibrium_constant(,)                 = reaction_kinetics.equilibrium_constant(,) ;
   liquid_bulk.pressure()          = reaction_kinetics.pressure() ;
   MTC.gas_density()           = gas_bulk.mass_density() ;
   MTC.gas_viscosity()         = gas_bulk.viscosity() ;
   MTC.gas_mass_fraction(,)    = gas_bulk.mass_fraction(,) ;
   MTC.gas_mass_flowrate()          = gas_bulk.mass_flowrate() ;
   MTC.pressure() = gas_bulk.pressure() ;
   MTC.liquid_density()        = liquid_bulk.mass_density() ;
   MTC.liquid_viscosity()      = liquid_bulk.viscosity() ;
   MTC.liquid_mass_flowrate()  = liquid_bulk.mass_flowrate() ;
   MTC.liquid_mass_fraction_phys_prop(,) = liquid_bulk.mass_fraction_phys_prop(,) ;
   MTC.liquid_total_volume_holdup() = liquid_bulk.total_volume_holdup() ;
   MTC.molar_concentration(,) = liquid_bulk.molar_concentration(,) ;
   MTC.gas_mass_transfer_coeff(,)      = interface.gas_mass_transfer_coefficient_Onda(,) ;
   MTC.liquid_mass_transfer_coeff()    = interface.liquid_mass_transfer_coefficient_Onda() ;
   MTC.liquid_diffusivity_CO2_solution()           = interface.liquid_diffusivity_CO2_solution() ;
   MTC.temperature() = interface.interface_temperature() ;
```

```
  liquid_bulk.column_height = gas_bulk.column_height ;
  liquid_bulk.column_diameter = gas_bulk.column_diameter ;
  liquid_bulk.packing_specific_area = gas_bulk.packing_specific_area ;
  liquid_bulk.packing_effective_area_ratio() = gas_bulk.packing_effective_area_ratio() ;
  liquid_bulk.packing_equivalent_diameter = gas_bulk.packing_equivalent_diameter ;


  interface.termolecular_forward_rate_constant_CO2()
        = reaction_kinetics.termolecular_forward_rate_constant_CO2() ;
  interface.interface_temperature() = reaction_kinetics.temperature() ;
  MTC.column_diameter = gas_bulk.column_diameter ;
  MTC.column_cross_section_area   = gas_bulk.column_cross_section_area ;
  MTC.packing_equivalent_diameter = gas_bulk.packing_equivalent_diameter ;
  MTC.packing_specific_area       = gas_bulk.packing_specific_area ;
  MTC.packing_void_fraction       = gas_bulk.packing_void_fraction ;
  MTC.packing_effective_area_ratio()       = liquid_bulk.packing_effective_area_ratio() ;
  MTC.column_height               = gas_bulk.column_height ;
```

Gas bulk sub-model

```
PARAMETER
  Components                AS ORDERED_SET
  phys_prop                 AS FOREIGN_OBJECT "PhysProp"
  molecular_weight          AS ARRAY(Components)     OF REAL   # [kg/mol]
  pi                   AS REAL DEFAULT 3.1415
  no_grid_points            AS INTEGER
  enthalpy_scale            AS REAL DEFAULT 1e4
  density_scale             AS REAL DEFAULT 1000
  viscosity_scale           AS REAL DEFAULT 1000
  pressure_scale            AS REAL DEFAULT 1000

DISTRIBUTION_DOMAIN
  column_axial              AS [ 0 : 1 ]      # Normalised distribution
  column_shifted_axial        AS [ 0 : 1 ]      # Normalised distribution
PORT
  inlet AS PMLMaterial
  Outlet AS PMLMaterial

PORTSET
  # Start Port Sets
    "flow" AS [inlet, outlet]
  # End Port Sets

VARIABLE
# Total quantities
  mass_flowrate               AS DISTRIBUTION(column_axial)       OF mass_flowrate
  mass_specific_enthalpy        AS DISTRIBUTION(column_axial)       OF mass_specific_enthalpy
  molar_flowrate              AS DISTRIBUTION(column_axial)       OF molar_flowrate
  mass_density                AS DISTRIBUTION(column_axial)       OF mass_density
  viscosity                 AS DISTRIBUTION(column_axial)       OF dynamic_viscosity
  velocity                  AS DISTRIBUTION(column_axial)       OF velocity
 energy_rate                  AS DISTRIBUTION(column_axial)       OF energy_rate
  heat_flux                  AS DISTRIBUTION(column_axial)       OF heat_flux_GLC

# Quantities of each component
  mass_fraction               AS DISTRIBUTION(Components,column_axial)        OF mass_fraction
  component_mass_flowrate     AS DISTRIBUTION(Components,column_axial)   OF mass_flowrate
  molar_fraction        AS DISTRIBUTION(Components,column_axial)        OF molar_fraction
component_molar_flowrate      AS DISTRIBUTION(Components,column_axial)     OF molar_flowrate
  component_molar_flux      AS DISTRIBUTION(Components,column_axial)     OF molar_flux

# Operating conditions
  pressure                  AS DISTRIBUTION(column_shifted_axial)           OF pressure
  temperature                 AS DISTRIBUTION(column_axial)                 OF temperature

# Design variables
  column_diameter             AS length_GLC
```

```
    column_height                  AS length_GLC
    column_height_input            AS length_GLC
    column_cross_section_area      AS area

# Packing speficification "parameters"
    packing_specific_area                AS no_type_gtzero
    packing_void_fraction              AS no_type_positive_fraction
    packing_equivalent_diameter         AS length
    packing_effective_area_ratio        AS DISTRIBUTION(column_axial)       OF no_type_gtzero

# Key Results
    capture_efficiency                       AS DISTRIBUTION(column_axial)       OF no_type
    capture_efficiency_input            AS no_type

SELECTOR
    column_height_selector      AS(input,result)    DEFAULT input

SET
    phys_prop := inlet.phys_prop ;
    Components := phys_prop.Components ;
    molecular_weight() := phys_prop.MolecularWeight()*1E-3 ;
    column_axial                  := [FFDM,1,no_grid_points];
    column_shifted_axial          := [BFDM,1,no_grid_points];

BOUNDARY
# z = 1 (at gas inlet)
    mass_flowrate(1) = inlet.mass_flowrate ;
    mass_fraction(,1) = inlet.mass_fraction ;
    mass_specific_enthalpy(1) = inlet.mass_specific_enthalpy ;

EQUATION
# Connectivity equations
# z = 1 (at gas inlet)
    inlet.mass_fraction() = inlet.info_mass_fraction() ;
    inlet.mass_specific_enthalpy = inlet.info_mass_specific_enthalpy ;
    pressure(1) = inlet.info_pressure ;

# z = 0 (at gas outlet)
    mass_flowrate(0)  = Outlet.mass_flowrate ;
  mass_fraction(,0) = Outlet.mass_fraction() ;
    mass_specific_enthalpy(0) = Outlet.mass_specific_enthalpy ;
    pressure(0) = Outlet.info_pressure ;

# Pressure drop along the column
    FOR z := 0|+ TO 1 DO
        (1/pressure_scale)
        * PARTIAL(pressure(z), column_shifted_axial) / column_height
      = (1/pressure_scale)
        *  (         (150*(1-packing_void_fraction)^2*velocity(z)*viscosity(z))
        / (packing_void_fraction^3*packing_equivalent_diameter^2)
        + (1.75*(1-packing_void_fraction)*mass_density(z)*velocity(z)^2)
        / (packing_void_fraction^3*packing_equivalent_diameter)
        ) ;
    END # For z

# Superficial velocity or velocity per empty column
    FOR z := 0 TO 1 DO
        mass_flowrate(z)
      = velocity(z) * column_cross_section_area * mass_density(z);
    END # For

# Cross section area of the column
    column_cross_section_area = (pi/4) * column_diameter^2 ;

# MASS BALANCE for each component
    FOR z := 0 TO 1|- DO
        FOR i in Components DO
```

```
            0 = - ( 1/column_cross_section_area
            * PARTIAL(component_mass_flowrate(i,z) , column_axial) / column_height )
            + ( component_molar_flux(i,z)*molecular_weight(i)
            * packing_specific_area*packing_effective_area_ratio(z) ) ;
        END # For i
    END # For z

# Definition of each component mass flowrate
    FOR z := 0 TO 1 DO
        FOR i IN Components DO
            component_mass_flowrate(i,z) = mass_fraction(i,z) * mass_flowrate(z) ;
        END # For i
    END # For z

# Definition of total mass flowrate
    FOR z := 0 TO 1|- DO
        mass_flowrate(z) = SIGMA(component_mass_flowrate(,z)) ;
    END # For z

# ENERGY BALANCE
    FOR z := 0 TO 1|- DO
        0
      =  ( -1/column_cross_section_area * PARTIAL(energy_rate(z) , column_axial) / column_height )
        + ( heat_flux(z) * packing_specific_area * packing_effective_area_ratio(z) ) ;
    END # For

# Relation between energy rate and mass flowrate
    FOR z := 0 TO 1 DO
        (1/enthalpy_scale) * energy_rate(z)
      = (1/enthalpy_scale) * mass_flowrate(z) * mass_specific_enthalpy(z) ;
    END # For

# Relation between mass flowrate and molar flowrate for each component
    FOR z := 0 TO 1 DO
        FOR i IN Components DO
            component_mass_flowrate(i,z) = component_molar_flowrate(i,z) * molecular_weight(i) ;
        END # For i
    END # For z

# Total molar flowrate
    FOR z := 0 TO 1 DO
        molar_flowrate(z) = SIGMA( component_molar_flowrate(,z) ) ;
    END # For z

# Molar fraction of each component
    FOR z := 0 TO 1 DO
        FOR i IN Components DO
            component_molar_flowrate(i,z) = molar_fraction(i,z) * molar_flowrate(z) ;
        END # For i
    END # For z

# Capture efficiency
    FOR z := 0 TO 1 DO
        capture_efficiency(z)
      = ( component_mass_flowrate('CO2',1) - component_mass_flowrate('CO2',z) )
        / component_mass_flowrate('CO2',1) * 100 ;
    END # For z

# Physical Properties calculation
    FOR z := 0 TO 1 DO
        (1/enthalpy_scale)*mass_specific_enthalpy(z)
      = (1/enthalpy_scale)
        * phys_prop.VapourEnthalpy( temperature(z), pressure(z), mass_fraction(,z) ) ;
        (1/density_scale)*mass_density(z)
      = (1/density_scale)
        * phys_prop.VapourDensity( temperature(z), pressure(z), mass_fraction(,z) ) ;
        (1*viscosity_scale)*viscosity(z)
```

```
     = (1*viscosity_scale)
       * phys_prop.VapourViscosity( temperature(z), pressure(z), mass_fraction(,z) ) ;
   END # For z

# Column height selector
   CASE column_height_selector OF
      WHEN input:
         column_height = column_height_input ;
         capture_efficiency_input = 1 ;
      WHEN result:
         capture_efficiency(0) = capture_efficiency_input ;
         column_height_input = 1e-5 ;
   END # Case
```

Interface sub-model

```
PARAMETER
   Components                  AS ORDERED_SET
   phys_prop                   AS FOREIGN_OBJECT "PhysProp"
   molecular_weight             AS ARRAY(Components)       OF REAL
   Pure_MEA_coeff               AS ARRAY(Components)       OF REAL
   Pure_H2O_coeff              AS ARRAY(Components)       OF REAL
   henry_binary_coefficient    AS ARRAY(4)                OF REAL
   ideal_gas_constant          AS REAL DEFAULT 8.314
   no_grid_points              AS INTEGER
   henry_scale                AS REAL DEFAULT 1e3
   flux_scale               AS REAL DEFAULT 1e3
   fraction_scale             AS REAL DEFAULT 1e3
   density_scale              AS REAL DEFAULT 1e3
   reaction_rate_scale        AS REAL DEFAULT 1e5

DISTRIBUTION_DOMAIN
   column_axial               AS [ 0 : 1 ]    # Normalised distribution

VARIABLE
# Quantities of each component
   gas_molar_fraction            AS DISTRIBUTION(Components,column_axial)        OF molar_fraction
  interface_gas_molar_fraction    AS DISTRIBUTION(Components,column_axial)     OF molar_fraction
   interface_molar_concentration  AS DISTRIBUTION(Components,column_axial) OF      molar_concentration
   molar_concentration     AS DISTRIBUTION(Components,column_axial)  OF molar_concentration
   gas_molar_flux               AS DISTRIBUTION(Components,column_axial)        OF molar_flux
   liquid_molar_flux            AS DISTRIBUTION(Components,column_axial)        OF molar_flux

# Total quantities
   gas_heat_flux                AS DISTRIBUTION(column_axial)          OF heat_flux_
   liquid_heat_flux             AS DISTRIBUTION(column_axial)          OF heat_flux_GLC
   liquid_molar_density           AS DISTRIBUTION(column_axial)          OF molar_concentration

# Operating conditions
   pressure                    AS DISTRIBUTION(column_axial)          OF pressure
   gas_temperature                AS DISTRIBUTION(column_axial)          OF temperature
  interface_temperature           AS DISTRIBUTION(column_axial)          OF temperature
   liquid_temperature             AS DISTRIBUTION(column_axial)          OF temperature

# Vapour-Liquid equilibrium variables
   henry_constant_CO2             AS DISTRIBUTION(column_axial)          OF no_type_gtzero
   henry_constant_N2O             AS DISTRIBUTION(column_axial)          OF no_type_gtzero
   henry_constant_CO2_in_water    AS DISTRIBUTION(column_axial)          OF no_type_gtzero
   henry_constant_N2O_in_water    AS DISTRIBUTION(column_axial)          OF no_type_gtzero
   henry_constant_N2O_in_MEA       AS DISTRIBUTION(column_axial)          OF no_type_gtzero
   henry_excess                 AS DISTRIBUTION(column_axial)          OF no_type
   vapour_pressure_H2O            AS DISTRIBUTION(column_axial)          OF pressure
   molar_volume_MEA               AS DISTRIBUTION(column_axial)          OF molar_specific_volume
   molar_volume_H2O               AS DISTRIBUTION(column_axial)          OF molar_specific_volume
   liquid_volume_fraction         AS DISTRIBUTION(Components,column_axial)       OF molar_fraction
   molar_fraction_binary          AS DISTRIBUTION(Components,column_axial)       OF molar_fraction
```

```
# Mass transfer variables
   gas_mass_transfer_coefficient  AS DISTRIBUTION(Components,column_axial) OF no_type_gtzero
   gas_mass_transfer_coefficient_Onda          AS DISTRIBUTION(Components,column_axial)        OF
no_type_gtzero
   gas_mass_transfer_coefficient_input     AS DISTRIBUTION(Components) OF no_type_gtzero
   liquid_mass_transfer_coefficient            AS DISTRIBUTION(column_axial)       OF no_type_gtzero
   liquid_mass_transfer_coefficient_Onda       AS DISTRIBUTION(column_axial)  OF no_type_gtzero
   liquid_mass_transfer_coefficient_input      AS no_type_gtzero
   enhancement_factor                          AS DISTRIBUTION(column_axial)       OF no_type_gtzero
   termolecular_forward_rate_constant_CO2      AS DISTRIBUTION(column_axial)       OF reaction_rate_GLC
   liquid_diffusivity_CO2_solution             AS DISTRIBUTION(column_axial)       OF diffusivity

# Heat transfer variables
   gas_heat_transfer_coefficient                  AS no_type_gtzero
   gas_heat_transfer_coefficient_input          AS no_type_gtzero
   liquid_heat_transfer_coefficient             AS no_type_gtzero
   liquid_heat_transfer_coefficient_input      AS no_type_gtzero

SELECTOR
   mass_transfer_coeff_selector            AS(constant_k,Onda)     DEFAULT Onda
   heat_transfer_coeff_selector            AS(constant_h,corr_2)   DEFAULT constant_h

SET
   Components := phys_prop.Components ;
   phys_prop := 'Multiflash::ABSORPTION_COLUMN.mfl' ;
   henry_binary_coefficient() := [4.793, -7.446e-3, 0, -2.201] ;
   molecular_weight() := phys_prop.MolecularWeight()*1E-3 ;

#                  CO2, N2, O2, H2O, MEA, H3O+, MEA.CO2-, HMEA+
   Pure_MEA_coeff := [ 0 , 0 , 0 , 0 , 1 , 0 , 0 , 0 ] ;
   Pure_H2O_coeff := [ 0 , 0 , 0 , 1 , 0 , 0 , 0 , 0 ] ;
   column_axial := [CFDM,2,no_grid_points] ;

EQUATION
   FOR z := 0 TO 1 DO
      (1*flux_scale) * gas_molar_flux('CO2',z)
    = (1*flux_scale) * gas_mass_transfer_coefficient('CO2',z)
      * ( pressure(z) / ( ideal_gas_constant*interface_temperature(z) ) )
      * ( gas_molar_fraction('CO2',z) - interface_gas_molar_fraction('CO2',z) ) ;
      (1*flux_scale) * gas_molar_flux('H2O',z)
    = (1*flux_scale) * gas_mass_transfer_coefficient('H2O',z)
      * ( pressure(z) / ( ideal_gas_constant*interface_temperature(z) ) )
      * ( gas_molar_fraction('H2O',z) - interface_gas_molar_fraction('H2O',z) ) ;
   END # For z

 FOR z := 0 TO 1 DO
      (1*flux_scale) * liquid_molar_flux('CO2',z)
    = (1*flux_scale) * liquid_mass_transfer_coefficient(z)# * enhancement_factor(z)
      * ( interface_molar_concentration('CO2',z) - molar_concentration('CO2',z) ) ;
      (1*flux_scale) * liquid_molar_flux('H2O',z)
    = (1*flux_scale) * liquid_mass_transfer_coefficient(z)
      * ( interface_molar_concentration('H2O',z) - molar_concentration('H2O',z) ) ;
   END # For z

  FOR z := 0 TO 1 DO
      FOR i IN Components - ['CO2','H2O'] DO
         liquid_molar_flux(i,z) = 0 ;
          gas_molar_flux(i,z) = 0 ;
      END # For i
   END # For z

# Enhancement factor (dimensionless)
   FOR z := 0 TO 1 DO
      enhancement_factor(z)
    = ( 1 + liquid_diffusivity_CO2_solution(z)/liquid_mass_transfer_coefficient(z)^2
      * termolecular_forward_rate_constant_CO2(z) * molar_concentration('MEA',z) )^(1/2) ;
   END # For z
```

```
# Relation between gas molar flux and liquid molar flux for CO2 and H2O
  FOR z := 0 TO 1 DO
    (1*flux_scale) * gas_molar_flux('CO2',z)
   = (1*flux_scale) * liquid_molar_flux('CO2',z) ;
    (1*flux_scale) * gas_molar_flux('H2O',z)
   = (1*flux_scale) * liquid_molar_flux('H2O',z) ;
  END # For z

# Relation between gas molar fraction at the interface and the liquid molar fraction for CO2 and H2O
  FOR z := 0 TO 1 DO
    (1*fraction_scale) * interface_gas_molar_fraction('CO2',z)
   = (1*fraction_scale)
    * henry_constant_CO2(z)/pressure(z)
    * interface_molar_concentration('CO2',z);
  END # For z

  FOR z := 0 TO 1 DO
    (1*fraction_scale) * interface_gas_molar_fraction('H2O',z)
   = (1*fraction_scale) *
    ( vapour_pressure_H2O(z)/pressure(z) )
    * ( interface_molar_concentration('H2O',z) / liquid_molar_density(z) ) ;
  END # For z

# Analogy between Henry's constant for CO2 and N2O in amine solutions
  FOR z:= 0 TO 1 DO
    (1/henry_scale) * henry_constant_CO2(z)
   = (1/henry_scale) * henry_constant_N2O(z)
    * ( henry_constant_CO2_in_water(z) / (henry_constant_N2O_in_water(z)) ) ;
  END # For z
# Henry's constants in pure solutions
  FOR z := 0 TO 1 DO
    (1/henry_scale) * henry_constant_CO2_in_water(z)
   = (1/henry_scale) * 2.8249e6 * EXP( -2044/interface_temperature(z) ) ;
    (1/henry_scale) * henry_constant_N2O_in_water(z)
   = (1/henry_scale) * 8.5470e6 * EXP( -2284/interface_temperature(z) ) ;
    (1/henry_scale) * henry_constant_N2O_in_MEA(z)
   = (1/henry_scale) * 1.207e5 * EXP( -1136.5/interface_temperature(z) ) ;
  END # For z

# Henry's constants in amine solutions
  FOR z := 0 TO 1 DO
    (1/henry_scale) * henry_constant_N2O(z)
   = (1/henry_scale) * EXP( henry_excess(z) )
    * henry_constant_N2O_in_MEA(z)^(liquid_volume_fraction('MEA',z))
    * henry_constant_N2O_in_water(z)^(liquid_volume_fraction('H2O',z)) ;
  END # For z

# Determination of the Henry excess parameter
  FOR z := 0 TO 1 DO
    (1*henry_scale) * henry_excess(z)
   = (1*henry_scale)*liquid_volume_fraction('MEA',z)*liquid_volume_fraction('H2O',z)
    * ( henry_binary_coefficient(1)
    + henry_binary_coefficient(2)*interface_temperature(z)
    + henry_binary_coefficient(3)*interface_temperature(z)^2
    + henry_binary_coefficient(4)*liquid_volume_fraction('H2O',z) ) ;
  END # For z

# Liquid volume fractions for the binary mixture H2O/MEA
  FOR z := 0 TO 1 DO
    (1*fraction_scale) * liquid_volume_fraction('MEA',z)
   = (1*fraction_scale) * molar_fraction_binary('MEA',z) * molar_volume_MEA(z)
    / ( molar_fraction_binary('MEA',z) * molar_volume_MEA(z)
    + molar_fraction_binary('H2O',z) * molar_volume_H2O(z) ) ;

    molar_fraction_binary('MEA',z)
   = molar_concentration('MEA',z)
```

```
    * 1/( molar_concentration('MEA',z) + molar_concentration('H2O',z) ) ;

   1 = SIGMA(liquid_volume_fraction(,z)) ;
    1 = SIGMA( molar_fraction_binary(,z) ) ;
  END # For z

# Liquid volume fractions for each component except H2O and MEA
  FOR z := 0 TO 1 DO
    FOR i IN Components - ['MEA','H2O'] DO
      molar_fraction_binary(i,z) = 0 ;
      liquid_volume_fraction(i,z) = 0 ;
    END # For i
  END # For z

# Physical Properties calculation for pure components
  FOR z := 0 TO 1 DO
    molar_volume_MEA(z)
   = phys_prop.LiquidVolume( interface_temperature(z),pressure(z),Pure_MEA_coeff() ) ;
    molar_volume_H2O(z)
   = phys_prop.LiquidVolume( interface_temperature(z),pressure(z),Pure_H2O_coeff() ) ;
    vapour_pressure_H2O(z)
   = SIGMA( phys_prop.VapourPressure( interface_temperature(z) ) * Pure_H2O_coeff() ) ;
  END # For z

# Heat transfer at the interface
  FOR z := 0 TO 1 DO
    gas_heat_flux(z)
   = gas_heat_transfer_coefficient * ( gas_temperature(z) - interface_temperature(z) ) ;

    liquid_heat_flux(z)
   = liquid_heat_transfer_coefficient * ( interface_temperature(z) - liquid_temperature(z) ) ;
  END # For z

  FOR z := 0 TO 1 DO
    gas_heat_flux(z) = liquid_heat_flux(z) ;
  END # For z

# Mass transfer coefficient selector, default Onda
 CASE  mass_transfer_coeff_selector OF
  WHEN constant_k:
    FOR i IN Components DO
      gas_mass_transfer_coefficient(i,) = gas_mass_transfer_coefficient_input(i);
    END # For i
      liquid_mass_transfer_coefficient() = liquid_mass_transfer_coefficient_input;
  WHEN Onda:
    FOR i IN Components DO
      gas_mass_transfer_coefficient(i,) = gas_mass_transfer_coefficient_Onda(i,);
      gas_mass_transfer_coefficient_input(i) = 1 ;
    END # For i
      liquid_mass_transfer_coefficient() = liquid_mass_transfer_coefficient_Onda();
      liquid_mass_transfer_coefficient_input = 1 ;
 END # Case

# Heat transfer coefficient selector, default constant_h
 CASE  heat_transfer_coeff_selector OF
  WHEN constant_h:
    gas_heat_transfer_coefficient = gas_heat_transfer_coefficient_input;
    liquid_heat_transfer_coefficient = liquid_heat_transfer_coefficient_input;
  WHEN corr_2:
    gas_heat_transfer_coefficient = gas_heat_transfer_coefficient_input;
    liquid_heat_transfer_coefficient = liquid_heat_transfer_coefficient_input;
 END # Case
```

Liquid bulk sub-model

```
PARAMETER
  Components         AS ORDERED_SET
```

```
    phys_prop           AS FOREIGN_OBJECT
    molecular_weight    AS ARRAY(Components)    OF REAL
    Reactions_eq  AS ORDERED_SET
    Reactions_eq_stoichiometric_coeff       AS ARRAY(Reactions_eq,Components)    OF REAL
    no_invariant_components         AS INTEGER
    reactor_data                    AS FOREIGN_OBJECT
    reaction_equilibrium_matrix  AS ARRAY(no_invariant_components, Components.CARD)  OF REAL
    gravitacional_constant  AS REAL DEFAULT 9.81
    pi                   AS REAL DEFAULT 3.14
    no_grid_points          AS INTEGER
    Components_contraction              AS ORDERED_SET
    MW                              AS ARRAY(Components_contraction)      OF REAL
    enthalpy_scale  AS REAL DEFAULT 1e5
    density_scale   AS REAL DEFAULT 1e3
    viscosity_scale AS REAL DEFAULT 1e5
    mol_conc_scale  AS REAL DEFAULT 1e2

DISTRIBUTION_DOMAIN
    column_axial    AS [ 0 : 1 ] # Normalised distribution

PORT
    inlet AS PMLMaterial
   outlet AS PMLMaterial

PORTSET
    # Start Port Sets
    "flow" AS [inlet, outlet]
    # End Port Sets

VARIABLE
# Total quantities
    total_holdup    AS DISTRIBUTION(column_axial)   OF molar_holdup_GLC
    total_mass_holdup  AS DISTRIBUTION(column_axial)        OF mass_holdup
    molar_flowrate  AS DISTRIBUTION(column_axial)   OF molar_flowrate
    molar_density   AS DISTRIBUTION(column_axial)   OF molar_concentration
    mass_density    AS DISTRIBUTION(column_axial)   OF mass_density
    total_volume_holdup AS DISTRIBUTION(column_axial)   OF molar_holdup_GLC
    velocity    AS DISTRIBUTION(column_axial)   OF velocity
    viscosity   AS DISTRIBUTION(column_axial)         OF dynamic_viscosity
    equilibrium_constant    AS DISTRIBUTION(Reactions_eq,column_axial)  OF reaction_rate_GLC
    mass_flowrate   AS DISTRIBUTION(column_axial)   OF mass_flowrate
    energy_rate             AS DISTRIBUTION(column_axial)   OF  energy_rate
    mass_specific_enthalpy  AS DISTRIBUTION(column_axial)   OF mass_specific_enthalpy
    mass_specific_internal_energy   AS DISTRIBUTION(column_axial)   OF mass_specific_enthalpy
    volume_specific_internal_energy AS DISTRIBUTION(column_axial)   OF volume_energy
    heat_flux                   AS DISTRIBUTION(column_axial)   OF heat_flux_GLC
    heat_of_absorption_CO2            AS heat_of_absorption_GLC
    mass_fraction_phys_prop           AS DISTRIBUTION(Components,column_axial)    OF mass_fraction
    mass_fraction_contraction          AS DISTRIBUTION(Components_contraction,column_axial)    OF
mass_fraction
    molar_fraction_contraction  AS DISTRIBUTION(Components_contraction,column_axial)    OF molar_fraction
    total_molar_concentration   AS DISTRIBUTION(Components_contraction,column_axial)    OF
molar_concentration
    mass_density_phys_prop  AS mass_density
    local_loading    AS DISTRIBUTION(column_axial)   OF no_type_positive_fraction
    weight_concentration_MEA    AS DISTRIBUTION(column_axial)   OF no_type_positive_fraction

# Quantities of each component
    component_holdup        AS DISTRIBUTION(Components,column_axial)    OF molar_holdup_GLC
    molar_fraction          AS DISTRIBUTION(Components,column_axial)    OF molar_fraction
    component_molar_flux    AS DISTRIBUTION(Components,column_axial)    OF molar_flux
    invariant_holdup        AS DISTRIBUTION(no_invariant_components,column_axial)   OF reaction_rate_GLC
    component_global_reaction_rate  AS DISTRIBUTION(Components,column_axial)    OF reaction_rate_GLC
    molar_concentration     AS DISTRIBUTION(Components,column_axial)    OF molar_concentration
    mass_fraction           AS DISTRIBUTION(Components,column_axial)    OF mass_fraction
    component_mass_flowrate AS DISTRIBUTION(Components,column_axial)    OF mass_flowrate
```

```
# Operating conditions
    pressure    AS DISTRIBUTION(column_axial)   OF pressure
    temperature     AS DISTRIBUTION(column_axial)  OF temperature

# Design variables
    column_height   AS length_GLC
    column_diameter    AS length_GLC
    column_cross_section_area        AS area

# Packing specification "parameters"
    packing_specific_area   AS no_type_gtzero
    packing_effective_area_ratio    AS DISTRIBUTION(column_axial) OF no_type_gtzero
    packing_equivalent_diameter   AS no_type_positive_fraction

# Test variables
    a   AS ARRAY(no_invariant_components, Components.CARD)  OF no_type

SET
    Components := phys_prop.Components ;
    phys_prop := inlet.phys_prop;
    molecular_weight() := phys_prop.MolecularWeight()*1e-3 ;
    Reactions_eq := ['HMEA+H2O','electrical_neutrality'] ;

# Components                               ['CO2','N2','O2','H2O','MEA','H3O+','MEA.CO2-','HMEA+'] ;
    Reactions_eq_stoichiometric_coeff('HMEA+H2O',) := [0,0,0,0,1,1,0,-1] ;
    Reactions_eq_stoichiometric_coeff('electrical_neutrality',) := [0,0,0,0,0,1,-1,1] ;
    no_invariant_components := Components.CARD - Reactions_eq.CARD ;
    reactor_data              := "EquilibriumFO";
    FOR j := 1 TO no_invariant_components DO
        FOR i := 1 TO Components.CARD DO
            reaction_equilibrium_matrix(j,i)
         := reactor_data.CalculateNullVectors
            (Components.CARD,Reactions_eq.CARD,j,i,Reactions_eq_stoichiometric_coeff);
        END # For
    END # For
    column_axial := [BFDM,1,no_grid_points] ;
    Components_contraction := ['CO2','H2O','MEA'] ;
    MW := [44e-3, 18e-3, 61e-3] ;

BOUNDARY
# z = 0 (at liquid inlet)
    mass_flowrate(0) = inlet.mass_flowrate ;
    mass_fraction(,0) = inlet.mass_fraction ;
    (1/enthalpy_scale) * mass_specific_enthalpy(0)
        = (1/enthalpy_scale) * inlet.mass_specific_enthalpy ;

EQUATION
# Connectivity equations
# z = 0 (at liquid inlet)
    inlet.mass_fraction() = inlet.info_mass_fraction() ;
    (1/enthalpy_scale) * inlet.mass_specific_enthalpy
        = (1/enthalpy_scale) * inlet.info_mass_specific_enthalpy ;

# z = 1 (at liquid outlet)
    mass_flowrate(1)  = outlet.mass_flowrate ;
    mass_fraction(,1) = outlet.mass_fraction() ;
    (1/enthalpy_scale) * mass_specific_enthalpy(1)   = (1/enthalpy_scale) * outlet.mass_specific_enthalpy ;
    pressure(1) = outlet.info_pressure ;

# Relation between mass fractions and molar fractions
    FOR z := 0 TO 1 DO
        FOR i IN Components - Components.last DO
            mass_fraction(i,z) / molecular_weight(i)
          = molar_fraction(i,z) * SIGMA( mass_fraction(,z)/molecular_weight() ) ;
        END # For i
    END # For z
    FOR z := 0 TO 1 DO
```

```
        SIGMA(molar_fraction(,z)) = 1 ;
    END # For z

# Relation between mass flowrate and molar flowrate
    FOR z := 0|+ TO 1 DO
        mass_flowrate(z) = SIGMA(component_mass_flowrate(,z) ) ;
    END # For z
    FOR z := 0 TO 1 DO
        FOR i IN Components DO
            component_mass_flowrate(i,z) = mass_flowrate(z) * mass_fraction(i,z) ;
        END # For i
    END # For z
    FOR z := 0 TO 1 DO
        molar_flowrate(z) = SIGMA( component_mass_flowrate(,z) / molecular_weight() ) ;
    END # For z

# Relation between mass density and molar density
   FOR z := 0 TO 1 DO
        (1/density_scale) * molar_density(z)
            = (1/density_scale) * SIGMA( mass_fraction(,z)/molecular_weight() ) * mass_density(z) ;
    END # For z

# Molar concentration of each component
    FOR z := 0 TO 1 DO
        FOR i IN Components DO
            molar_concentration(i,z) = molar_fraction(i,z) * molar_density(z) ;
        END # For i
    END # For z

# Total holdup
    FOR z := 0 TO 1 DO
              total_holdup(z) = molar_density(z) * total_volume_holdup(z) ;
    END # For z

# Volume holdup below the loading point
    FOR z := 0 TO 1 DO
        total_volume_holdup(z)
      = (12/gravitacional_constant * viscosity(z)/mass_density(z)
        * velocity(z) * packing_specific_area^(2))^(1/3) ;
    END # For z

# Superficial velocity or velocity per empty column
    FOR z := 0 TO 1 DO
        mass_flowrate(z)
      = velocity(z) * column_cross_section_area * mass_density(z) ;
    END # For z

# Cross section area
    column_cross_section_area = pi/4 * column_diameter^2 ;

# Holdup of each component
    FOR z := 0 TO 1 DO
        FOR i IN Components DO
            component_holdup(i,z) = molar_fraction(i,z) * total_holdup(z) ;
        END # For i
    END # For z

# Invariant holdups
    FOR z := 0 TO 1 DO
        FOR k := 1 TO no_invariant_components DO
            invariant_holdup(k,z) = SIGMA( reaction_equilibrium_matrix(k,)*component_holdup(,z) ) ;
        END # For k
    END # For z

# Invariant material balances (molar)
    FOR z := 0|+ TO 1 DO
        FOR k := 1 TO no_invariant_components DO
```

```
      $invariant_holdup(k,z)
     = -1/(column_cross_section_area)
      * PARTIAL ( molar_flowrate(z) * SIGMA( reaction_equilibrium_matrix(k,)*molar_fraction(,z) )
      , column_axial ) / column_height
      + SIGMA( reaction_equilibrium_matrix(k,)*component_molar_flux(,z)
      * packing_specific_area * packing_effective_area_ratio(z) )
      + SIGMA( reaction_equilibrium_matrix(k,)
      * component_global_reaction_rate(,z) ) ;
    END # FOr k
  END # For z

# Equilibrium constants
  FOR z:= 0|+ TO 1 DO
    FOR j IN Reactions_eq - ['electrical_neutrality'] DO
      equilibrium_constant(j,z)
     = PRODUCT( molar_concentration(,z)^Reactions_eq_stoichiometric_coeff(j,) ) ;
    END # For j
  END # For z

# Electrical neutrality constrain
  FOR z := 0|+ TO 1 DO
    equilibrium_constant('electrical_neutrality',z) * molar_concentration('MEA.CO2-',z)
   = molar_concentration('HMEA+',z) + molar_concentration('H3O+',z) ;
  END # For z

# Total mass holdup
  FOR z := 0 TO 1 DO
    total_mass_holdup(z) = SIGMA(component_holdup(,z) * molecular_weight()) ;
  END # For z

# Matrix of null vectors
  a(,) = reaction_equilibrium_matrix(,) ;

# Energy balance
  FOR z := 0|+ TO 1 DO
       $volume_specific_internal_energy(z)
   = (( -1/column_cross_section_area * PARTIAL( energy_rate(z),column_axial ) / column_height )
    + ( heat_flux(z) * packing_specific_area * packing_effective_area_ratio(z) )
    + ( heat_of_absorption_CO2 * component_molar_flux('CO2',z) )
    * packing_specific_area * packing_effective_area_ratio(z)
    )/(1e8)*(1e8) ;
  END # For

# Energy holdup (relation between volume specific internal energy and mass specific internal energy
  FOR z := 0 TO 1 DO
    (1/enthalpy_scale) * volume_specific_internal_energy(z)
   = (1/enthalpy_scale)
    * mass_specific_internal_energy(z) * mass_density(z) ;
  END # For z

# Relation between mass specific internal energy and mass specific enthalpy
  FOR z := 0 TO 1 DO
    (1/enthalpy_scale) * mass_specific_internal_energy(z)
   = (1/enthalpy_scale)
    * ( mass_specific_enthalpy(z) - pressure(z)/mass_density(z) ) ;
  END # For

# Relation between energy rate and total mass flowrate
  FOR z := 0 TO 1 DO
    (1/enthalpy_scale) * energy_rate(z)
   = (1/enthalpy_scale)
    * mass_flowrate(z) * mass_specific_enthalpy(z) ;
  END # For
  FOR z := 0 TO 1 DO
    local_loading(z) * total_molar_concentration('MEA',z) = total_molar_concentration('CO2',z) ;
  END # For z
  FOR z := 0 TO 1 DO
```

```
        total_molar_concentration('MEA',z) * molecular_weight('MEA')
      = weight_concentration_MEA(z) * total_molar_concentration('H2O',z) * molecular_weight('H2O') ;
    END # For z

# Physical Properties calculation
# Contraction of the list of components to exclude the ion species
    FOR z := 0 TO 1 DO
        total_molar_concentration('CO2',z) = molar_concentration('CO2',z) + molar_concentration('MEA.CO2-',z) ;
        total_molar_concentration('MEA',z)
      = molar_concentration('MEA',z) + molar_concentration('MEA.CO2-',z) + molar_concentration('HMEA+',z) ;
        total_molar_concentration('H2O',z) = molar_concentration('H2O',z) + molar_concentration('H3O+',z) ;
    END # For z

    FOR z := 0 TO 1 DO
        (1*mol_conc_scale) * molar_fraction_contraction('CO2',z) / (molar_fraction_contraction('MEA',z))
      = (1*mol_conc_scale) * total_molar_concentration('CO2',z) / (total_molar_concentration('MEA',z)) ;
    END # For z

    mass_density_phys_prop = 1000 ;
    FOR z:= 0 TO 1 DO
        (1/mol_conc_scale) * total_molar_concentration('MEA',z)
      = (1/mol_conc_scale) * mass_density_phys_prop
        * ( mass_fraction_contraction('MEA',z) / molecular_weight('MEA') ) ;
    END # For z

    FOR z := 0 TO 1 DO
        SIGMA ( molar_fraction_contraction(,z) ) = 1 ;
    END # For z

    FOR z := 0 TO 1 DO
        FOR i IN Components_contraction DO
            mass_fraction_contraction(i,z)
         =  molar_fraction_contraction(i,z) * MW(i)
            / SIGMA( molar_fraction_contraction(,z) * MW() ) ;
        END # For i
    END # For z

    FOR z := 0 TO 1 DO
        FOR i IN Components_contraction DO
            mass_fraction_phys_prop(i,z) = mass_fraction_contraction(i,z) ;
              END # For i
    END # For z

    FOR z := 0 TO 1 DO
            mass_fraction_phys_prop('N2',z) = 0 ;
            mass_fraction_phys_prop('O2',z) = 0 ;
            mass_fraction_phys_prop('MEA.CO2-',z) = 0 ;
            mass_fraction_phys_prop('H3O+',z) = 0 ;
            mass_fraction_phys_prop('HMEA+',z) = 0 ;
    END # For z

    FOR z := 0 TO 1 DO
            (1/enthalpy_scale) * mass_specific_enthalpy(z)
          = phys_prop.LiquidEnthalpy( temperature(z), pressure(z), mass_fraction_phys_prop(,z) )
            * (1/enthalpy_scale) ;
            (1/density_scale) * mass_density(z)
          = phys_prop.LiquidDensity( temperature(z), pressure(z), mass_fraction_phys_prop(,z) )
            * (1/density_scale) ;
             (1*viscosity_scale) * viscosity(z)
          = phys_prop.LiquidViscosity( temperature(z), pressure(z), mass_fraction_phys_prop(,z) )
            * (1*viscosity_scale) ;
    END # For z
```

Mass transfer sub-model

```
PARAMETER
    Components                          AS ORDERED_SET
```

```
    phys_prop                       AS FOREIGN_OBJECT "PhysProp"
    gravitacional_constant          AS REAL DEFAULT 9.81
    pi                              AS REAL DEFAULT 3.1415
    ideal_gas_constant              AS REAL DEFAULT 8.314
    no_grid_points                  AS INTEGER
    molecular_weight                AS ARRAY(Components)    OF REAL

# Scaling parameters
    scale_factor        AS REAL DEFAULT 1e4

DISTRIBUTION_DOMAIN
    column_axial                    AS [ 0 : 1 ] # Normalised distribution

VARIABLE
# Packing specifications
    packing_specific_area                AS no_type_gtzero
    packing_equivalent_diameter          AS length
    packing_void_fraction                AS no_type_gtzero
    packing_effective_area_ratio         AS DISTRIBUTION(column_axial)   OF no_type_gtzero
    packing_critical_surface_tension     AS surface_tension
    column_cross_section_area            AS area
    effective_transfer_area              AS DISTRIBUTION(column_axial)   OF no_type_gtzero

# Properties of the components, the solvent and/or their molecules
    atomic_diffusion_volume              AS ARRAY(Components)          OF no_type_gtzero
    solvent_diffusivity_coeff            AS no_type_gtzero

# Operating conditions
    pressure                             AS DISTRIBUTION(column_axial) OF pressure
    temperature                          AS DISTRIBUTION(column_axial) OF temperature

# Gas side
    gas_mass_flowrate                    AS DISTRIBUTION(column_axial) OF mass_flowrate
    gas_mass_fraction                    AS DISTRIBUTION(Components,column_axial) OF mass_fraction
    gas_density                          AS DISTRIBUTION(column_axial) OF mass_density
    gas_viscosity                        AS DISTRIBUTION(column_axial) OF dynamic_viscosity
    gas_mass_superficial_velocity        AS DISTRIBUTION(column_axial)   OF no_type_gtzero
    gas_diffusivity                      AS DISTRIBUTION(Components,column_axial)    OF diffusivity

# Liquid side
    liquid_mass_flowrate                 AS DISTRIBUTION(column_axial) OF mass_flowrate
   liquid_mass_fraction_phys_prop  AS DISTRIBUTION(Components,column_axial)  OF mass_fraction
   liquid_mass_fraction_st     AS DISTRIBUTION(Components,column_axial)    OF mass_fraction
    liquid_density                       AS DISTRIBUTION(column_axial)   OF mass_density
    liquid_viscosity                     AS DISTRIBUTION(column_axial)   OF dynamic_viscosity
    liquid_mass_superficial_velocity     AS DISTRIBUTION(column_axial)   OF no_type_gtzero
    liquid_diffusivity                   AS DISTRIBUTION(column_axial)   OF diffusivity
    liquid_surface_tension               AS DISTRIBUTION(column_axial)   OF surface_tension
    liquid_total_volume_holdup           AS DISTRIBUTION(column_axial)   OF volume_holdup_GLC

# Mass transfer coefficient
    liquid_mass_transfer_coeff           AS DISTRIBUTION(column_axial) OF diffusivity
    gas_mass_transfer_coeff              AS DISTRIBUTION(Components,column_axial) OF diffusivity

# Ko correlation for liquid diffusivity
liquid_diffusivity_N2O_water           AS DISTRIBUTION(column_axial)   OF diffusivity
liquid_diffusivity_CO2_water           AS DISTRIBUTION(column_axial)   OF diffusivity
liquid_diffusivity_N2O_solution           AS DISTRIBUTION(column_axial)   OF diffusivity
liquid_diffusivity_CO2_solution           AS DISTRIBUTION(column_axial)   OF diffusivity
molar_concentration     AS DISTRIBUTION(Components,column_axial)   OF molar_concentration

# Wetted area
    liquid_Reynolds AS DISTRIBUTION(column_axial)   OF no_type_gtzero
    liquid_Froude   AS DISTRIBUTION(column_axial)   OF no_type_gtzero
    liquid_Weber    AS DISTRIBUTION(column_axial)   OF no_type_gtzero
    surface_tension_ratio   AS DISTRIBUTION(column_axial)   OF no_type_gtzero
    packing_wetted_area_ratio AS DISTRIBUTION(column_axial)   OF no_type_positive_fraction
```

```
    column_height   AS length_GLC

# Flooding point
    flow_factor                        AS DISTRIBUTION(column_axial)   OF no_type_gtzero
    flooding_point_resistance_factor    AS DISTRIBUTION(column_axial)   OF no_type_gtzero
    flooding_point_packing_constant     AS DISTRIBUTION(column_axial)   OF no_type_gtzero
    flooding_point_packing_exponent     AS DISTRIBUTION(column_axial)   OF no_type
    flooding_point_gas_velocity         AS DISTRIBUTION(column_axial)   OF velocity
    flooding_liquid_holdup              AS DISTRIBUTION(column_axial)   OF volume_holdup_GLC
    column_diameter         AS length_GLC
    column_diameter_input   AS length_GLC
    new_column_diameter     AS DISTRIBUTION(column_axial)   OF length_GLC

SELECTOR
    column_diameter_selector      AS(input,result)    DEFAULT input

SET
    Components := phys_prop.Components ;
    phys_prop := "Multiflash::ABSORPTION_COLUMN.mfl" ;
    column_axial := [CFDM,2,no_grid_points] ;
    molecular_weight() := phys_prop.MolecularWeight() * 1e-3 ;

EQUATION
# Constants and assignments for the diffusions and the mass transfer coefficients:
    solvent_diffusivity_coeff = 2.6;
    atomic_diffusion_volume("CO2") = 26.9
    atomic_diffusion_volume("N2") = 18.5 ;
    atomic_diffusion_volume("O2") = 16.3 ;
    atomic_diffusion_volume("H2O") = 13.1 ;
    atomic_diffusion_volume("MEA") = 1 ;
    atomic_diffusion_volume("MEA.CO2-") = 1 ;
    atomic_diffusion_volume("H3O+") = 1 ;
    atomic_diffusion_volume("HMEA+") = 1 ;

# Liquid film [properties - mass transfer coefficient]:
    FOR z := 0 TO 1 DO
        liquid_diffusivity_CO2_solution(z)/liquid_diffusivity_N2O_solution(z)
      = liquid_diffusivity_CO2_water(z)/liquid_diffusivity_N2O_water(z) ;
    END # For z

    FOR z := 0 TO 1 DO
        (1e10)*liquid_diffusivity_CO2_water(z)
      = (1e10)*2.35e-6*EXP(-2119/temperature(z)) ;
        (1e10)*liquid_diffusivity_N2O_water(z)
      = (1e10)*5.07e-6*EXP(-2371/temperature(z)) ;
        (1e10)*liquid_diffusivity_N2O_solution(z)
      = (1e10)*(
        (5.07e-6 + 8.65e-7*(molar_concentration('MEA',z)/1000) + 2.78e-7*(molar_concentration('MEA',z)/1000)^2)
        * EXP( (-2371-93.4*(molar_concentration('MEA',z)/1000)) / temperature(z) ) );
    END # For z

    FOR z := 0 TO 1 DO # for SI units
        (1*scale_factor) * liquid_diffusivity(z)
      = (1*scale_factor) * 1.173 * 10^(-16) * temperature(z)
        * (solvent_diffusivity_coeff*molecular_weight("H2O")*1e3)^(1/2)
        / (liquid_viscosity(z)*0.034^(0.6));
    END # For z

# Liquid mass transfer coefficient
    FOR z := 0 TO 1 DO
        (1*scale_factor) * liquid_mass_transfer_coeff(z)
      = (1*scale_factor) * 0.0051
        * ( liquid_mass_superficial_velocity(z)/effective_transfer_area(z)/liquid_viscosity(z) )^(2/3)
        * ( liquid_viscosity(z)/liquid_density(z)/liquid_diffusivity_CO2_solution(z) )^(-1/2)
        * ( packing_specific_area*packing_equivalent_diameter )^(0.4)
        * ( liquid_density(z)/liquid_viscosity(z)/gravitacional_constant )^(-1/3) ;
    END # For z
```

```
# Diffusivity of each components in air for low pressures
    FOR z := 0 TO 1 DO
        FOR i IN Components DO
            (1*scale_factor) * gas_diffusivity(i,z)
          = (1*scale_factor) * 1e-4 * 0.00143 * temperature(z)^(1.75)
            / ( pressure(z)/1e5 * 2^(1/2)*( 1/molecular_weight(i)/1e3 + 1/18 )^(-1/2)
            * ( atomic_diffusion_volume(i)^(0.3333) +13.1^(0.3333) )^(2) ) ; #19.7^(0.3333) )^(2) ) ;        END # For i
    END # For z

# Gas mass transfer coefficient
    FOR z := 0 TO 1 DO
        FOR i IN Components DO
            gas_mass_transfer_coeff(i,z)
          = 5.23 * packing_specific_area * gas_diffusivity(i,z)
            * ( gas_mass_superficial_velocity(z) / packing_specific_area / gas_viscosity(z) )^(0.7)
            * ( gas_viscosity(z) / gas_density(z) / gas_diffusivity(i,z) )^(1/3)
            * ( packing_specific_area * packing_equivalent_diameter )^(-2) ;
        END # For i
     END # For z

# Effective packing transfer area
    FOR z := 0 TO 1 DO
        effective_transfer_area(z)
      = packing_specific_area * packing_effective_area_ratio(z) ;
    END # For z

# Relation between liquid mass flowrate and Mass superficial velocity
    FOR z := 0 TO 1 DO
        liquid_mass_flowrate(z) = liquid_mass_superficial_velocity(z) * column_cross_section_area ;
    END # For z

# Relation between gas mass flowrate and Mass superficial velocity
    FOR z := 0 TO 1 DO
        gas_mass_flowrate(z) = gas_mass_superficial_velocity(z) * column_cross_section_area ;
    END # For z

# Reynolds number ( 0.04 < Re < 500 )
    FOR z := 0 TO 1 DO
        liquid_mass_superficial_velocity(z) = liquid_Reynolds(z) * packing_specific_area * liquid_viscosity(z) ;
    END # For z

# Froude number ( 5e-9 < Fr < 1.8e-2 )
    FOR z := 0 TO 1 DO
        liquid_mass_superficial_velocity(z)^2 * packing_specific_area
      = liquid_Froude(z) * liquid_density(z)^2 * gravitacional_constant ;
    END # For z

# Weber number ( 1.2e-8 < We < 0.272 )
    FOR z := 0 TO 1 DO
        liquid_mass_superficial_velocity(z)^2
      = liquid_Weber(z) * liquid_density(z) * liquid_surface_tension(z) * packing_specific_area ;
    END # For z

# surface tension ratio ( 0.3 < ratio < 2 )
    FOR z := 0 TO 1 DO
        surface_tension_ratio(z) = packing_critical_surface_tension/liquid_surface_tension(z) ;
    END # For z

# Wetted area (Onda et Al.)
    FOR z := 0 TO 1 DO
        packing_wetted_area_ratio(z)
      = 1 - EXP( -1.45 * (packing_critical_surface_tension/liquid_surface_tension(z))^(0.75)
        * liquid_Reynolds(z)^(0.1) * liquid_Froude(z)^(-0.05) * liquid_Weber(z)^(0.2) ) ;
    END # For z

    FOR z := 0 to 1 do
```

```
    packing_effective_area_ratio(z)
   = 0.310 * (liquid_surface_tension(z)*1e3)^(1/2)/(column_height)^(0.4)
    * ABS ( liquid_viscosity(z)*(liquid_mass_flowrate(z)/column_cross_section_area)
    / (liquid_density(z)*liquid_surface_tension(z))  *
  (6*(gas_mass_flowrate(z)/column_cross_section_area)/(packing_specific_area*gas_viscosity(z))
    ) )^(0.392) ;
#packing_effective_area_ratio(z) = 0.06 ;
  END # For

# Physical properties calculation
  FOR z := 0 TO 1 DO
    liquid_surface_tension(z)
   = phys_prop.SurfaceTension
    ( temperature(z), pressure(z), liquid_mass_fraction_st(,z), gas_mass_fraction(,z) ) ;
  END # For z

# Liquid mass fractions for surface tension calculation
  FOR z := 0 TO 1 DO
    liquid_mass_fraction_st('H2O',z)
   = liquid_mass_fraction_phys_prop('H2O',z)/(1-liquid_mass_fraction_phys_prop('CO2',z)) ;
    liquid_mass_fraction_st('MEA',z)
   = liquid_mass_fraction_phys_prop('MEA',z)/(1-liquid_mass_fraction_phys_prop('CO2',z)) ;
  END # For z

  FOR z:= 0 TO 1 DO
    FOR i IN Components - ['H2O','MEA'] DO
      liquid_mass_fraction_st(i,z) = 0 ;
    END # For i
  END # For z

# Flooding calculations:
# flow factor (dimensionless)
  FOR z := 0 TO 1 DO
       flow_factor(z) = liquid_mass_flowrate(z)/gas_mass_flowrate(z) * (gas_density(z)/liquid_density(z))^(1/2) ;
  END # For z

# Constants for the Resistance at flooding point calculation
 FOR z := 0 TO 1 DO
    IF flow_factor(z) < 0.4 THEN
      flooding_point_packing_constant(z) = 2.178 ;
      flooding_point_packing_exponent(z) = -0.194 ;
    ELSE
      flooding_point_packing_constant(z) = 0.6244 * 2.178 * (liquid_viscosity(z)/gas_viscosity(z))^(0.1028) ;
      flooding_point_packing_exponent(z) = -0.708 ;
    END # If
  END # For z

# Resistance at Flooding point
  FOR z := 0 TO 1 DO
    flooding_point_resistance_factor(z)
   = gravitacional_constant/flooding_point_packing_constant(z)^(2)
    * ( flow_factor(z)*( liquid_viscosity(z)/gas_viscosity(z) )^(0.2) )^(-2*flooding_point_packing_exponent(z)) ;
  END # For z

# Gas velocity at Flooding point
  FOR z := 0 TO 1 DO
    flooding_point_gas_velocity(z)
   = 2^(1/2) * (gravitacional_constant/flooding_point_resistance_factor(z))^(1/2)
    * ABS( packing_void_fraction - flooding_liquid_holdup(z) )^(3/2)
    / (packing_void_fraction)^(1/2)
    * (flooding_liquid_holdup(z)/packing_specific_area)^(1/2)
    * (liquid_density(z)/gas_density(z))^(1/2) ;
  END # For z

# Liquid holdup at flooding point ( voidage/3 < holdup at flooding < voidage )
  FOR z := 0 TO 1 DO
    flooding_liquid_holdup(z)^3 * (3*flooding_liquid_holdup(z) - packing_void_fraction)
```

```
    = 6/gravitacional_constant * packing_specific_area^2 * packing_void_fraction
      * liquid_viscosity(z)/liquid_density(z) * liquid_mass_flowrate(z)/gas_mass_flowrate(z)
      * gas_density(z)/liquid_density(z) * flooding_point_gas_velocity(z) ;
   END # For z

# Column diameter as function of gas velocity at loading point
   FOR z := 0 TO 1 DO
      gas_mass_flowrate(z)
    = 0.8*flooding_point_gas_velocity(z) * (pi/4 * new_column_diameter(z)^2) * gas_density(z) ;
   END # For z

# Column diameter selector
   CASE column_diameter_selector OF
      WHEN input:
         column_diameter = column_diameter_input ;
      WHEN result:
         column_diameter = MAX( new_column_diameter() ) ;
         column_diameter_input = 1e-5 ;
   END # Case
```

Reaction kinetics sub-model

```
PARAMETER
   Components                          AS ORDERED_SET
   phys_prop                          AS FOREIGN_OBJECT
   Reactions                          AS ORDERED_SET
   Reactions_eq                        AS ORDERED_SET
   ideal_gas_constant                    AS REAL DEFAULT 8.314
   no_grid_points                      AS INTEGER

# Reactions parameters
   Reactions_stoichiometric_coefficient    AS ARRAY(Reactions,Components)    OF REAL
   reaction_rate_scale             AS REAL DEFAULT 1000

DISTRIBUTION_DOMAIN
   column_axial                     AS [ 0 : 1 ] # Normalised distribution

VARIABLE
   component_molar_concentration       AS DISTRIBUTION (Components,column_axial)     OF
molar_concentration
   molar_concentration_CO2_eq  AS DISTRIBUTION (column_axial)       OF molar_concentration
   component_reaction_rate  AS DISTRIBUTION (Components,column_axial)  OF reaction_rate_GLC
   equilibrium_constant   AS DISTRIBUTION (Reactions_eq,column_axial)     OF reaction_rate_GLC
   equilibrium_constant_MEA           AS DISTRIBUTION (column_axial)  OF reaction_rate_GLC
  reaction_rate                    AS DISTRIBUTION (Reactions,column_axial)     OF reaction_rate_GLC
   temperature                     AS DISTRIBUTION (column_axial)                OF temperature
   pressure                       AS DISTRIBUTION (column_axial)                OF pressure
   termolecular_reaction_rate_MEAAS DISTRIBUTION (column_axial) OF reaction_rate_GLC
   termolecular_reaction_rate_H2O             AS DISTRIBUTION (column_axial) OF reaction_rate_GLC
 termolecular_forward_rate_constant_CO2 AS DISTRIBUTION (column_axial)  OF reaction_rate_GLC

SET
   Components := phys_prop.Components ;
   phys_prop := 'Multiflash::ABSORPTION_COLUMN.mfl' ;
   Reactions_eq := ['HMEA+H2O','electrical_neutrality'] ;
   Reactions := ['CO2+MEA+H2O'] ;

# Components                          ['CO2','N2','O2','H2O','MEA','H3O+','MEA.CO2-','HMEA+'] ;
   Reactions_stoichiometric_coefficient('CO2+MEA+H2O',) := [-1,0,0,-1,-1,1,1,0] ;
   column_axial := [BFDM,1,no_grid_points];

EQUATION
# Equations for termolecular mechanism
   FOR z:= 0 TO 1 DO
      (1*reaction_rate_scale)*termolecular_reaction_rate_MEA(z)
    = (1*reaction_rate_scale)*4.61e9 * EXP( -4412 / temperature(z) ) * 1e-6 ;
      (1*reaction_rate_scale)*termolecular_reaction_rate_H2O(z)
```

```
      = (1*reaction_rate_scale)*4.55e6 * EXP( -3287 / temperature(z) ) * 1e-6 ;
    END # For z

# Equilibrium constants dependence with temperature
    FOR z := 0 TO 1 DO
        (1*reaction_rate_scale)*equilibrium_constant_MEA(z)
      = (1*reaction_rate_scale)* 6E-9 * EXP( 2856 / temperature(z) ) ;
    END # For z
    FOR z := 0 TO 1 DO
        (1*reaction_rate_scale)*equilibrium_constant('HMEA+H2O',z)
      = (1*reaction_rate_scale)*1e3 * EXP( -5811.11/temperature(z) - 3.3636 ) ;
    END # For z

# Global reaction rate of each component
    FOR z:= 0 TO 1 DO
        FOR i IN Components DO
            component_reaction_rate(i,z)
          = SIGMA( reaction_rate(,z) * Reactions_stoichiometric_coefficient(,i) ) ;
        END # For i
    END # For z

# Forward reaction rate constant for termolecular mechanism
    FOR z := 0 TO 1 DO
        termolecular_forward_rate_constant_CO2(z)
      = termolecular_reaction_rate_MEA(z)*component_molar_concentration('MEA',z)
        + termolecular_reaction_rate_H2O(z)*component_molar_concentration('H2O',z) ;
    END # For z

# Reaction rate for the reaction CO2+MEA+H2O - termolecular mechanism
    FOR z := 0 TO 1 DO
        reaction_rate('CO2+MEA+H2O',z)
      = termolecular_forward_rate_constant_CO2(z)
        * ( component_molar_concentration('CO2',z) * component_molar_concentration('MEA',z)
        - 1/equilibrium_constant_MEA(z)
        * component_molar_concentration('MEA.CO2-',z) * component_molar_concentration('H3O+',z) ) ;
    END # For z
```